MODELING AND PRECISION CONTROL OF IONIC POLYMER METAL COMPOSITE

A Thesis

by

NIKHIL DILIP BHAT

Submitted to the Office of Graduate Studies of
Texas A&M University
in partial fulfillment of the requirements for the degree of

MASTER OF SCIENCE

August 2003

Major Subject: Mechanical Engineering

MODELING AND PRECISION CONTROL OF IONIC POLYMER METAL COMPOSITE

A Thesis

by

NIKHIL DILIP BHAT

Submitted to Texas A&M University
in partial fulfillment of the requirements
for the degree of

MASTER OF SCIENCE

Approved as to style and content by:

Won-Jong Kim (Chair of Committee)	J. N. Reddy (Member)
James. G. Boyd (Member)	Dennis L. O'Neal (Interim Head of Department)

August 2003

Major Subject: Mechanical Engineering

ABSTRACT

Modeling and Precision Control of Ionic Polymer Metal Composite.
(August 2003)
Nikhil Dilip Bhat, B.E., Pune University
Chair of Advisory Committee: Dr. Won-jong Kim

This thesis describes the open-loop behavior of an ionic polymer metal composite (IPMC) strip as a novel actuator, the empirical force and position models, the control system and the improved dynamic characteristics with the feedback control implemented. Ionic polymer metal composite is a novel polymer in the class of electroactive polymers. IPMC consists of a base polymer coated with electrodes made up of highly conducting pure metals such as gold. The actuation behavior of IPMC can be attributed to the bending of an IPMC strip upon application of voltage across its thickness. The main reasons for the bending are ion migration on the application of voltage and swelling and contraction caused by water content. An experimental setup to study the open-loop force and tip displacement of an IPMC strip in a cantilever configuration was developed, and real time controllers were implemented.

In open loop, the force response of the IPMC strip of dimensions 25 mm × 3.9 mm × 0.16 mm to a 1.2-V step input is studied. The open-loop rise time was 0.08 s and the percent overshoot was 131.62 %, while the settling time was about 10 s. Based on this open-loop step response using a least-square curve-fitting methodology, a fourth-order empirical transfer function from the voltage input to the force output was derived. The tip displacement response of an IPMC strip of dimensions 23 mm × 3.96 mm × 0.16 mm to a

1.2-V step input was also studied. The step response exhibited a 205.34 % overshoot with a rise time of 0.08 s, and the settling time was 27 s. A fourth-order empirical transfer function from the step input to the tip displacement as output was also derived.

Based on the derived transfer functions lead-lag feedback controllers were designed for precision control of both force and displacement. The control objectives were to decrease the settling time and the percent overshoot, and achieve reference input tracking. After implementing the controllers, the percent overshoot decreased to 30% while the settling time was reduced to 1.5 s in case of force control. With position control, the settling time was reduced to 1 s while the percent overshoot decreased to 20%. Precision micro-scale force and position-control capabilities of the IPMC were also demonstrated. A 4-μN force resolution was achieved, with a force noise of 0.904-μN rms. The position resolution was 20 μm with a position noise of 7.6-μm rms.

ACKNOWLEDGMENTS

First of all I would like to thank Dr. Won-jong Kim. I am greatly honored to get the opportunity to work with him. Whenever I had problems in my research he was always there to help. He was a constant source of inspiration and motivation to me. During my association with him, I have learned a lot. I am really amazed by his knowledge and insight into different technical fields.

I would like to thank Dr. J. N. Reddy for serving on my thesis committee. I am highly privileged to have him on my thesis committee. I would also like to thank Dr. James G. Boyd for serving on my thesis committee. I am grateful to him for giving me a lot of technical material to read on adhesion forces in micro-domain during Spring 2002.

My special thanks go to Dr. Donald Leo and Mr. Matt Bennett of Virginia Polytechnic Institute for supplying the IPMC sample. Without their help this entire research could not have been possible. I would also like to take this opportunity to thank Dr. Yoseph Bar-Cohen at NASA Jet Propulsion Laboratory at Caltech. His passion towards electroactive polymers and his wonderful effort in setting up the webhub for electroactive polymers was one of the reasons for my fascination in IPMC.

I would like to thank all my past and present labmates. They have helped me whenever I had a problem, and helped in making the working environment very friendly. I share a special friendship with each one of them.

To my parents Dilip and Nilima Bhat, I have the utmost respect and appreciation. They have been always there for me at all times. During times of my happiness they rejoiced with me. During the times when I was sad and depressed, they motivated me and made me feel good. They have always supported me to learn and stressed achievement of

knowledge. I cannot ever forget the sacrifices they have made so that I could get this education. I will always throughout my life be highly indebted to them. I would also like to thank my young brother Anuj Bhat. By looking at his smiling face and seeing his excitement, I will never forget my childhood. I love him a lot.

TABLE OF CONTENTS

Page

CHAPTER Page

LIST OF TABLES

Page

LIST OF FIGURES

Page

Page

Page

Page

Page

CHAPTER I

INTRODUCTION

The development of mankind and human civilization can be correlated to the discovery and manufacture of new materials. In 300,000 BC flint was found to be useful in making new tools as it could be made into many shapes quite easily. By 5500 BC gold and copper were used for tools and weapons. In 1450 BC iron was discovered and by 1500 AD a blast furnace was invented leading to the era of iron [1]. In present times new materials are discovered and manufactured at a very high frequency. We can christen this to be the decade of smart materials .

Structures and materials that sense external stimuli and respond accordingly in real- or near-real-time are called as “smart” [2]. Polymers have many attractive characteristics; they are lightweight, inexpensive, fracture tolerant, and pliable. Polymers that respond to electrical stimulation with a significant shape or size change are called as electroactive polymers (EAPs) [2]. Generally electroactive polymers can be classified into two major categories based on their active mechanism-electronic and ionic. Electronic polymers include electrostrictive, electrostatic, piezoelectric, and ferroelectric polymers. They require high activation voltage. Their position can be controlled in a better manner as they can hold the induced displacement on the application of a dc voltage [2]. Ionic electroactive materials include ionic gels, ionic polymer metal composites, conducting polymers, and carbon nanotubes. They require low activation

---

This thesis follows the style and format of *IEEE/ASME Transactions on Mechatronics.*

voltages as low as 1−5 V. But it is difficult to maintain their position constant under dc-activation [2]. Electroactive polymers have great potential as polymer-based actuators and sensors.

Ionic Polymer Metal Composite (IPMC) is a novel polymer material belonging to the class of ionic electroactive polymers. IPMC consists of a base polymer coated with electrodes made up of highly conducting pure metals like gold. Two types of base polymers can be used to form IPMC: Nafion® (made by DuPont) and Flemion® (made by Asahi Glass) [2]. Figure 1.1 shows the chemical structure of Nafion based IPMC [3]. IPMC requires wet environment to function correctly. The water present on the surface of IPMC serves as a medium for ion migration, so the quantity of water molecules present on the surface of the IPMC is very important factor which influences the performance of IPMC. Figure 1.2 shows the picture of a Nafion based IPMC sample.

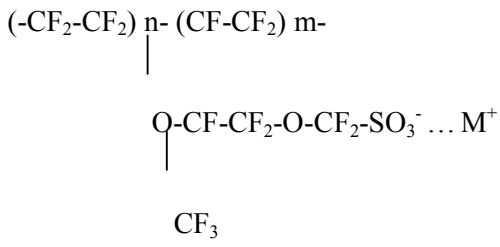

Figure 1.1. Chemical structure of IPMC.

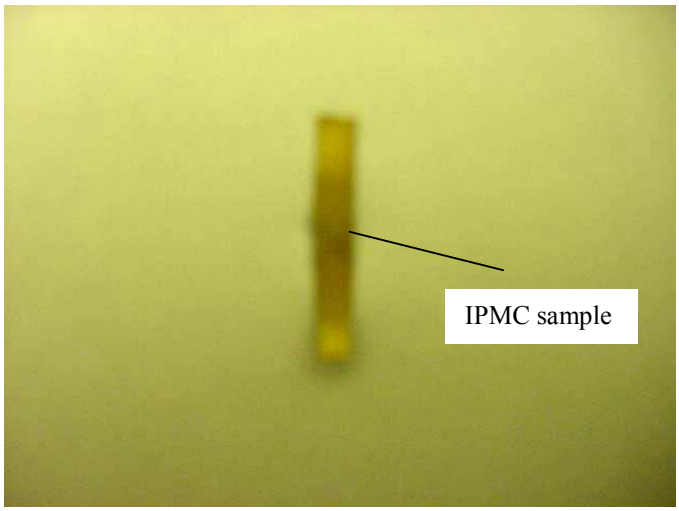

Figure 1.2. Picture of a Nafion-based IPMC sample.

1.1 History of IPMC

As mentioned earlier, IPMC is a type of ionic electroactive polymer, which bends on a voltage stimulus. This electroactive behavior of IPMC for the first time discovered by Shahinpoor [4], Oguru, et al. [5] and Shadeghipour, et al. [6] in 1992. Nafion was widely used in fuel cells for production of hydrogen [2]. But only in 1992 the application of Nafion in creating electroactive polymers was realized. Shadeghipour, et al. developed a novel accelerometer cell based on Nafion. They developed a platinum coated Nafion accelerometer cell and also calibrated it. Shahinpoor presented a conceptual design of swimming robotic structures using ionic polymer gel muscles. In this design concept, all the onboard electronics was to be placed in a head-like structure. A flexible membrane was attached to this head and was filled with an aqueous ionic gel. It was possible to electrically control the expansion and contraction of this polymeric fiber filled gel. Oguru, et al. showed that mechanical deformation is produced across the thickness of a Nafion-based membrane.

1.2 Working Principle of IPMC

Tadokoro, et al. [7] presented a model for the working principle of IPMC based on physicochemical hypotheses. According to that model, on the application of voltage an electric field is created through the IPMC. Sodium ion migration takes place from the anode to the cathode by electrostatic force (Lithium ion was the mobile cation in the IPMC sample used in this research). At the same time due to hydration water molecules travel with the sodium ions. Due to the net migration of sodium ions and water molecules the following forces are applied on the IPMC.

- Swelling and contraction caused by the water content.
- Electrostatic force generated by deviation of fixed charges of sulphonic acid groups.
- Momentum conservation effect concerning the ion migration and the water travel.
- Conformation change of the polymer structure according to the ionic migration.

This conformation change actually represents bending of the polymer. This is just one of the several models developed to explain the behavior of IPMC. But there are still few accurate models, which can completely explain all the internal electro-chemical-mechanical reactions.

1.3 Applications of IPMC

IPMC has many advantages. They (1) require low drive voltage (less than 3 V), (2) produce high displacement, (3) can operate very well in wet environment, and (4) can be cut into small strips and have just one moving part. Table 1.1 presents the comparison between IPMC and other smart materials. From the table we can see that the stress generated by IPMC is small compared to that generated by shape memory alloys (SMAs) and lead zirconium titanate (PZT). The efficiency of IPMC is higher than that of SMA and almost the same as that of PZT. Therefore, IPMC shows significant potential in low mass, high-displacement actuation and other applications.

Table 1.1. Comparison of IPMC with other smart materials [8].

Smart Materials	Strain (%)	Stress (MPa)	Efficiency (%)
Piezoelectric	0.09	35	> 30
SMA	> 5	> 200	> 3
Magnetostrictive	0.2	70	< 30
Electrostatic	> 10	0.04	> 20
IPMC	> 40	0.3	> 30

1.3.1 Human-Machine Interface

There is a need to create better human-machine interfaces, which can help our sensory system efficiently. For example, in case of telesurgery a doctor needs a highly developed interface to avoid realizing the difference due to his physical absence from the operation. Some of the important human-machine interfaces are tactile sensors and haptic devices [2]. IPMC actuators [9] were used to produce artificial tactile feel display to provide a human operator with the required stimuli. Bar-Cohen presented the idea of

using electroactive polymers in active tactile display device to present textual and graphical information to a blind person. The display medium can be constructed as a planar array of small cones called ‘reading pins’ [2].

1.3.2 Space Applications

Space applications are the most challenging and technologically demanding amongst all hence new technologies and materials find immediate application in space. Bar-Cohen, et al. developed an IPMC-based planetary dust wiper to remove planetary dust particles from the surface of a Nanorover [10]. It was a joint effort of NASA and NASDA (National Space Development Agency of Japan). NASA found that operations on mars involve an environment that causes accumulation of dust on hardware surfaces. Hence they proposed a planetary dust wiper. This dust may be a cause of serious concern as it may damage delicate and precious instruments such as a high-resolution camera, etc. Thus it is important to deal with this planetary dust.

1.3.3 Robotic Applications

The human fascination to create humanoids or robots, which resemble man, is well known. For years efforts have been made in the direction of creating robots which can walk, talk, and more importantly, show emotions like man. With the development of ionic polymer metal composites this goal appears closer. IPMC shows a potential to act like human muscles. Hence we might be able to build robots which are now more closer to a human. Developing biomimetic robots requires (1) development of specific circuitry, (2) power and regulators integrated into the mobility elements to allow a limited degree

of self-powered maneuvering [2]. Shahinpoor presented a conceptual design of a swimming robotic struture,which uses IPMC [4]. The general structural design of such a swimming robotic structure is considered to be in the form of a submarine structure which is partially encapsulated in an elastic or flexible membrane filled with an electrolyte like water. Incidently the first commercial application of IPMC was a swimming fish robot developed by EAMEX, Japan was exhibited recently [11]. Bar-Cohen, et al. designed and created a miniature robotic arm at JPL [12]. It consists of a gripper of four fingers made up of IPMC with hooks at the bottom emulating fingernails. The other reason for use of hooks was the low grasping force generated by IPMC.

1.3.4 Medical Applications

IPMC show great potential in medical applications due to their unique properties. IPMC operates similar to biological muscles in terms of flexibility, softness, and large displacement, thus making them good candidates to operate as substitutes for human muscles [2]. Shahinpoor [13] used IPMC as artificial muscles. A human body has a large percentage of water present in it. IPMC operates very well in presence of a solvent medium like water. Thus this property of IPMC, makes it a very good material for making robots, etc. which can be inserted in out body to perform surgeries and a closed-loop real-time control system will control it and a haptic interface like joystick will be used in the closed loop. IPMC can also be used in developing micro-robots, which can guide catheters in the blood stream [2].

1.3.5 Micro-Manipulation Applications

In this decade there has been a tremendous growth in the field of micro-electro-mechanical systems (MEMS). Primarily-silicon based applications like miniaturized pumps, miniaturized sensors, etc. have become common and are used in several places like automobile industries, etc. EAPs in general and IPMCs in particular can be of tremendous importance in next generation MEMS devices. Presently MEMS devices for example micro-pumps cannot achieve very high displacements or forces. This is because the present actuators have many limitations in terms of power consumption or applied voltage to produce the known force. IPMC due to their large displacements and low power consumption, can be a suitable material in MEMS [2].

Micromanipulation is important in microassembly of small parts, in microfabrication, etc. IPMCs are well suited as actuators in micromanipulation devices. Lumia and Shahinpoor gave a design of a micro-gripper, which used both the actuation and sensing capabilities of IPMC [14]. Kim and Bhat initiated an idea of using IPMC strips as fingers for a micro-gripper system [15]. To develop a micro-gripper system, many issues pertinent to IPMC and micro-domain manipulation should be addressed. Consider the case that we pick and place a micro-sphere using a micro-gripper. When we place the micro-sphere at the desired position, the micro-sphere may not be released from the finger surface. This is because adhesion forces are much bigger than the gravitational force in micro-domain. Also in the manipulation of micro-objects the precision control of force is of critical importance, as excessive force may damage the micro-object.

1.4 Manufacture of IPMC

This section presents a brief overview of the manufacturing method of IPMC. The IPMC samples, which were used in this thesis, were obtained from Dr. Donald Leo and his student Mr. Matt Bennett of the Virginia Polytechnic Institute. The samples were also gold plated while the manufacturing process mentioned here is for producing platinium coated IPMC. But still this gives a very good idea about the manufacturing method for IPMC. The method stated in this section is given by Dr. Oguru [16].

Raw Materials required.

- Base polymer: Nafion 117 (DuPont)
- Aqueous solution of platinum ammine complex ($[Pt(NH_3)_4]Cl_2$ or $[Pt(NH_3)_6]Cl_4$) [Can be purchased from: Aldrich Chemical Co., Milwackee, WI phone 800-558-9160, Catalog #275905].
- Sodium borohydride ($NaBH_4$, reducing agent for primary reduction).
- Hydrazine hydrate (NH_2NH_2- ~$1.5H_2O$, reducing agent for secondary reduction)
- Hydroxylamine hydrochloride (NH_2OH-HCl, reducing agent for secondary reduction)
- Dilute ammonium hydroxide solution (NH_4OH 5% solution)
- Dilute hydrochloric acid (HCl aq, 2 *N* solution and 0.1 *N* solution)
- Deionized water

1.4.1 Surface Roughening of the Membrane

a. Mild Sandblast: The surface of the membrane is sandblasted in order to increase the surface area. Fine glass beads (GP 105A, Toshiba Co. Ltd.) that are blown onto the dry membrane by compressed air are used for the sandblasting process. The speed of sandblasting is approximately 1 s/cm^2 membrane area. It is also possible to use emery paper to sand the material.

b. Ultrasonic Washing: The glass beads and residues are removed by washing the membrane with water preferably using ultrasonic cleaner.

c. Treatment with HCl: The membrane is boiled in dilute hydrochloric acid (HCl aq, 2 *N* solution) for 30 minutes to remove impurities and ions in the membrane After boiling, it is rinsed with deionized water.

d. Treatment with Water: Then the membrane is boiled in deionized water for 30 minutes to remove acid and to swell the membrane. The roughened membrane is then stored in deionized water.

1.4.2 Ion-Exchange (Adsorption)

Platinum complex ($[Pt(NH_3)_4]Cl_2$ or $[Pt(NH_3)_6]Cl_4$) solution of 2 mg Pt/ml is prepared. Although the adsorbing amount depends on charge of the complex, either complex gives good electrodes. The membrane is then immersed in the solution containing more than 3 mg of Pt per cm^2 membrane area. For instance, more than 45 ml of the Pt solution is required for a membrane of 30 cm^2. Excess amount of the Pt solution is preferable. After immersing the membrane, 1 ml of ammonium hydroxide solution (5

%) is added to neutralize the solution. Then the membrane is kept in the solution at room temperature for more than 3 hours (one night usually).

1.4.3 Primary Plating (Reduction)

A 5-wt% aqueous solution of sodium borohydride is prepared. After rinsing the membrane with water, the membrane of 30 cm^2 is placed in stirring water of 180 ml in a water bath at 40^oC. Then, 2 ml of the sodium borohydride solution (5 wt% $NaBH_4$ aq) is added every 30 min for 7 times. The amount of the reagent is proportional to the area of the membrane. In the sequence of addition, the temperature is raised up to 60^oC gradually. Then, 20 ml of the reducing agent is added and stirred for 1.5 hr at 60^oC. Black layer of fine Pt particles deposits only on the surface of the membrane. Finally the membrane is rinsed with water and immersed in dilute hydrochloric acid (0.1 *N*) for an hour.

1.4.4 Secondary Plating (Developing)

The amount of platinum deposited by the first plating (reduction process) is only less than 0.9 mg/cm^2, which depends on the ion exchange capacity, thickness of the membrane and the structure of the Pt complex. Additional amount of platinum is plated by developing process on the deposited Pt layer. For 2 mg/cm^2 of Pt added on the area of 60 cm^2 (both sides of 30 cm^2 of membrane), Pt complex solution containing 120 mg of Pt is needed. A 240 ml aqueous solution of the complex ($[Pt(NH_3)_4]Cl_2$ or $[Pt(NH_3)_6]Cl_4$) containing 120 mg of Pt is prepared and 5 ml of the 5% ammonium hydroxide solution is added. Plating amount is determined by the content of Pt in the solution. Then a 5%

aqueous solution of hydroxylamine hydrochloride (NH_2OH-HCl) and a 20% solution of hydrazine (NH_2NH_2) is prepared. After doing that the membrane is placed the stirring Pt solution at 40^oC. 6 ml of the hydroxylamine hydrochloride solution and 3 ml of the hydrazine solution is added every 30 minutes. In the sequence of addition, the temperature is raised up to 60^oC gradually for 4 hours, and gray metallic layers start forming. At the end of this process, a small amount of the solution is sampled and boiled with the strong reducing agent ($NaBH_4$) to check the end point. It is dangerous to add $NaBH_4$ powder in a hot solution, because of possible gas explosion. So $NaBH_4$ solution added to a cold solution, and the solution is warmed on a water bath. If any Pt ion remains in the plating solution, the color of the solution turns black. In such cases, development of Pt is continued with addition of the NH_2OH-HCl and NH_2NH_2 solutions. If there is none of Pt ion in the chemical plating solution, the membrane is rinsed with water, and boiled in dilute hydrochloric acid (0.1 *N*) to remove the ammonium cation in the membrane. After washing with water, H^+ in the composite can be exchanged for any cation by immersing in a solution of the chloride salt of the cation.

1.5 Need for Closed-Loop Control

In open-loop operation, on the application of a dc voltage IPMC cannot maintain their position or force at a constant value. This is because the open-loop response of IPMC is characterized by fast bending towards the anode followed by slow movement towards the cathode and finally bending towards the initial position. Also the open-loop overshoot is sometimes very high in the order of 100 to 200% for IPMC while the open-loop settling time is on the order of 10 to 30 seconds.

Consider an application like a robotic manipulator, which has to move from one specified position to another, and has to maintain the position constant. If we are to use IPMC as the actuators then in open loop, it becomes very difficult to maintain the position constant and also to move the IPMC the specified distance. Hence closed-loop precision position control becomes of critical importance in such applications to ensure proper functioning, repeatability, and reliability.

Precision force control equal importance in many future applications of IPMC. Consider a micro-gripper system having IPMC as the fingers. In micro-domain the force required to grip a micro-object is small due to the dominance of adhesion forces as compared to the gravitational force. Van der Waals force is a big constituent of the adhesion force experienced in micromanipulation. Van der Waals force is greatly influenced by the applied force. Hence the control of force generated by IPMC is important to maintain the adhesion forces within particular limits [17]. This will facilitate better micromanipulation. Excessive force may also damage the micro-object. Thus micro-scale precision force control of force produced by IPMC becomes important in the next-generation micro-domain manipulation systems using IPMC as actuators.

1.6 Contributions of the Thesis

This thesis focused on the force and displacement control of ionic polymer metal composite. The following summarizes the contributions of this research.

- The open-loop force and position responses of IPMC in a cantilever configuration were studied.

- Based on the force response to a step input, an empirical model between the voltage input and force output was obtained by using a least-square curve fitting methodology.
- Based on the tip displacement to a step input, an empirical model between the voltage input and position output was also obtained.
- Feedback control systems were designed and implemented based on a lead-lag compensation methodology for force control and also position control. The objectives of the control system were to decrease the per-cent overshoot and the settling time, and reference input tracking.
- Performance characteristics of the IPMC actuator were found out experimentally.

After implementing the feedback force control system on the IPMC the percent overshoot was decreased from 131.62% in open loop to 30% in closed loop. The settling time also decreased from 10 s to nearly 1.5 s. Also when the feedback position control system was implemented the percent overshoot decreased to 20% from nearly 205.34% in open loop and the settling time reduced to about 1 s from 27 s in open loop.

1.7 Overview of the Thesis

Chapter II presents the experimental setup. The open-loop force and position response of ionic polymer metal composites is also presented.

Chapter III presents the modeling methodology followed to obtain the transfer function between input voltage and output force and also input voltage and output tip displacement.

Chapter IV describes the feedback position and force controller development on the basis of lead-lag methodology. The objectives were to reduce the settling time, the percent overshoot and input tracking.

Chapter V presents the closed-loop experimental results. Closed-loop precision micro-scale force and position control is achieved and is presented.

Chapter VI presents the conclusion and the future work.

CHAPTER II

OPEN-LOOP EXPERIMENTAL RESPONSE OF IPMC

This chapter will give a brief overview of the experimental setup used in the open-loop analysis of IPMC. Both open-loop force response of IPMC and open-loop position response of IPMC are presented. Water affects the performance of IPMC and hence the effect of water on the open-loop frequency response is studied and presented. The need for closed-loop control of IPMC will be stressed at the end of this chapter.

2.1 Specification of the IPMC Strips

Ionic polymer metal composite is a new generation smart material and when this research was started, no commercial vendor of IPMC was available. It is fabricated only in research laboratories in the academia and research institutions like NASA Langley Research Center, etc. The IPMC strips used in this research were cut from a sample provided by Dr. Donald Leo and Mr. Matt Bennett of the Virginia Polytechnic and Technical Institute. Table 2.1 lists the specifications of the three IPMC strips used in the research. The three strips will be referred to as strip *A*, *B*, and *C* throughout this document. As they were cut from the same base strip, the thickness of each strip is the same. In all the experiments the IPMC strips were held in a cantilever position.

Table 2.1. Specifications of the IPMC strips used.

Strip	A	B	C
Thickness (mm)	0.16	0.16	0.16
Length (mm)	28	25	23
Width (mm)	4.5	3.9	3.96

2.2 Experimental Setup for Open-Loop Force Tests

Figure 2.1 shows the schematic of the experimental setup used for conducting open-loop force experiments. A standard clamp as seen in the figure was bought from McMaster, Inc[1]. It was modified by attaching 2 copper electrodes of dimensions 11.43 mm × 4.28 mm × 1.27-mm (99.9% pure copper foil from Alfa Aesar[2]). Two holes were drilled on the jaws of the clamp behind the copper electrodes for allowing wires to be connected to the electrodes. The wires were soldered to the electrodes. A precision load cell (Model GM2 from SCAIME[3]) with a force resolution of 900 nN, was used for the force sensing purpose. It was mounted on the platform, such that the tip of IPMC after clamping between the modified clamp would touch the tip of the load cell. The output of the load cell was very small, thus was amplified using a signal amplifier (CMJ-CEB Series). A differential instrument preamplifier (Model ADA 400 from Tektronix[4]) was used to amplify the output further, and also for noise rejection. The output from the differential preamplifier was fed to a 16-bit analog-to-digital (A/D) converter board of a DSP (digital signal processor) controller board (Model DS1102 from dSPACE[5]). The controller board has a Texas Instruments' TMS320C31 floating-point DSP. Figure 2.2 shows the picture of the experimental setup. The IPMC held between the modified clamps is seen in Figure 2.3.

[1] McMaster-Carr: P.O. Box 740100 Atlanta, GA 30374-0100. Phone-404-346-7000.
[2] Alfa Aesar: 30 Bond Street, Ward Hill, MA 01835. Phone-800-343-0660.
[3] PTC Electronics: P. O. Box, Wyckoff, NJ 07481-0072. Phone-800-989-9518.
[4] Tektronix, Inc: P.O. Box 500, Beaverton, Oregon 97077-0001. Phone-503-627-7111.
[5] dSPACE, Inc., 28700 Cabot Drive – Suite 1100, Novi, MI 48377. Phone-248-567-1270.

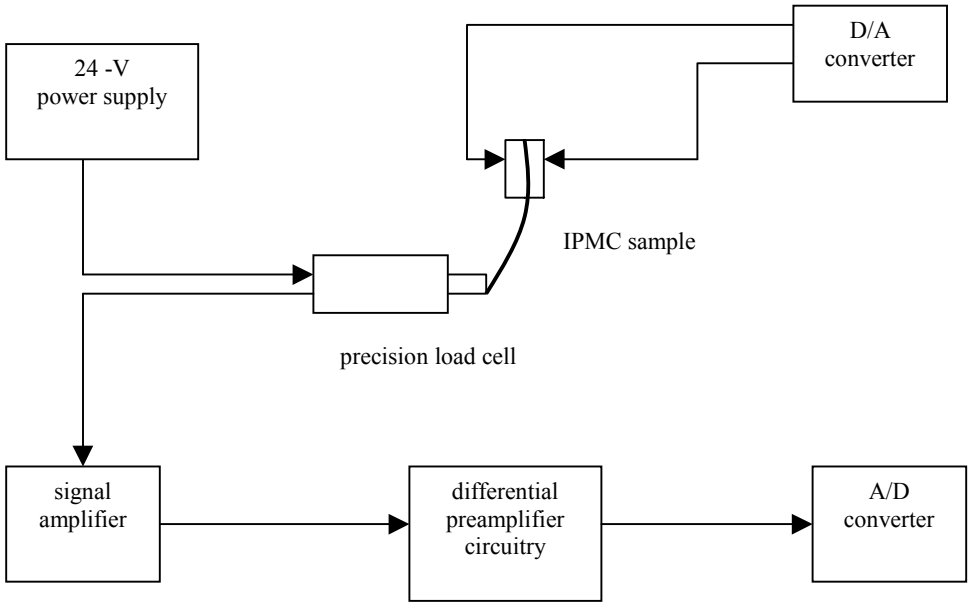

Figure 2.1. Experimental setup for open-loop force experiments.

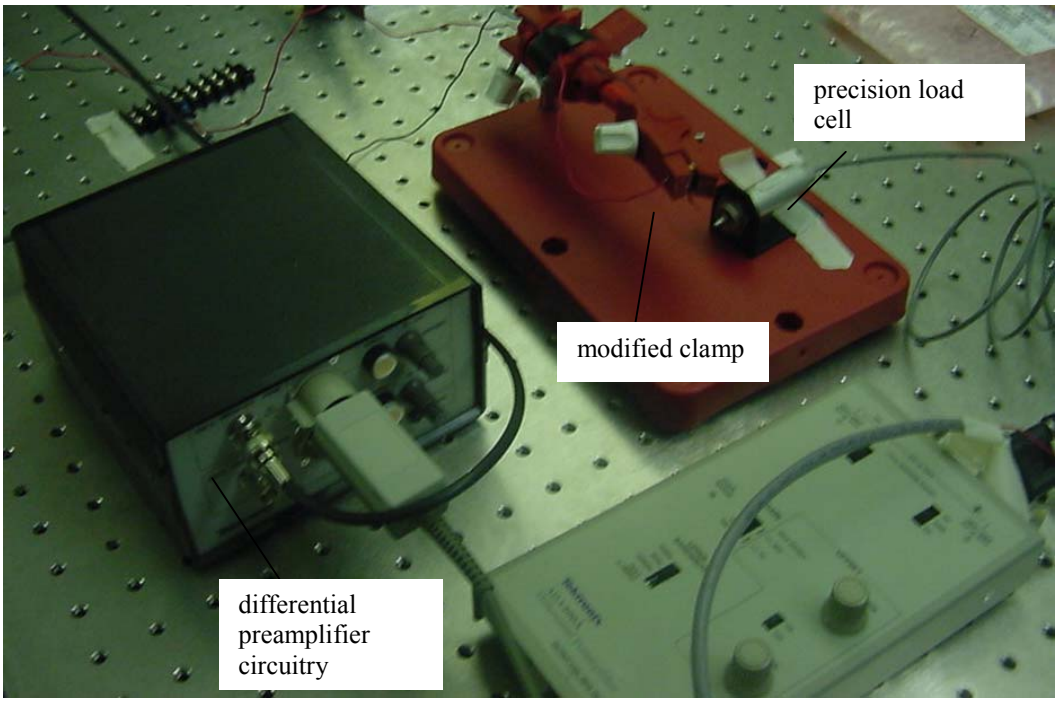

Figure 2.2. Experimental setup. The setup shows the modified clamp, the precision load cell, and the differential preamplifier circuitry.

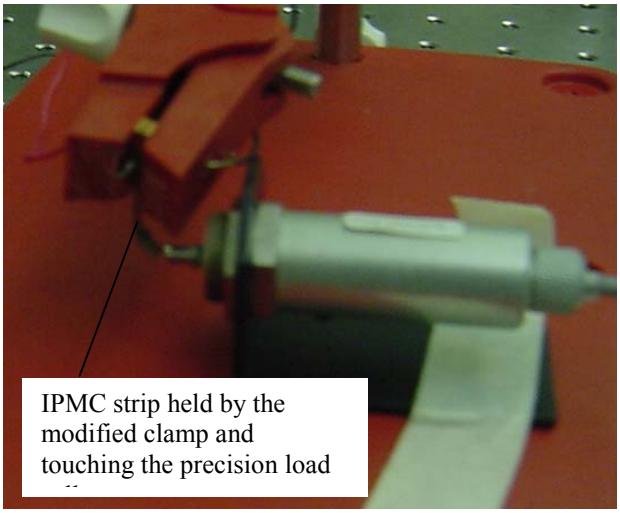

Figure 2.3. Zoomed-in picture of the setup, showing the modified clamp holding the IPMC strip and the precision load cell.

2.3 Open-Loop Force Responses

IPMC strip *A* with the specifications given in Table 2.1 was used to perform the open-loop experiments. Figure 2.4 shows the response of the IPMC strip to a −1.2 V step input. The motivation for giving a negative voltage in case of open-loop force experiments was that in the experimental setup the load cell was so placed that on the application of a positive voltage the IPMC strip initially bend away from the load cell.

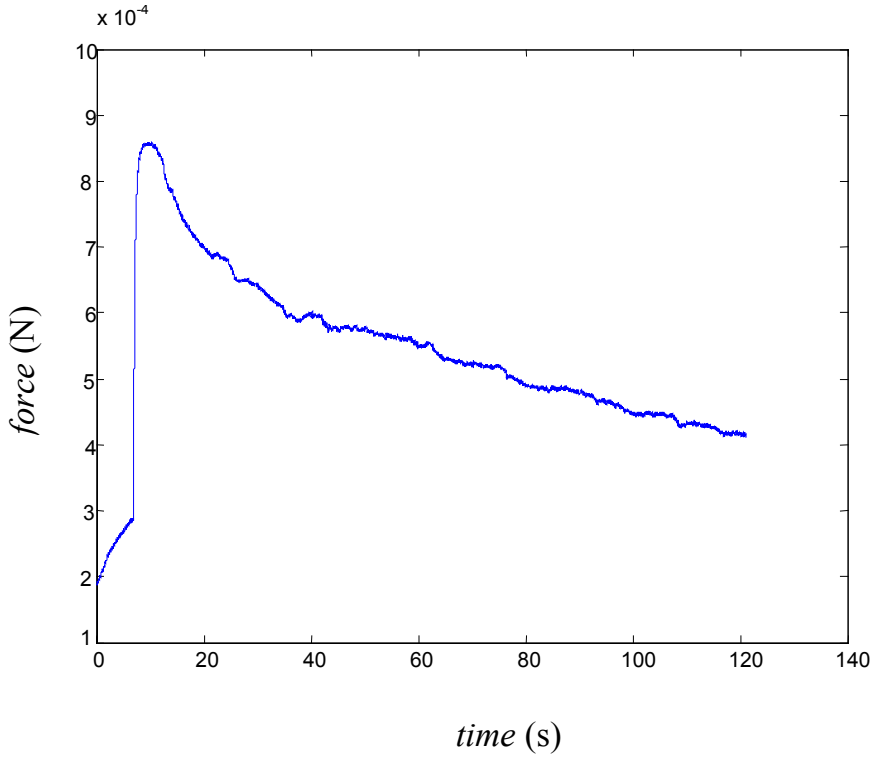

Figure 2.4. Open-loop response of IPMC strip *A* to −1.2 V step input.

The maximum force generated for a 1.2-V step input was 5.716×10^{-4} N. From the step response it is seen that the IPMC strip initially generates its maximum force within 2.618 s after the application of the step input then, it takes about 20 s to settle back

to its steady-state value. It was observed that the IPMC strip response in time domain was non-repeatable and hence it became difficult to quantify the performance characteristics.

As mentioned in Chapter I, one of the factors observed to affect the performance of IPMC is the water content. Leary and Bar-Cohen states that a hydrolysis reaction starts after about 1.23 V and hence water level present goes on decreasing rapidly [18]. Also exposure to air for a long period of time causes evaporation of water from the surface of IPMC. Mallavapuru [19] and Kothera [20] tried to find a correlation between the shift of resonant frequency due to change in water content. They both used position data obtained from position sensing devices. The effect on the frequency spectrum obtained from force response data, due to the decrease in the water level was studied. Time domain force data of the IPMC strip was taken every 2 minutes for a period of 30 minutes, with sweep-sine signal input. This time domain data obtained was converted into corresponding frequency spectrum by performing fast fourier transform on the data. Figures 2.5–2.7 show the frequency response when the IPMC was completely rehydrated, after 16 minutes and after 30 minutes respectively. It was observed that even without maintaining the water concentration constant (i.e., without rehydration), the frequency response does not show any appreciable change over this 30-minute period. Some of the reasons for this observation which actually differs from the previous work can be as follows

- It was observed during the experiments that at the point of contact between the IPMC tip and the precision load cell a localized layer of water was formed. The presence of this layer might have contributed to the lack of frequency shift observed.

- The applied voltage range was less than 1.23 V, hence it is possible that hydrolysis reaction did not occur and hence water decrease on the surface of IPMC was less than what it would have been if hydrolysis had occurred.

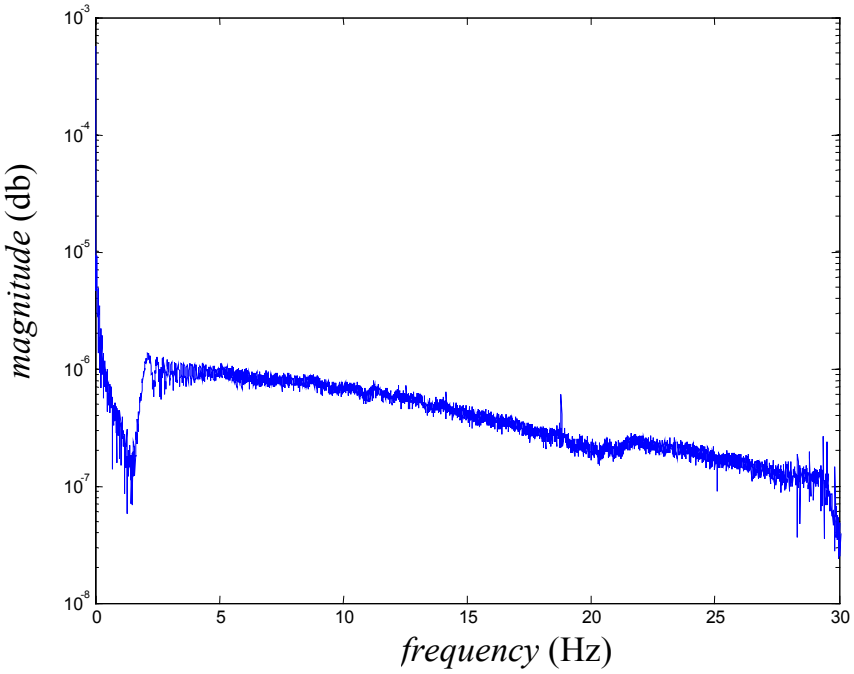

Figure 2.5. Frequency response of the IPMC when it was completely rehydrated.

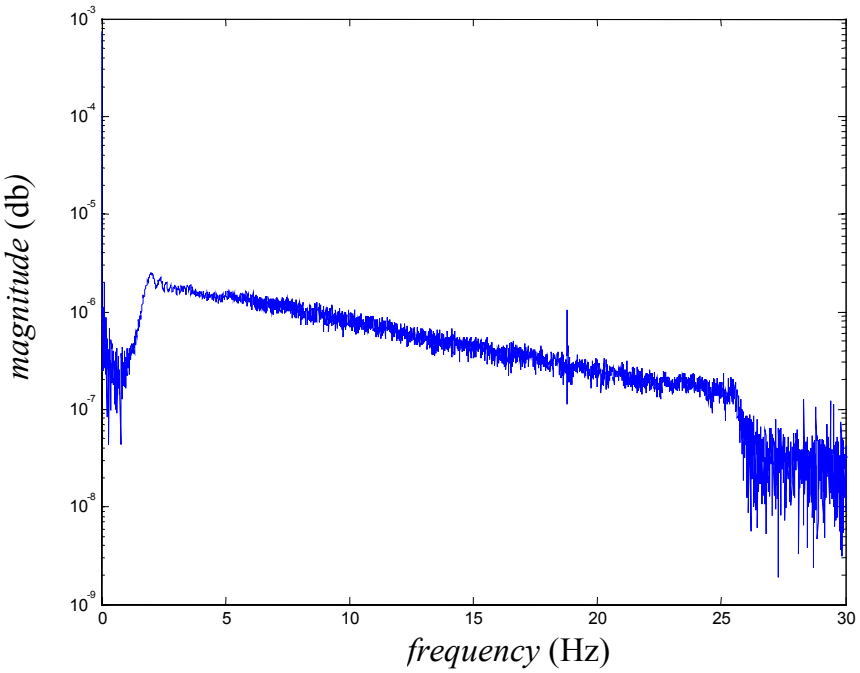

Figure 2.6. Frequency response taken after 16 minutes without rehydration.

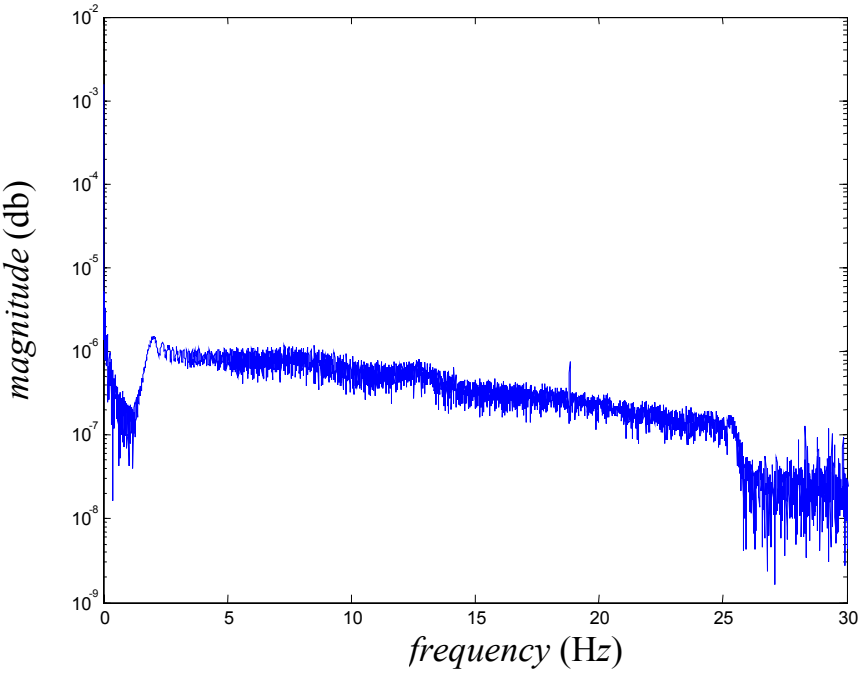

Figure 2.7. Frequency response taken after 30 minutes without rehydration.

Due to repeated use of this IPMC strip *A* over a period of time its performance was degraded and was not used for closed-loop force or position control.

IPMC strip *B* as specified in Table 2.1 was used to develop an empirical model between voltage input and force output. Figure 2.8 shows the open-loop step response of strip *B* to −1.2 V input voltage. From the Figure 2.8 it can seen that maximum force achieved was about 0.9 mN on the application of 1.2 V step input. Its rise time is also

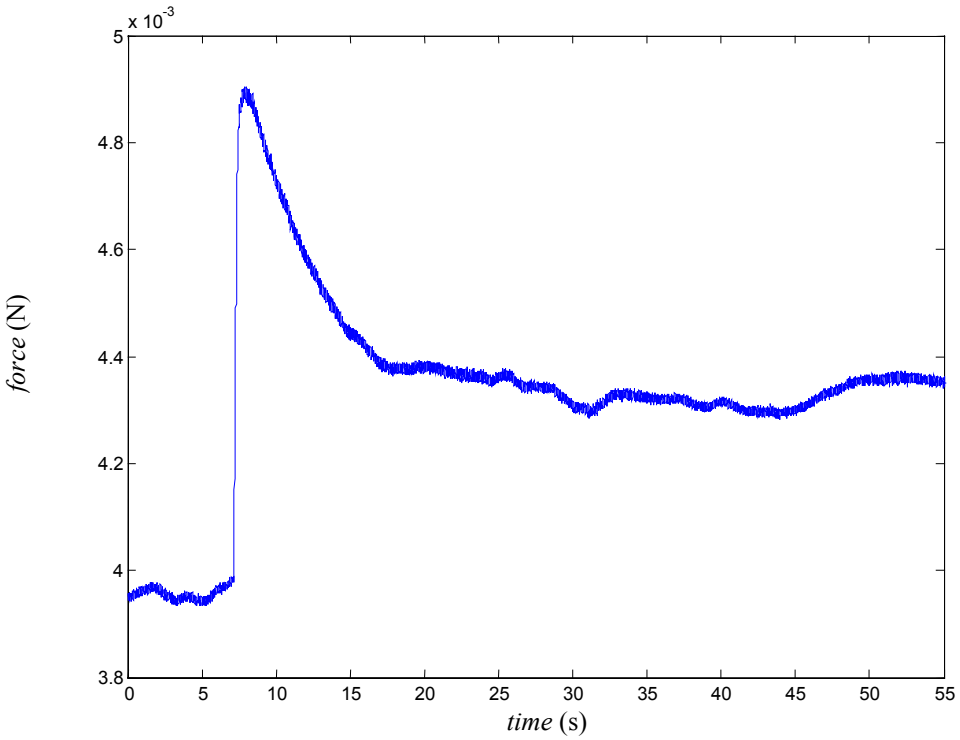

Figure 2.8. Open loop step response of IPMC strip *B* to −1.2 V step input.

about 0.0805 s. The open-loop settling time was observed to be nearly 10 s.

Figure 2.9 shows the IPMC response to a 5-Hz sine wave of 1 V amplitude. From the figure it can be seen that the IPMC strip follows the frequency quite well. Figure 2.10 shows the open loop response to 1 V amplitude, 0.5 Hz frequency sine wave. It can be

seen from these responses that the IPMC strip responded very well to the commanded input frequencies.

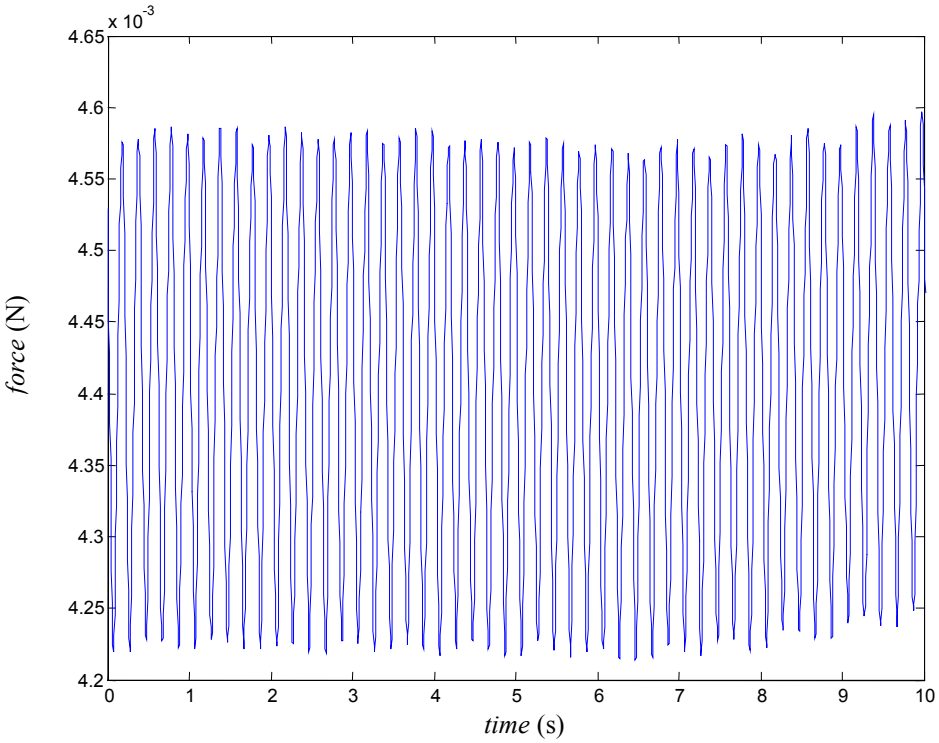

Figure 2.9. Open-loop response of IPMC strip to a sinewave of amplitude 1 V and frequency 5 Hz.

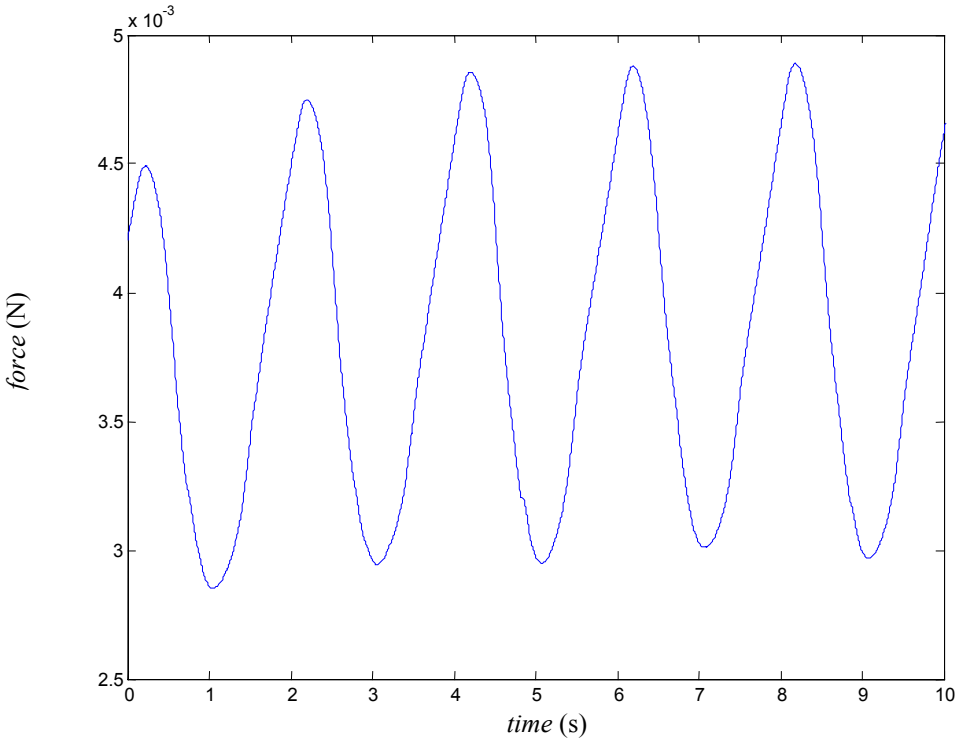

Figure 2.10. Open-loop response of IPMC strip *B* to 1V amplitude and 0.5 Hz sine wave.

2.4 Open-Loop Position Response

IPMC strip *C* having specifications 23 mm × 3.96 mm × 0.16 mm as in Table 2.1, was used to conduct open-loop position experiments. The experimental setup used for the open-loop position response is shown in Figure 2.11. Figure 2.12 shows the picture of the experimental setup. It is very similar to the setup used for open-loop force experiments, the only difference being the use of a laser distance sensor (Model OADM 20144/404790) from Baumer Electric[6] to sense the tip position. Also no differential pre-amplifier was used in this case as the output voltage was in the range of 0–10 V. The

[6] Baumer Electric Ltd: 122 Spring Street, Unit C-6, Southington, CT 06489. Phone-860-621-2121.

laser distance sensor has a resolution of 5 μm and the operation range was 10 mm with a standoff of 15mm. The response time is less than 10 ms. This sensor works on the principle of optical triangulation. The sensor could detect position up to a bending angle of 30° [21].

IPMC is a bending type of actuator. When held in a cantilever position as in this case, the IPMC strip starts bending. The displacement of the tip of IPMC was of interest. Hence the laser sensor was so placed that the laser was incident on the free end of the polymer strip. It should be noted that the tip displacement also referred to as position in this thesis does not stand for linear movement of the IPMC strip but the deflection of the free end, which can also be calibrated into the bending angle of the IPMC strip. Figure 2.13 shows the close up picture of the IPMC strip clamped between the modified clamps and the laser sensor.

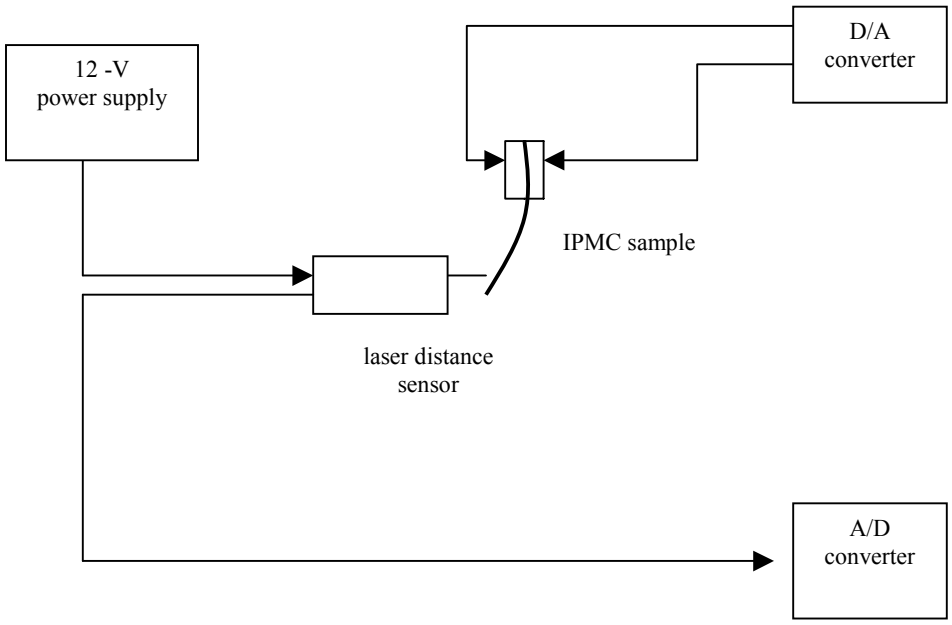

Figure 2.11. Schematic of the experimental setup for open loop position response.

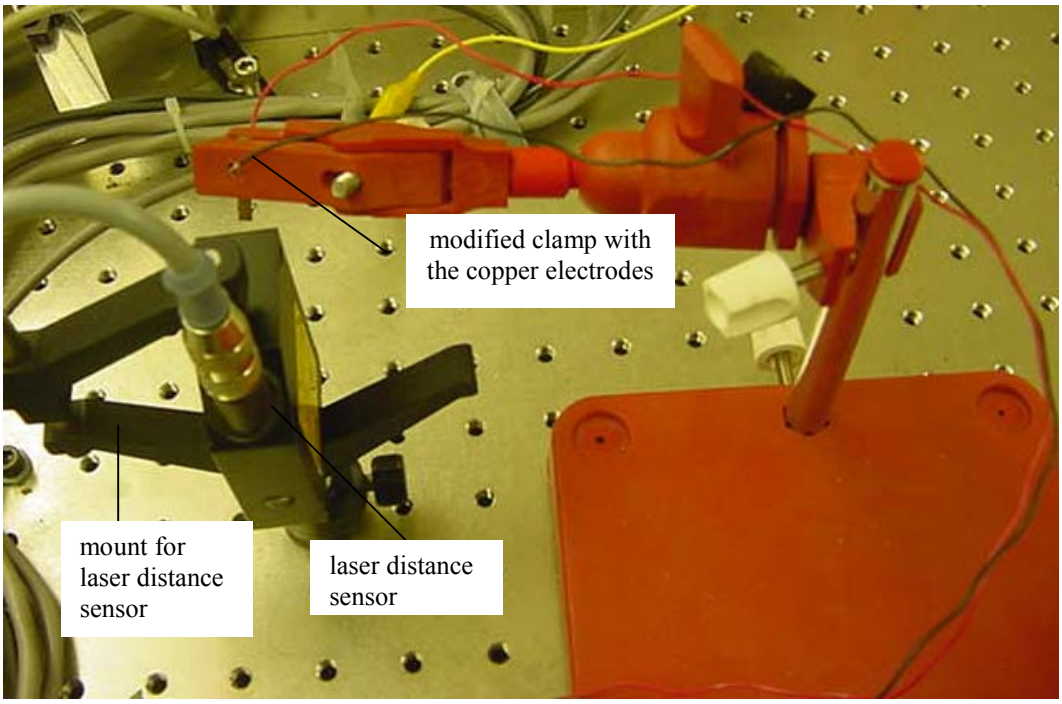

Figure 2.12. Picture of the experimental setup used for both open loop and closed loop position response.

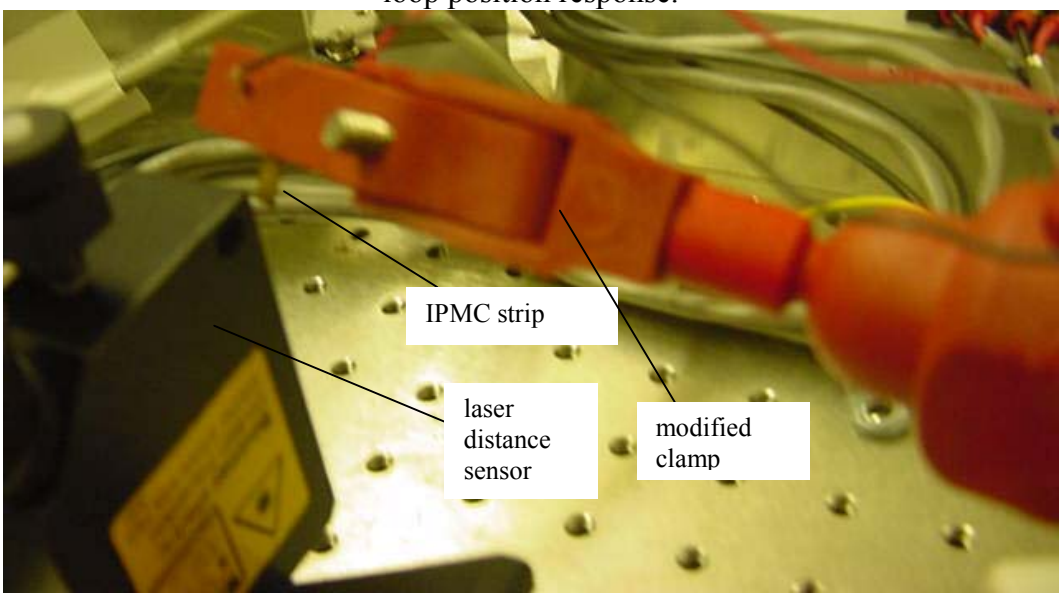

Figure 2.13. Zoomed-in picture showing the clamp with the IPMC strip and the laser distance sensor.

Figure 2.14 shows the open-loop position response of the IPMC strip *C* to 1.2-V step input. From the figure the rise time is about 0.078 s, the settling time is about 27 s and the

overshoot is 205.34 %. The maximum tip displacement is 1.7710 mm. Figure 2.15 shows the sinusoidal response of the IPMC strip to a 1.2-V sine wave of 5 Hz frequency. It can be seen that the IPMC strip is following the commanded frequency very well.

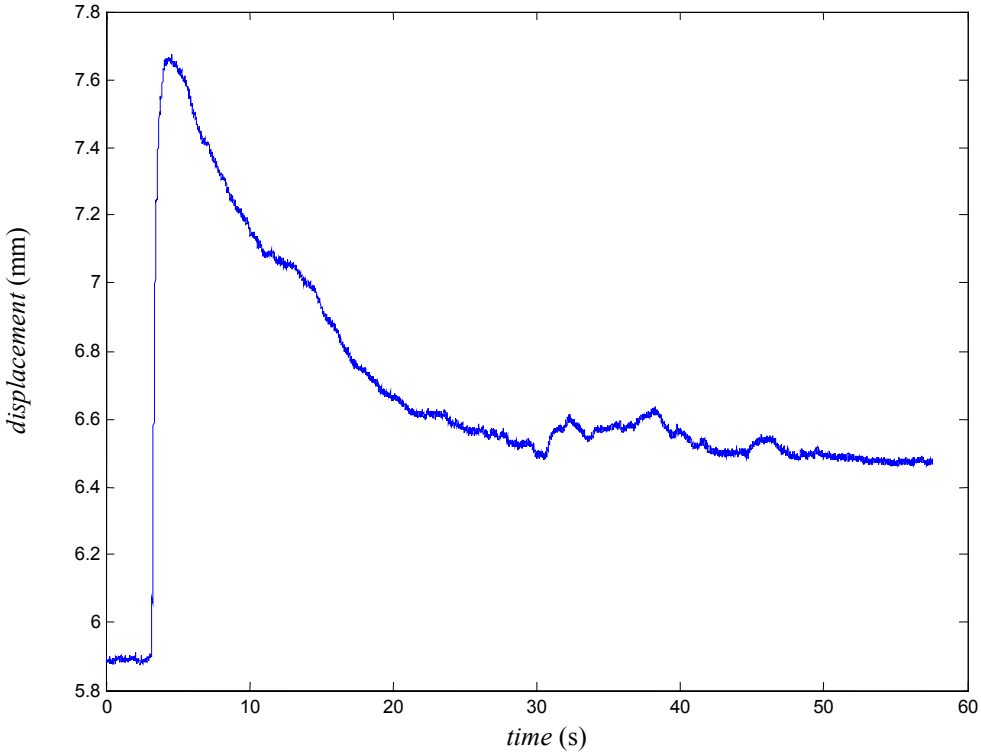

Figure 2.14. Open-loop position response of IPMC strip *C* to 1.2-V input voltage.

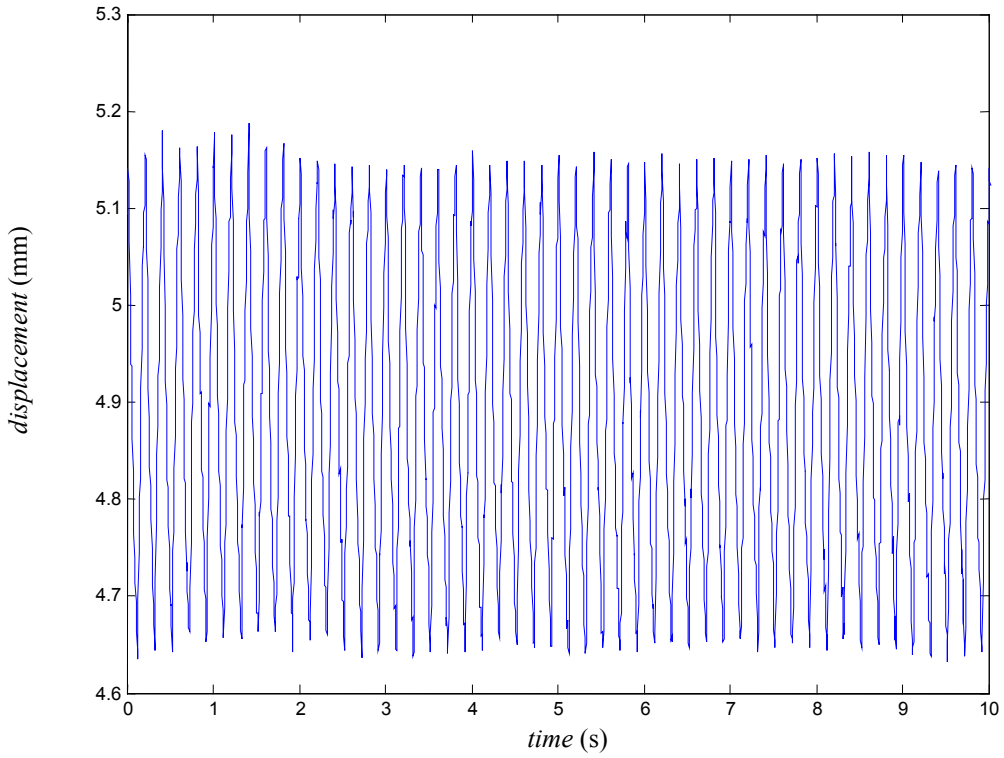

Figure 2.15. Open-loop position response of IPMC *C* to 1.2-V amplitude and 5 Hz-frequency sine wave.

2.5 Conclusions for Chapter II

Both open-loop position and force experiments show similar behavior of IPMC. The rise time for the IPMC very small about 0.080 s for force response and 0.078 s for position response, as compared to the settling time which is about 10 s for force response and 27 s for position response. The percent overshoot is also very high, about 131.62% in force response and about 205.34% in the position response. Both the open-loop force and position behavior of IPMC was found out to be not repeatable, thus arises the need for closed-loop position and force control.

CHAPTER III

MODELING

In this Chapter, Sections 3.2, and 3.3 will deal with the development of an empirical force model based on the obtained step response data, while Section 3.4 will deal with the development of an empirical tip displacement model for IPMC.

3.1 Prior Methodologies

Many physical models have been developed for IPMC. Kanno, et al. presented a three-stage model of IPMC [22]. Shahinpoor [23], Nemat-Nasser and Li [24], and Xiao and Bhattacharya [25] presented a model based on the electromechanics of ionic polymer gels. Tadokoro, et al. presented a white-box model for IPMC [6]. These models consisted of partial differential equations representing individual phenomenon, which had to be solved independently and not simultaneously to obtain the position and force. Therefore, it was difficult to develop a controller based on these physical models.

In 1994, Kanno, et al. presented an empirical model for IPMC [26]. Mallavarapu modified this model to include its resonance behavior [19]. Mallavarapu, et al. also presented an empirical pole-zero model for IPMC [27]. However, all these models focused on the position response of IPMC, and did not address the problem of force control. Only Newbury has presented a model, which can empirically give both the force generation capability and the tip displacement of the IPMC polymer [28]. He presented a two port empirical model for the IPMC polymer in which the coupling term was made frequency dependent.

3.2 Force Modeling

For the development of a controller, it is important to develop good empirical models. We follow a similar methodology as done by Kanno, et al [26] to derive a model between the step input and the force output of the IPMC strip. The difficulties, which are intrinsic in developing an empirical force model of IPMC, are as follows:

- To measure the force there should be physical contact between the load cell and the IPMC strip. The presence of water layer on the IPMC strip creates wet stiction between the IPMC strip and the load cell tip.
- Due to this stiction, some residual force exists. Thus, it is required to compensate the force measured by the load cell.

A negative 1.2-V step input was given continuously to IPMC strip *B* with dimensions in Table 2.1 for a period of about 55 s at a sampling rate of 250 Hz, and an open-loop step response of IPMC was obtained (Figure 3.1). After the step response data was collected, it was normalized to take care of the stiction force present (Figure 3.2). For normalizing the average value of stiction force which was 3.9 mN was subtracted from all the readings.

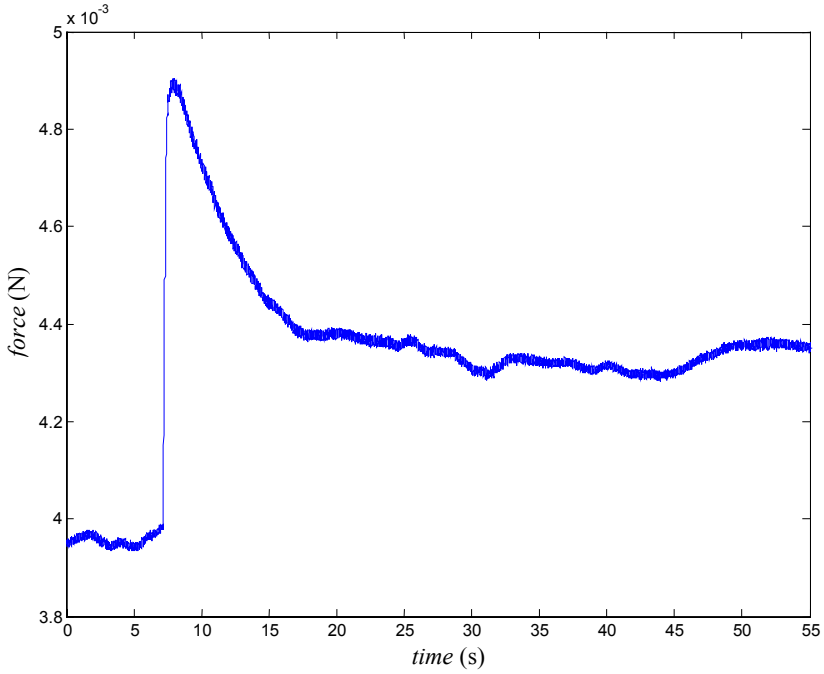

Figure 3.1. Open-loop force response of the IPMC strip to a −1.2 V step input.

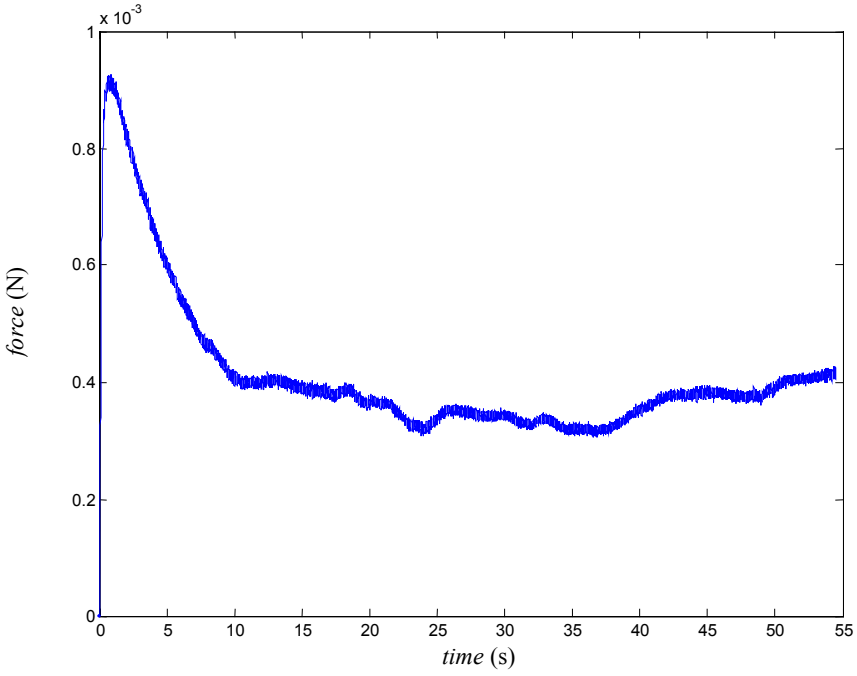

Figure 3.2. Open-loop force response of the IPMC strip to a −1.2 V step input after normalizing by subtracting 3.9 mN from the load cell reading at all times.

For the model development Matlab toolbox of non-linear curve fitting was used [29]. It solves nonlinear curve-fitting (data-fitting) problems in least-squares sense. That is, given input data *xdata,* and the observed output *ydata*, it find coefficients *x* that gives the best fit of the equation.

min sum {(fun(*x*, *xdata*)-*ydata*).^2}

x

where *x*, *xdata*, *ydata* and the values returned by fun can be vectors or matrices.

[*x*, *resnorm*]=lsqcurvefit(fun,x_0,*xdata*,*ydata*) returns the value of the squared 2-norm of the residual at x: sum {(fun(*x*, *xdata*)-*ydata*).^2}.

The step response shows exponential decay after its peak value, so various exponential decay terms were used to fit the data. Initially, the data obtained was fitted with only one exponential decay term to be

$$y(t) = y_1 e^{-at} + C_1. \tag{3.1}$$

Here 'C_1' is the steady-state value. From Figure 3.2 this value is taken as 0.4 mN. By using the LSQCURVEFIT function the parameters y_1 and *a* were estimated to be

y_1= 0.0005

a= 0.2158

The squared residual norm for this curve fit was 5.3933×10^{-5}. Figure 3.3 shows the modeled response verses the actual response for this case.

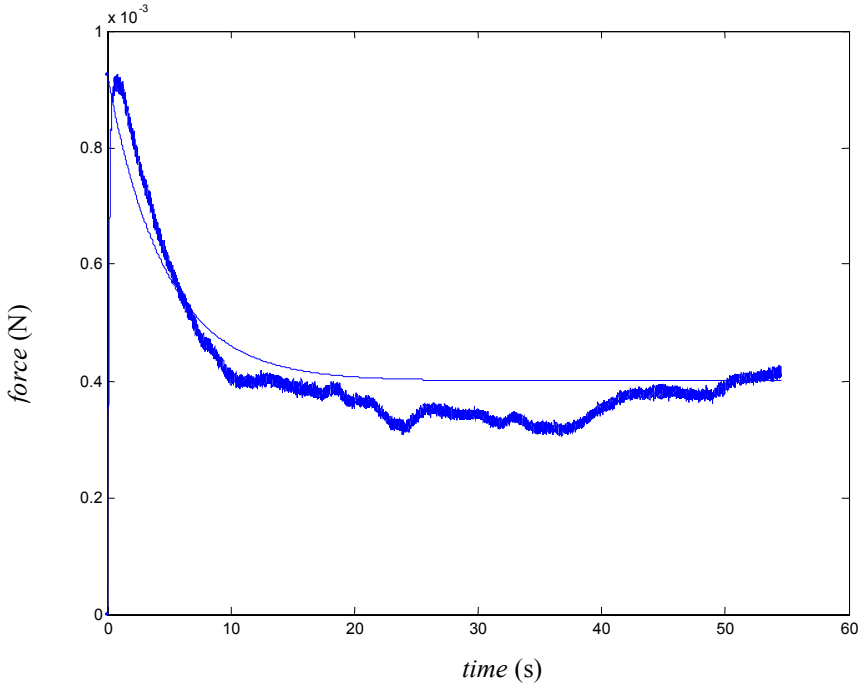

Figure 3.3. Actual response versus modeled response with one exponential decay term.

To decrease the residual norm, one more exponential decay term was added to the model. Now the step response was fitted to be

$$y(t) = y_1 e^{-at} + y_2 e^{-bt} + C_1. \tag{3.2}$$

By using the LSQCURVEFIT function the parameters y_1, y_2, a, and b were estimated to be

$y_1 = -0.0034$

$y_2 = 0.0038$

$a = 0.0587$

$b = 0.0658$

The squared residual norm for this curve fit was 3.4774×10^{-5}. Figure 3.4 shows the modeled response for this model verses the actual response. It can be seen that the squared residual norm is decreased by 35.523 % by adding one more exponential decay term in (3.2).

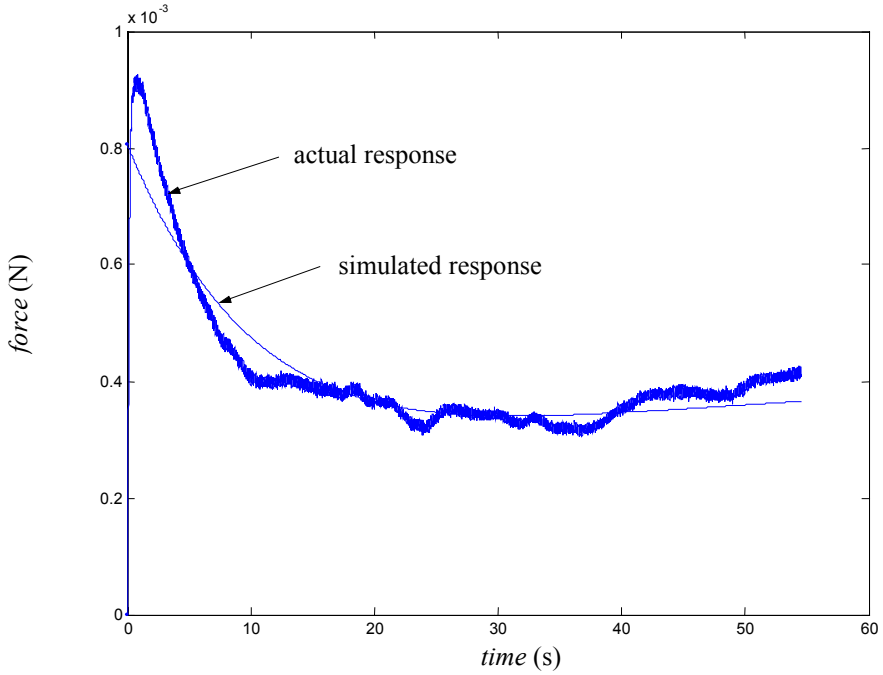

Figure 3.4. Actual response versus modeled response for model with two exponential decay terms.

Although there is a significant decrease in the squared residual norm when this model is used, this model does not account for the small rise time of 0.08 s observed in the open-loop force response of IPMC. From the figure we see that the model predicts the IPMC reaching its peak value at time t = 0 s. The same can also be seen from the model with one exponential term. The main reason for this error can be traced to the real values for all the parameters obtained [30]. To account for this rise time of 0.08 s an empirical model with 3 complex parameters was developed and the data obtained was fitted to be

$$y(t) = y_1 e^{-at} + y_2 \mathrm{e}^{-bt} - y_3\left(e^{ct} - e^{dt}\right) + C_1. \tag{3.3}$$

Again by using LSQCURVEFIT the parameters y_1, y_2, y_3, a, b, c, and d were estimated to be

$y_1 = 0.0886$

$y_2 = -0.0888$

$y_3 = 0.0029\, i$

$a = 0.5008$

$b = 0.5060$

$c = -1.4036 + 0.2574\, i$

$d = -1.4036 - 0.2574\, i$

The squared residual norm in this case was 2.7135×10^{-5}. Therefore, we can see that the squared residual norm decreased significantly in this case. Figure 3.5 shows the modeled verses actual response for this case. From the figure we can see that the model predicts the rise time very well.

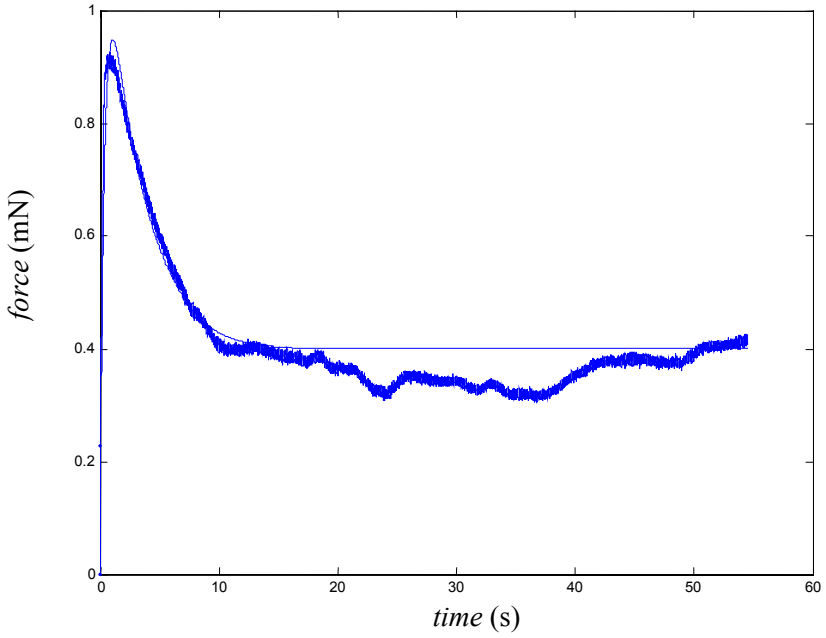

Figure 3.5. Actual versus modeled response for the model with three complex parameters.

Taking the Laplace transformation of the output and input equations we get

$$Y(s) = \frac{y_1}{s+a} + \frac{y_2}{s+b} - y_3\left(\frac{1}{s-c} - \frac{1}{s-d}\right) + \frac{C_1}{s} \tag{3.4}$$

$$U(s) = \frac{step\ voltage}{s} \tag{3.5}$$

where the 'step voltage' is the –1.2-V step input. After substituting the values of y_1, y_2, y_3, a, b, c, and d obtained previously and taking the ratio of $Y(s)$ and $U(s)$, the transfer function from the input voltage and the output force of the IPMC strip B was found to be

$$\frac{Y(s)}{U(s)} = -\frac{0.0002365\,s^4 + 0.002947\,s^3 + 0.004299\,s^2 + 0.002266\,s + 0.0002065}{1.2\,s^4 + 4.577\,s^3 + 6.14\,s^2 + 3.314\,s + 0.6194} \tag{3.6}$$

The negative sign seen in the model is due to the application of negative step voltage as mentioned earlier. Table 3.1 lists the different values for the parameters and the residual norm obtained by the LSQCURVEFIT function in matlab.

Table 3.1. Tabulation of the different parameters obtained from modeling process for strip *B*.

Eq. No.	y_1	y_2	y_3	a	b	c	d	Res-norm ($\times 10^{-5}$)
3.1	0.0005	-	-	0.2158	-	-	-	5.3933
3.2	–0.0034	0.0038	-	0.0587	0.0658	-	-	3.4774
3.3	0.0886	–0.0888	0.0029 *i*	0.5008	0.5060	–1.4036 + 0.2574 *i*	–1.4036 – 0.2574 *i*	2.7135

3.3 Generalized Algorithm for Force Model Development

A generalized method for model development for IPMC strips based on empirical step response data is proposed herein. As seen in Figure 3.6 we assume the IPMC to be a black box and give it a step input of say 1.2 V. By using a high precision load cell we measure its force output for a finite period of about 55 s (or by the time it reaches its steady state value). When we have both the input voltage data and the output force data, an empirical model for controller development and implementation can be generated.

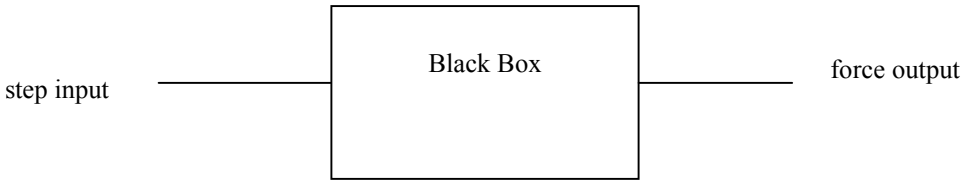

Figure 3.6. Block diagram for generalized model development.

The proposed generalized method is as follows

1. Capture the force output data *y* corresponding to step input *x* for 60 s.
2. Normalize *y* by removing the initial force present before the step is being applied.
3. Change the size of *x* and time *t* to match size of *y*.
4. Curve fit the data to the equation given in (3.3).
5. Obtain the transfer function as mentioned in (3.4) and (3.5).

3.4 Position Modeling

After the development of the model between voltage input and force output, a model was also identified between the voltage input and the tip displacement. IPMC strips *B* and *C* as listed in Table 2.1, were used to identify two different models. Table 3.2 again lists the specifications of the two different strips used for identifying the position model.

Table 3.2. Specifications of the IPMC strip.

Strip	B	C
Length (mm)	25	23
Width (mm)	3.9	3.96
Thickness (mm)	0.16	0.16

Figure 3.7 shows the open-loop step response of the tip displacement of IPMC strip *B* to the application of 1.2-V step voltage.

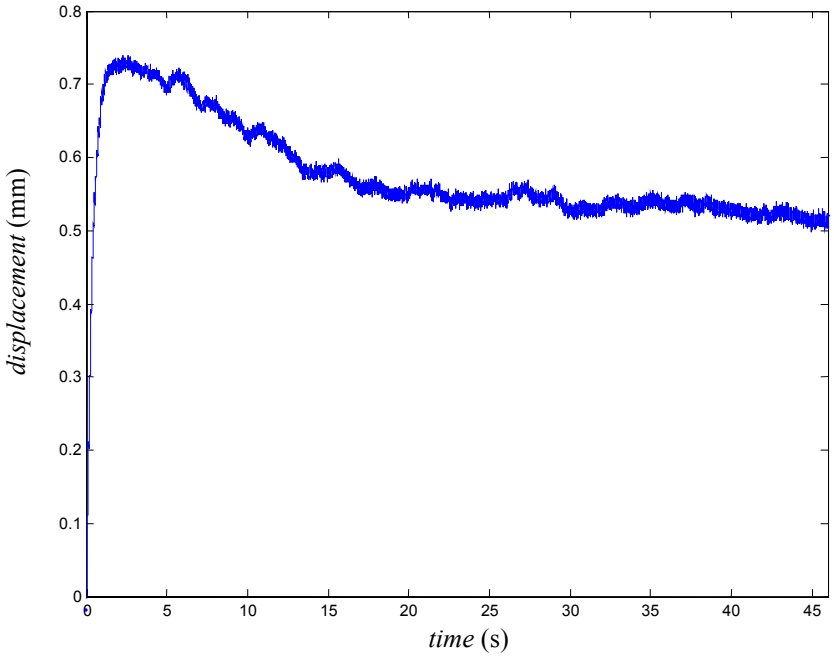

Figure 3.7. Tip displacement of IPMC strip *B* to open-loop step input of 1.2-V.

To identify the model between the voltage input and tip displacement, similar methodology as one used for identifying the force model was utilized. The step response shows exponential decay after its peak value, so various exponential decay terms were used to fit the data. Initially, the data obtained was fitted with only one exponential decay term to be

$$y(t) = y_1 e^{-at} + C_2. \tag{3.7}$$

In this case 'C_2' is the steady-state value, i.e., 0.54-mm as seen in Figure 3.7. By using the LSQCURVEFIT function the parameters y_1 and a were estimated to be

y_1= 0.1820

a= 0.0651

The squared residual norm for this curve fit was 122.3507. Figure 3.8 shows the modeled response verses the actual response.

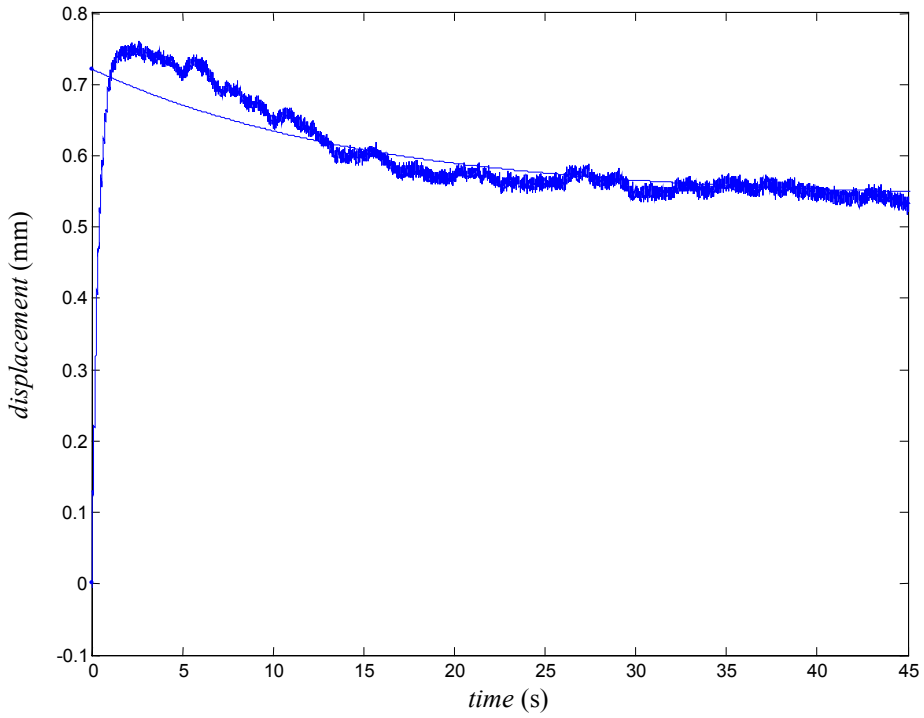

Figure 3.8. Actual versus modeled position response for model with one exponential decay term for strip *B*.

To decrease the residual norm, one more exponential decay term was added to the model. Now the step response was fitted to be

$$y(t) = y_1 e^{-at} + y_2 e^{-bt} + C_2. \tag{3.8}$$

By using the LSQCURVEFIT function the parameters y_1, y_2, a, and b were estimated to be

$$y_1 = 0.2905$$

$$y_2 = -0.8112$$

$$a = 0.0985$$

$$b = 2.0760$$

The squared residual norm for this curve fit was 5.4068. Figure 3.9 shows the modeled response for this model verses the actual response. It can be seen that the squared residual norm is decreased by 95.580 % by adding one more exponential decay term in (3.8).

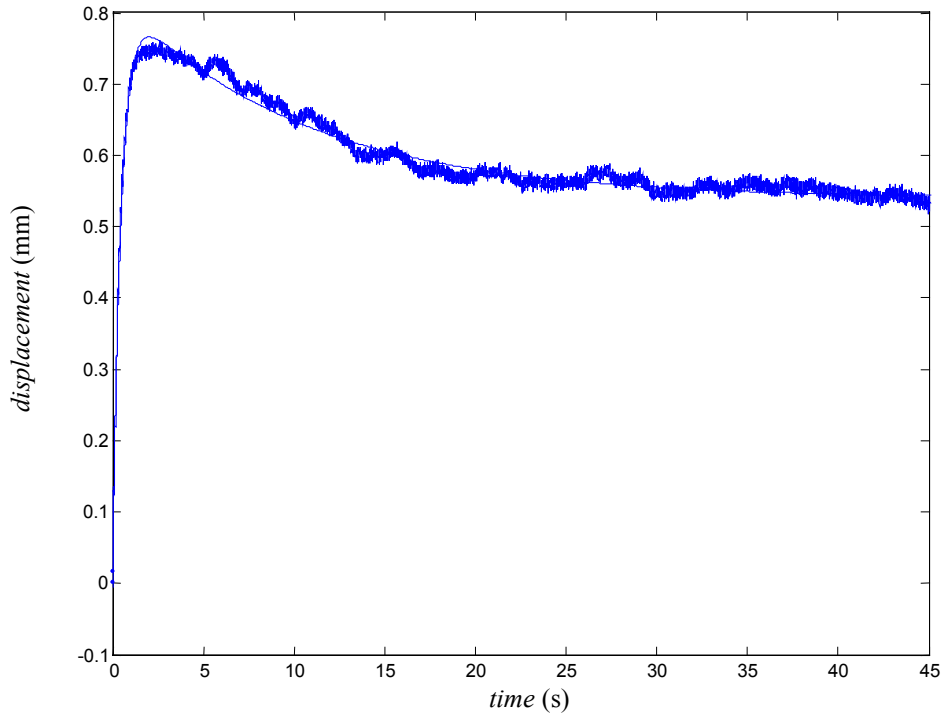

Figure 3.9. Actual versus modeled position response for model with two exponential decay terms for strip *B*.

From the Figure 3.9 it can be seen that as compared to the force model, addition of one additional real parameter actually did account for the rise time of 0.37 s while in case of force model it was not the case. To decrease the residual norm more, an empirical model with 3 complex parameters was developed and the data obtained was fitted to be

$$y(t) = y_1 e^{-at} + y_2 e^{-bt} - y_3\left(e^{ct} - e^{dt}\right) + C_2. \tag{3.9}$$

Again by using LSQCURVEFIT the parameters y_1, y_2, y_3, a, b, c, and d were estimated to be

$y_1 = -0.8915$

$y_2 = 0.3584$

$y_3 = -0.0011 + 0.6246i$

$a = 0.5008$

$b = 0.1144$

$c = -1.3752 + 0.7899i$

$d = -1.3772 - 0.7908i$

Actually c and d should be a complex conjugate pair, but due to the rounding error in Matlab there was a small difference in the values obtained. The squared residual norm in this case was 3.7090. Figure 3.10 shows the modeled verses actual response for this case.

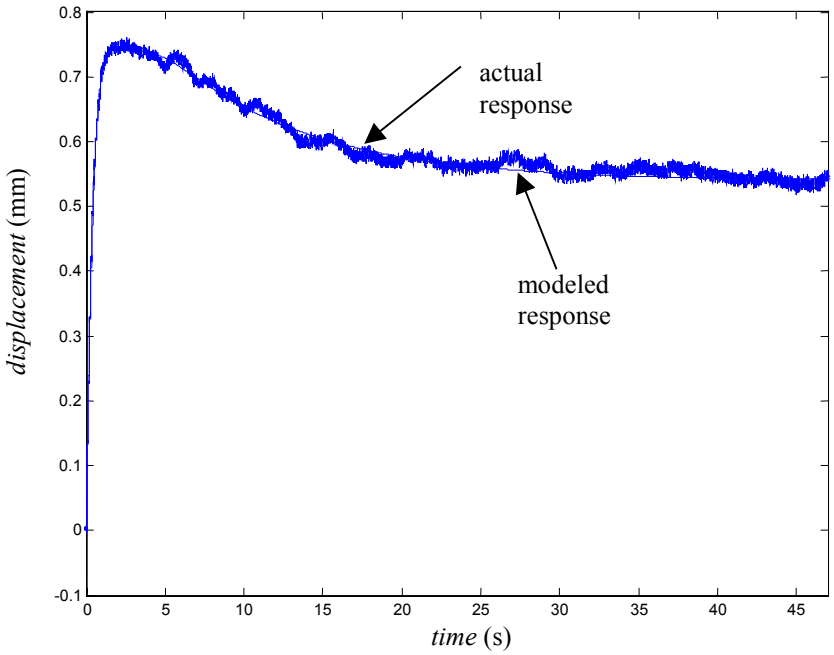

Figure 3.10. Actual versus modeled position response for model with complex parameters for strip *B*.

Compared to the force model developed the introduction of these exponential decay terms does not actually decrease the residual norm significantly. And we can see that even the model with only real terms account for the small rise time observed. But to maintain similarity with the force model developed, the model mentioned in (3.9) was used for IPMC strip *B*.

Taking the Laplace transformation of the output and input equations we get

$$Y(s) = \frac{y_1}{s+a} + \frac{y_2}{s+b} - y_3\left(\frac{1}{s-c} - \frac{1}{s-d}\right) + \frac{C_2}{s} \tag{3.10}$$

$$U(s) = \frac{stepvoltage}{s} \tag{3.11}$$

where 'step voltage' is the 1.2-V step input. After substituting the values of y_1, y_2, y_3, a, b, c, and d obtained previously and taking the ratio of $Y(s)$ and $U(s)$, the transfer function from the input voltage and the output force of the IPMC was found to be

$$\frac{Y(s)}{U(s)} = \frac{0.006895\,s^4 + 1.735\,s^3 + 3.034\,s^2 + 2.078\,s + 0.1332}{1.2\,s^4 + 4.467\,s^3 + 6.345s^2 + 3.256\,s + 0.296} \tag{3.12}$$

For IPMC strip *C*, a fourth-order model was developed by using similar methodology. Table 3.3 lists the different parameters identified for the IPMC strip *C* by using LSQCURVEFIT function. Figures 3.11–3.13 show the modeled response verses the actual response obtained for models developed on the basis of (3.7)–(3.9).

Table 3.3. Tabulation of the different parameters obtained from least square curve fitting method for IPMC strip *C*.

Eq. No.	y_1	y_2	y_3	a	b	c	d	Res-norm
1	1.1959	-	-	0.0924	-	-	-	140.4293
2	–1.9841	1.4143	-	3.3852	0.1082	-	-	20.9230
3	–1.9313+ 0.0003*i*	1.4155	–0.0507*i*	1.4155	0.1083	–5.0364+ 14.3825*i*	–5.0166– 14.3416*i*	20.8687

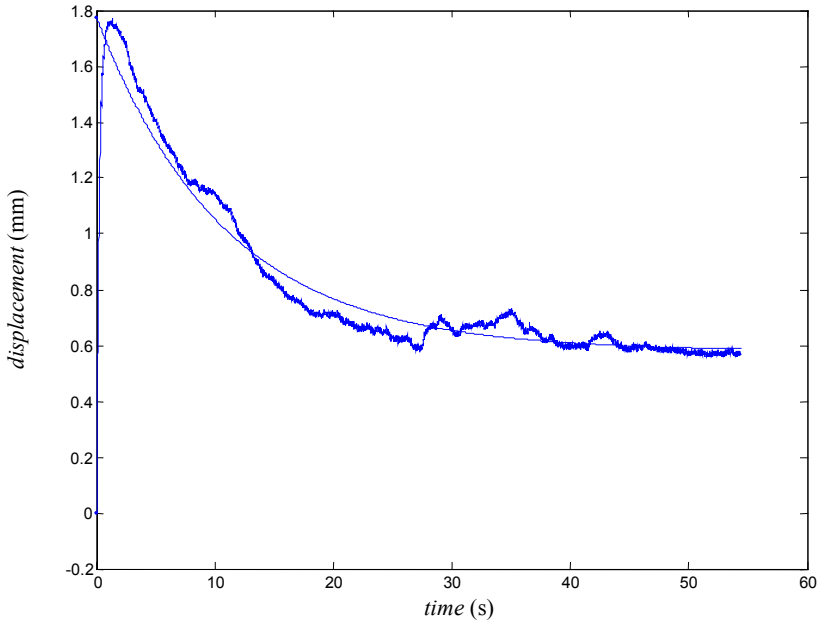

Figure 3.11. Actual versus modeled position response for model with one exponential decay term for strip *C*.

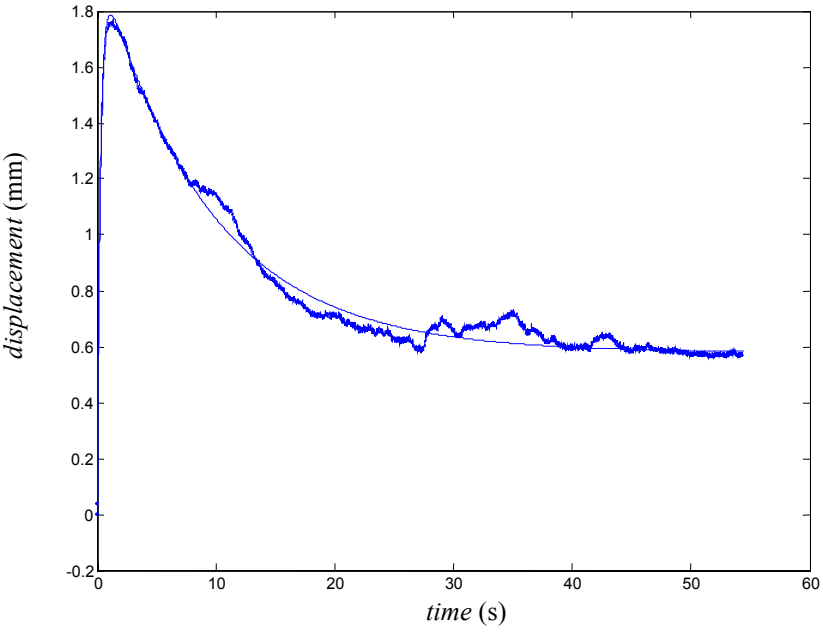

Figure 3.12. Actual versus modeled position response for model with two exponential decay terms for strip *C*.

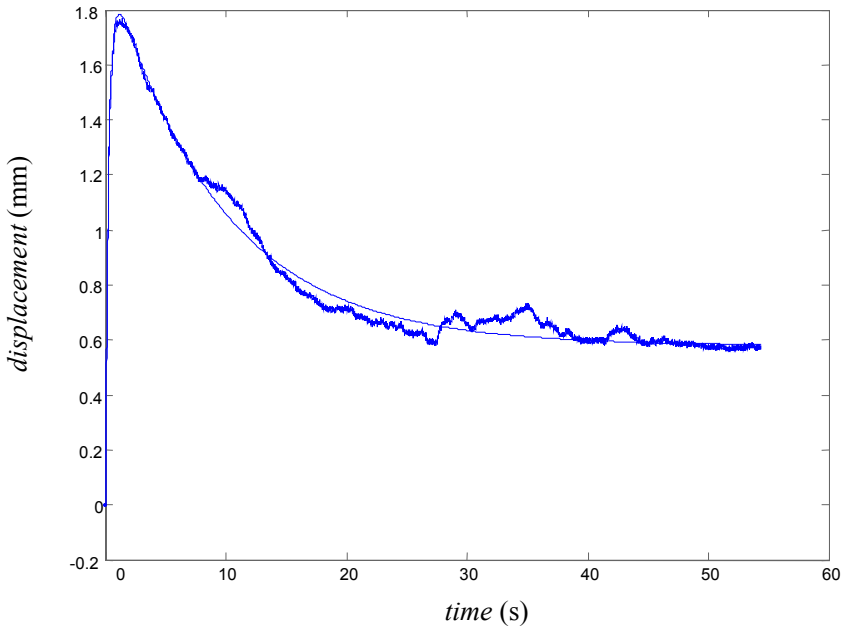

Figure 3.13. Actual versus modeled position response for model with complex parameters for strip *C*.

Again for the IPMC strip *C* taking the Laplace transformation of the output and input equations we get

$$Y(s) = \frac{y_1}{s+a} + \frac{y_2}{s+b} - y_3\left(\frac{1}{s-c} - \frac{1}{s-d}\right) + \frac{C_3}{s} \tag{3.13}$$

$$U(s) = \frac{step\ voltage}{s} \tag{3.14}$$

where 'C_3' is the steady state value which is 0.58 mm in this case and the 'step voltage' is the 1.2-V step input. After substituting the values of y_1, y_2, y_3, a, b, c, and d listed in Table 3.3 and taking the ratio of $Y(s)$ and $U(s)$, the transfer function from the input voltage and the output position of the IPMC was found to be

$$\frac{Y(s)}{U(s)} = \frac{0.06464\,s^4 + 5.647\,s^3 + 75.02\,s^2 + 1496s + 48.1}{1.2\,s^4 + 16.16\,s^3 + 319.5\,s^2 + 953.7s + 99.53} \tag{3.15}$$

In the case of IPMC strip *C* the difference in the squared residual norm when the step response is fitted to an equation having only 2 decaying terms (3.7) and equation having some additional complex parameters (3.8), is almost negligible. But in case of the force modeling part the square residual norm was affected to a large extent by the addition of complex parameters.

3.5 Conclusions for Chapter III

In this chapter by using least-square curve fitting methodology, the real step response force and position data were fitted to obtain fourth-order empirical models between voltage as an input and force and position as outputs. The presence of additional complex parameters in case of development of a position model did not affect the squared residual norm significantly as it did in case of development of a force model.

CHAPTER IV

CONTROL SYSTEM DESIGN

This chapter will describe in detail the design of a feedback control scheme, to meet the performance objectives. Based on the force model and the position model developed in Chapter III, controllers based on the lead-lag compensation technique were designed and implemented. The objectives were to precisely control the force generated by the IPMC and the tip displacement of the IPMC.

4.1 Force Controller Development

In Chapter III, we developed an empirical fourth-order model between voltage input and force output for the IPMC strip *B* of dimensions 23 mm × 3.9 mm × 0.16 mm. The transfer function for this model is

$$\frac{Y(s)}{U(s)} = -\frac{0.0002365\,s^4 + 0.002947\,s^3 + 0.004299\,s^2 + 0.002266\,s + 0.0002065}{1.2\,s^4 + 4.577\,s^3 + 6.14\,s^2 + 3.314\,s + 0.6194} \qquad (4.1)$$

As mentioned in Chapter III, the negative sign is due to the application of a –1.2 V step input. The open-loop Bode plot for this model is shown in Figure 4.1. The control objectives were to reduce the per-cent overshoot, to track the commanded input force, and to decrease the settling time. Initially a lag compensator was developed. A free pole was placed at the origin to eliminate the steady-state error [31]. The matlab tool ‘rltool’ was used for controller design. Figure 4.2 shows the control loop used for force controller development. It was recommended that the voltage applied to the IPMC strip be on the

order of 1-3 V. Due to the limited quantity of the material available, the voltage applied to the IPMC strip was limited to ±2 V to prevent any damage. The saturation block shown in the Figure 4.2 was used to achieve this voltage cutoff. The lag compensator initially designed was

$$G_c(s) = -236 \times \left(\frac{s + 239}{s} \right) \tag{4.2}$$

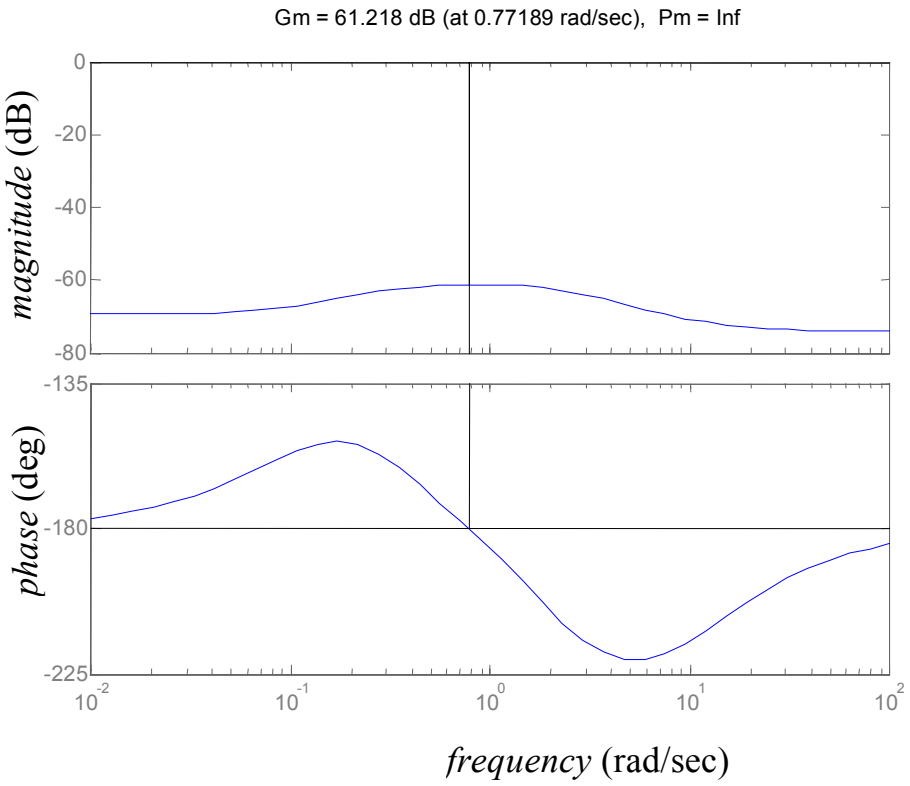

Figure 4.1. Open-loop Bode plot of the force model of IPMC.

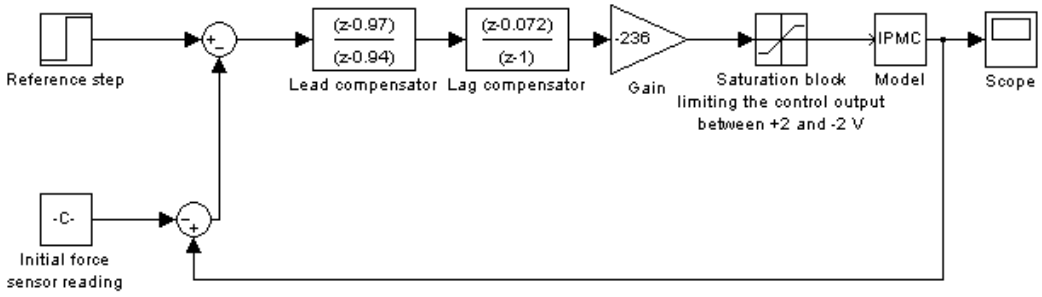

Figure 4.2. Force control loop.

Figure 4.3 shows the loop transfer function Bode plot for this closed-loop system with the lag compensator given in (4.2). The phase margin was 62.297° at a crossover frequency of 2.2 Hz (13.863 rad/sec). The closed-loop Bode plot of the system with lag compensator is shown in Figure 4.4.

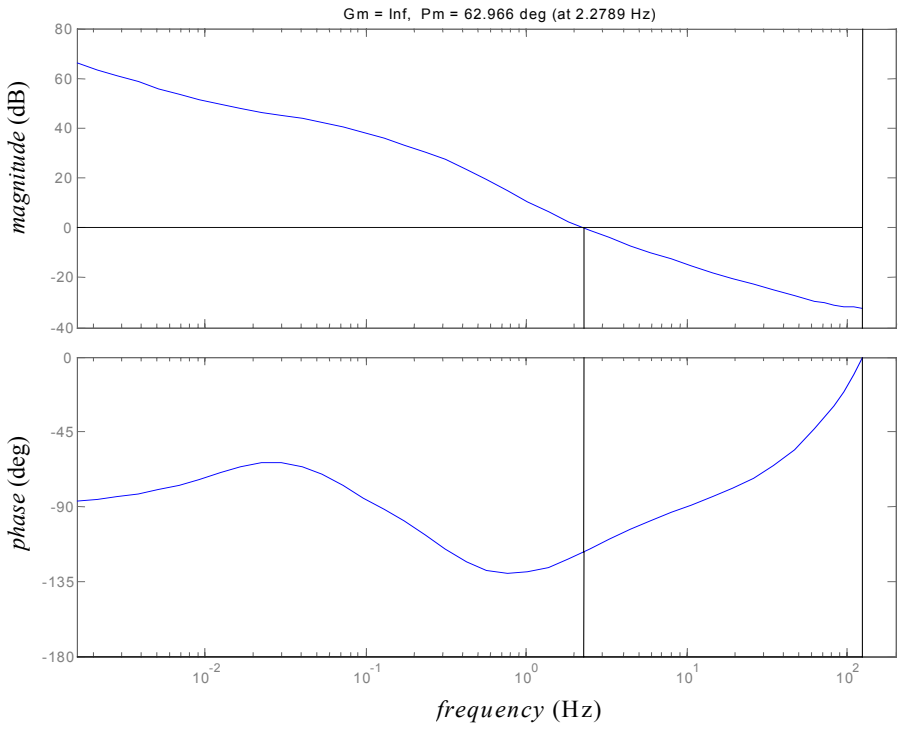

Figure 4.3. Loop transfer Bode plot of the system with lag compensator.

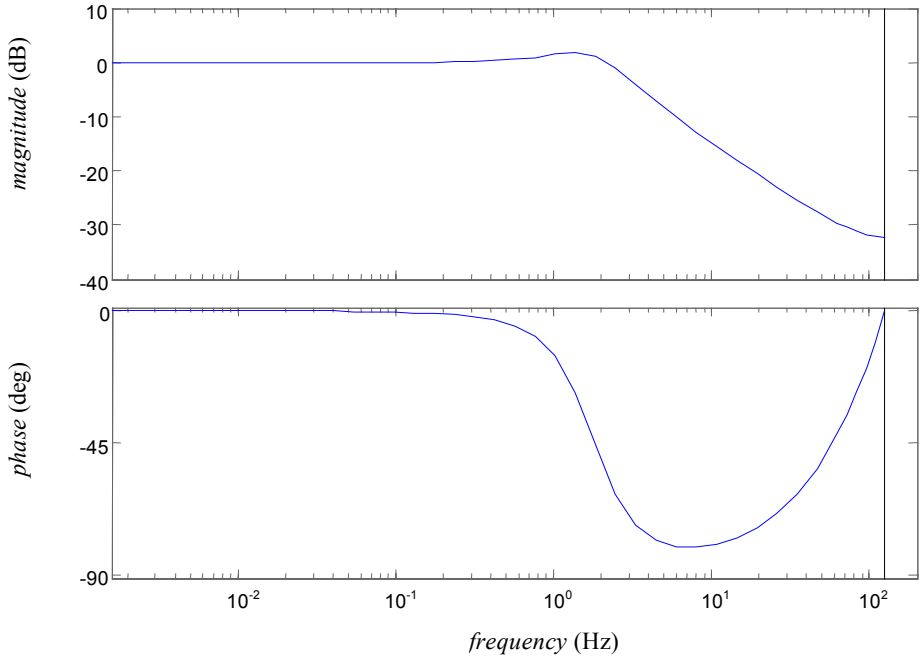

Figure 4.4. Closed-loop Bode plot of the system with lag-compensator.

The controller developed in the *s*-domain was converted into the *z*-domain, by using the zero order hold method and is given in (4.3).

$$G_C(z) = -236 \times \frac{(z - 0.0432)}{(z - 1)} \tag{4.3}$$

This digital lag controller was implemented at a sampling rate of 250 Hz, by using the dSPACE DSP (digital signal processing) board 1102. Figure 4.5 shows a schematic of the setup used for real-time closed-loop control. The control loop was first constructed in Simulink. The Simulink model was then built using Real Time Workshop, which also loaded the real-time code on the DSP of 1102 board. The virtual interface was built in ControlDesk.

As a contact-type sensor (GM2 load cell) was used, there was some initial force created due to wet stiction between IPMC and the sensor tip. This force was almost a magnitude higher than the actual force generated by IPMC. This initial stiction force was problematic in real-time controller implementation. When the control action was started, the error was very high due to the initial sensor reading being an magnitude higher than the targeted force value. Due to the presence of the integrator in the control loop, this error was integrated and it increased quite rapidly. The controller outputted a voltage higher than + 2 V or lower than –2 V at time t = 0 making the actuator already be saturated. Due to the limitation on the voltage swing of the controller, this led to no control action.

To address this problem the following approaches could be taken:

- Resetting the precision load cell to zero at the start of the control action. This would involve offsetting the load cell output by manually turning the zero-adjustment knob present on the signal amplifier. This method does not guarantee zero value, as the precision load cell used in the experiment was very sensitive to small changes and gave an analog output. Thus everytime it would be difficult to ascertain the output is exactly zero.
- Subtracting a force comparable to the initial force, from the sensor reading at all times. This reduces the magnitude of the force being fed back in the control loop to that actually developed by the IPMC.

The second method was utilized in the control loop. From Figure 3.1 the initial force before the step commences is nearly 4 mN, hence constant force 4 mN was subtracted at all times from the sensor reading. And this lead to a successful operation of

the control scheme. Figure 4.2 shows the residual force of 4 mN being subtracted at all times from the sensor reading. This actually is an offline resetting of the sensor to a known value.

After implementing this controller, the IPMC strip could follow the commanded step value, but the objectives of decreasing the settling time and the per-cent overshoot were not achieved. Figure 4.6 shows the actual 0.4-mN step response obtained after implementing this controller.

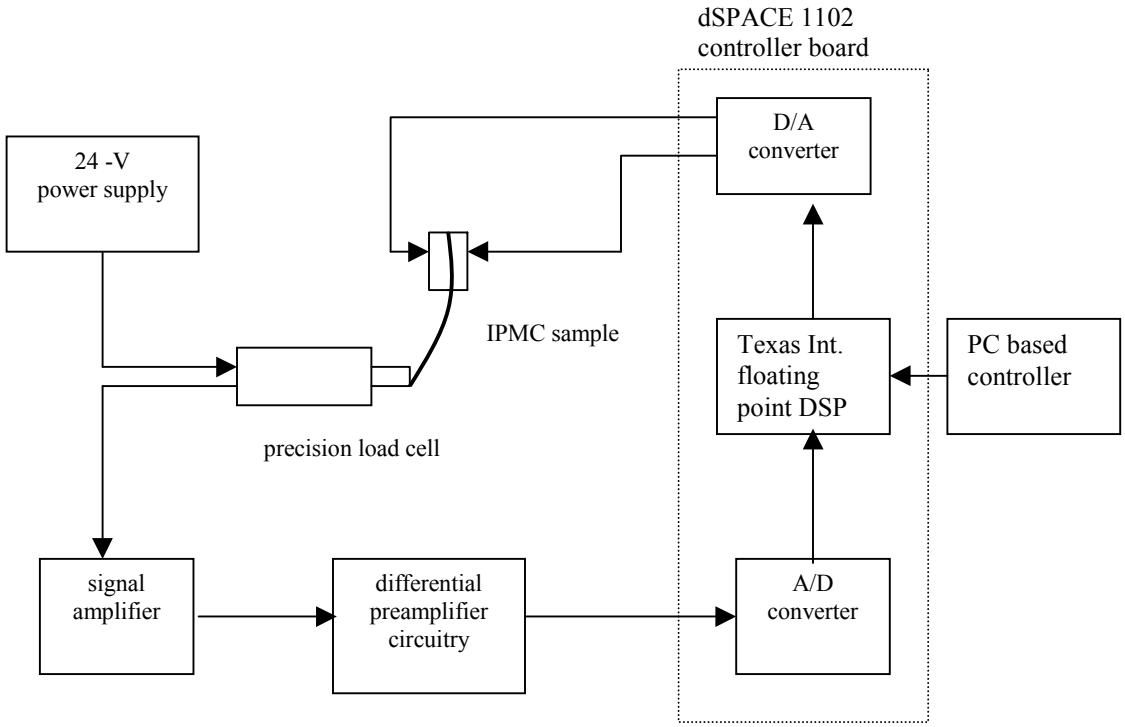

Figure 4.5. Schematic of the setup used for real time force control.

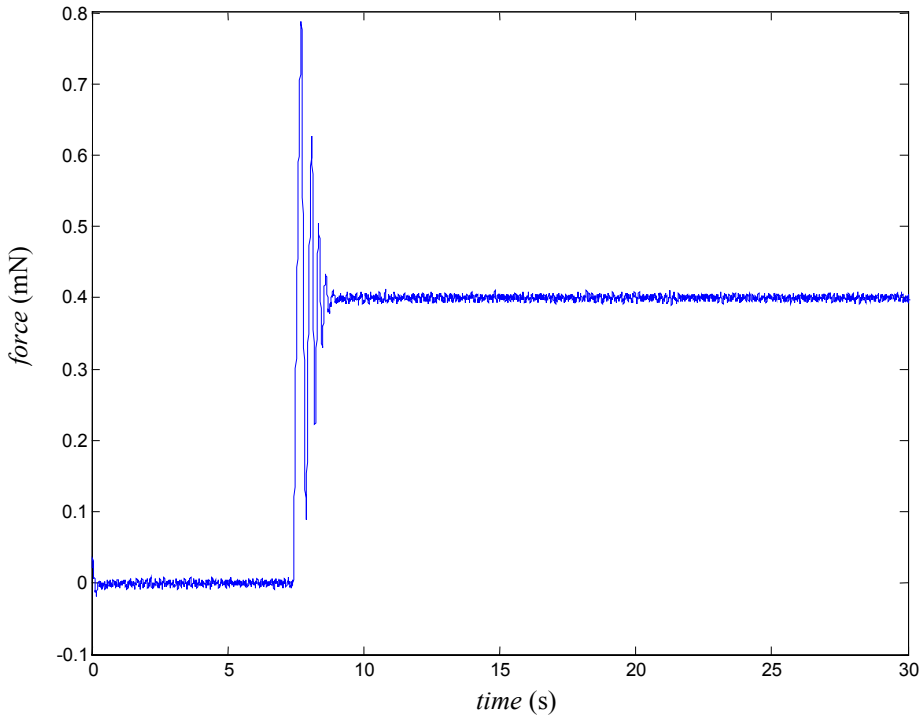

Figure 4.6. Closed-loop response of IPMC to 0.4 mN step input after implementing the lag compensator.

A lead compensator was then designed based on the lag-compensator already designed. With this new lead-lag compensator the phase margin was increased to 80.714° at a crossover frequency of 1.31 Hz (8.2838 rad/sec). The new lead-lag compensator is given below.

$$G_C(s) = -236 \times \frac{(s+239)(s+7.5)}{s(s+22.5)} \tag{4.4}$$

Figure 4.7 shows the loop transfer function Bode plot after incorporating the new lead-lag compensator. The controller specified by (4.4) was converted into a z-domain controller by using the zero order hold method. The z-domain controller is given below in (4.5).

$$G_C(z) = -236 \times \frac{(z-0.072)(z-0.97)}{(z-1)(z-0.914)} \tag{4.5}$$

As mentioned previously, the digital lead-lag controller was implemented at a sampling frequency of 250 Hz. Figure 4.8 shows the closed-loop Bode plot of the new closed-loop system. The closed-loop step response to 0.4 mN step input after implementing the lead-lag compensator is shown in Figure 4.9. The settling time was now reduced to 1.5 s from nearly 10 s in open loop, while the percent overshoot was decreased to 30% from about 131.62% in open loop. The controller output (Figure 4.10) shows a drift in the voltage. The reason for this drift in voltage may be attributed to the behavior of IPMC as a parallel-plate capacitor. From Figure 4.10 it is also observed that even after reaching the steady state value the controller output is not a straight line. The reason for this may be related to the response of IPMC to a change in voltage and not a constant-voltage. Hence even after reaching the commanded force the controller has to output changing voltage to maintain that force at the specified value.

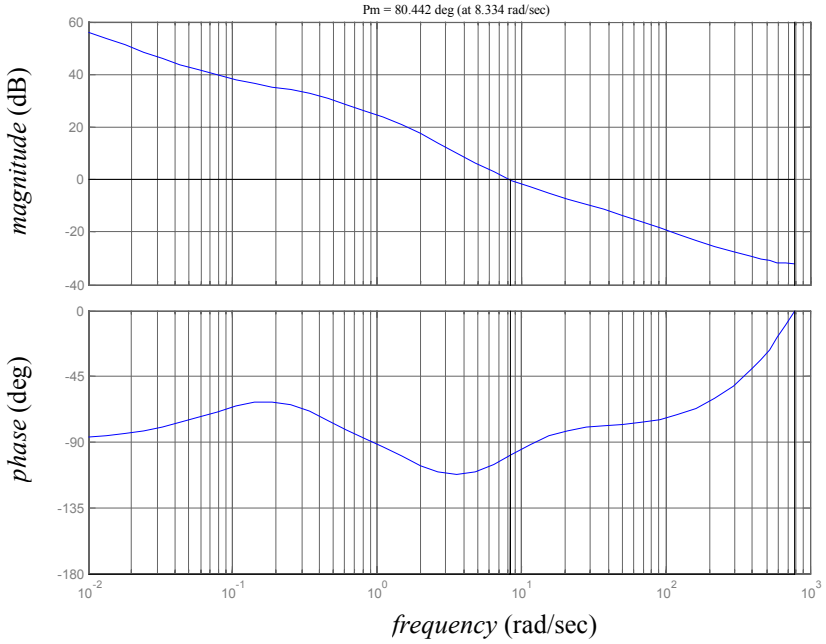

Figure 4.7. Bode magnitude and phase plots for the loop transfer function with the lead-lag controller.

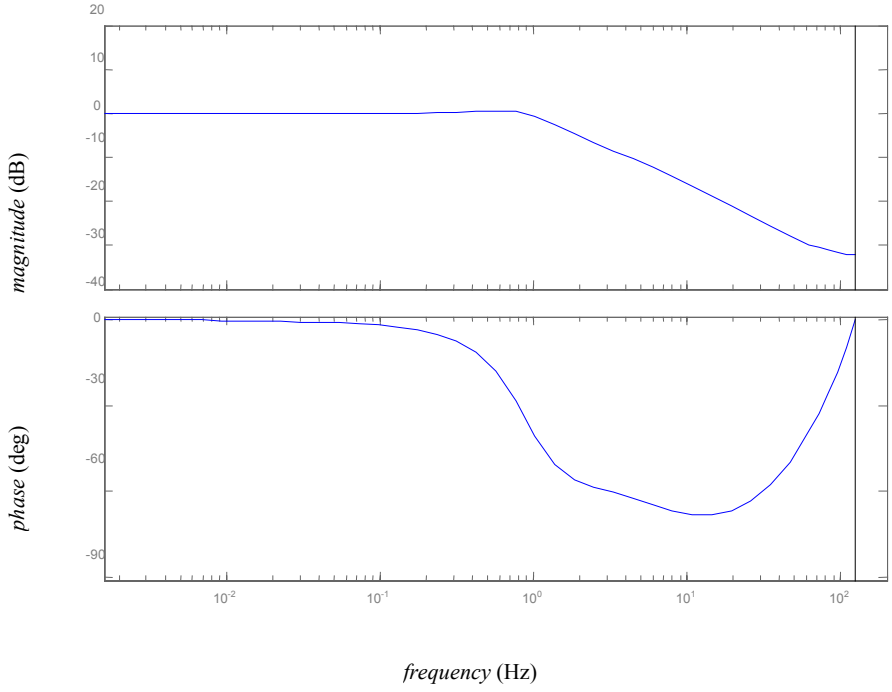

Figure 4.8 Closed-loop Bode plot of system with the lead-lag controller.

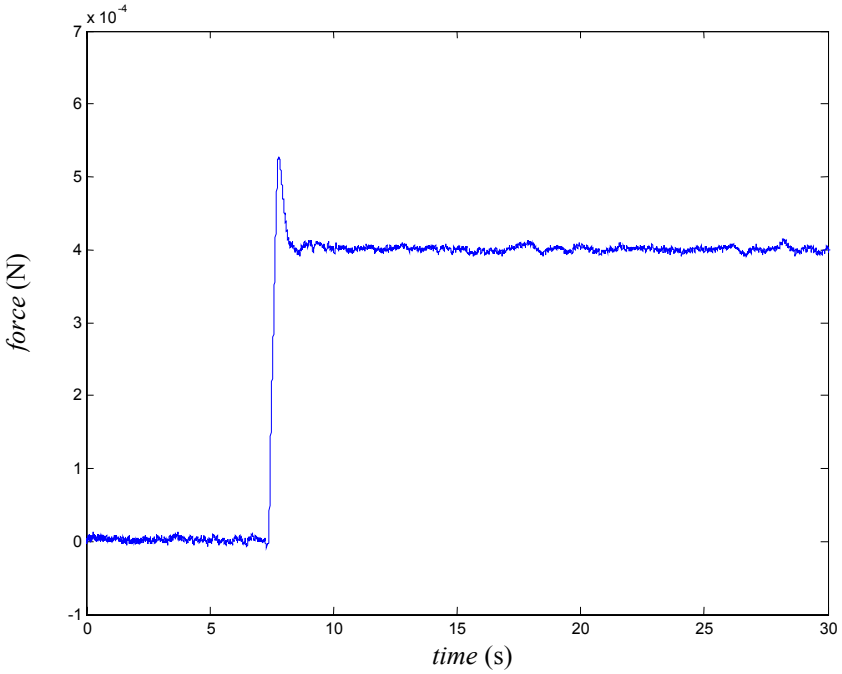

Figure 4.9. Closed-loop step response to 0.4 mN step input after implementation of the lead-lag compensator.

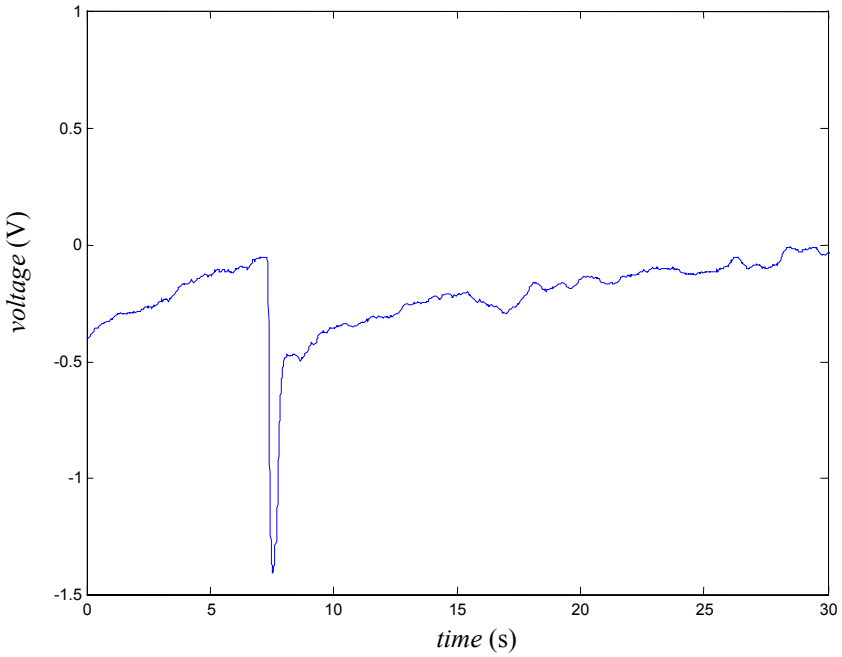

Figure 4.10. Controller output for the 0.4 mN closed-loop step response.

4.2 Position Controller Design

After the control of force produced by IPMC was achieved, the control of tip displacement was the next course of action. The model developed empirically between voltage input and position output for IPMC strip *C* in Chapter III was used to develop different control strategies for position control. The model is again

$$\frac{Y(s)}{U(s)} = \frac{0.06464\,s^4 + 5.647\,s^3 + 75.02\,s^2 + 1496s + 48.1}{1.2\,s^4 + 16.16\,s^3 + 319.5\,s^2 + 953.7s + 99.53} \quad . \tag{4.6}$$

The control objective in this case was, decreasing the per-cent overshoot and the settling time present in the open-loop response of IPMC. The second objective was to achieve position tracking. The open-loop Bode plot of the model given in (4.6) is shown in Figure 4.11 below. The open-loop Bode plot shows a phase margin of 129.67° at a crossover frequency of 0.691 Hz.

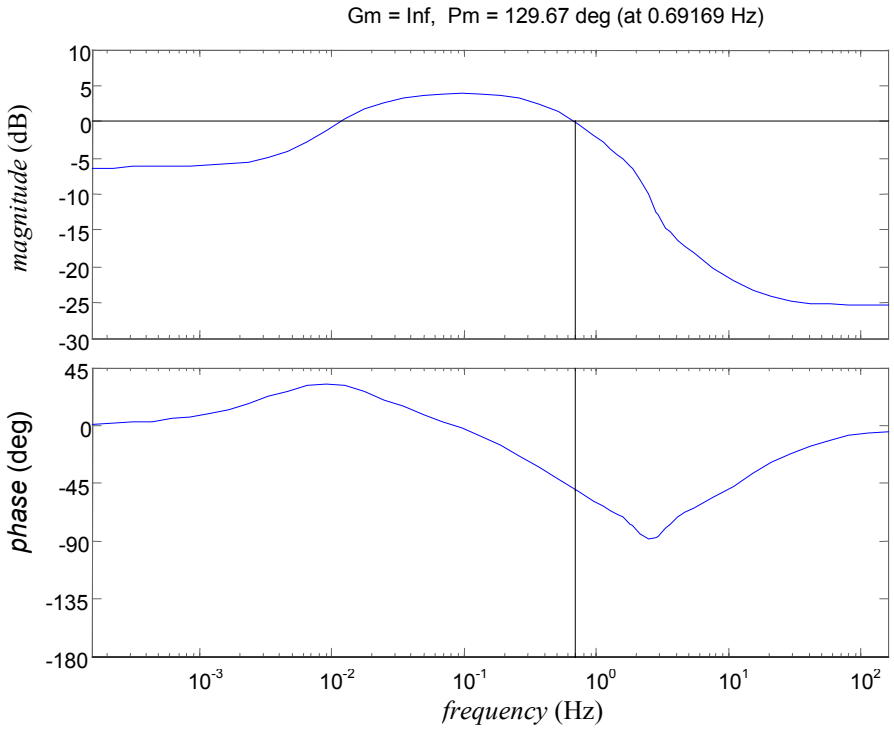

Figure 4.11. Open-loop Bode plot of the position model.

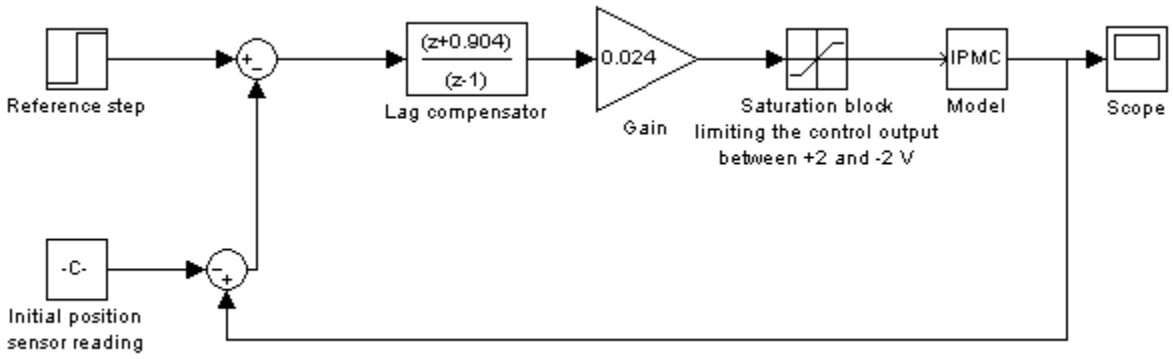

Figure 4.12. Control-loop for position control

A lag-compensator was designed to meet the control objectives. Matlab tool 'rltool' was extensively used to design the compensator. Figure 4.12 shows the control

loop developed for precision position control. The compensator, which was designed, is given below

$$G_c(s) = 6 \times \frac{(s + 476)}{s} \tag{4.7}$$

Figure 4.13 shows the loop transmission Bode plot with this compensator. The phase margin was 34.5° at a crossover frequency of 0.84241 Hz. Figure 4.14 shows the closed-loop Bode plot.

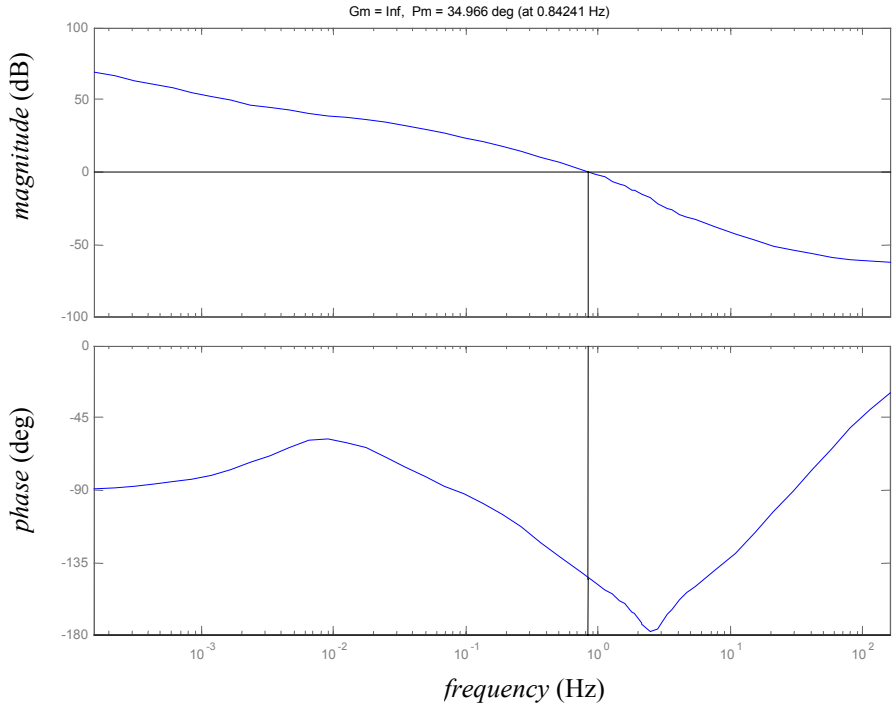

Figure 4.13. Bode magnitude and phase plots for the loop transfer function with the lag controller.

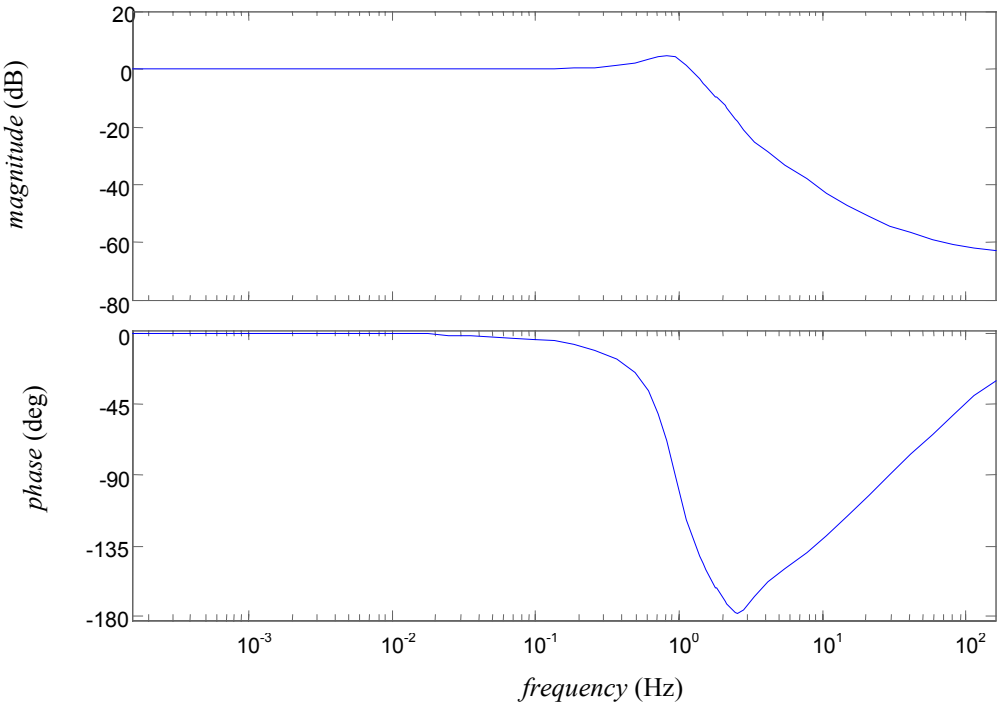

Figure 4.14. Bode magnitude and phase plots for the closed-loop system with the lag-controller.

The controller mentioned in (4.7) was converted to *z*-domain by using zero order hold method. The *z*-domain controller is given below

$$G_C(z) = 0.024 \times \frac{(z + 0.904)}{(z - 1)} \tag{4.8}$$

This digital controller was implemented at a sampling frequency of 250 Hz. Figure 4.15 shows the schematic of the experimental setup used in real time controller implementation. Figure 4.16 shows the closed loop position response to a 0.4 mm commanded value. From the figure we can see that the percent overshoot was decreased to 20% from 205.34% in open loop, while the settling time was decreased to 1 s from nearly 27 s in open loop. The controller output voltage captured after the saturation block

for this closed-loop position response is shown in Figure 4.17. A drift in the controller output is also observed in this case.

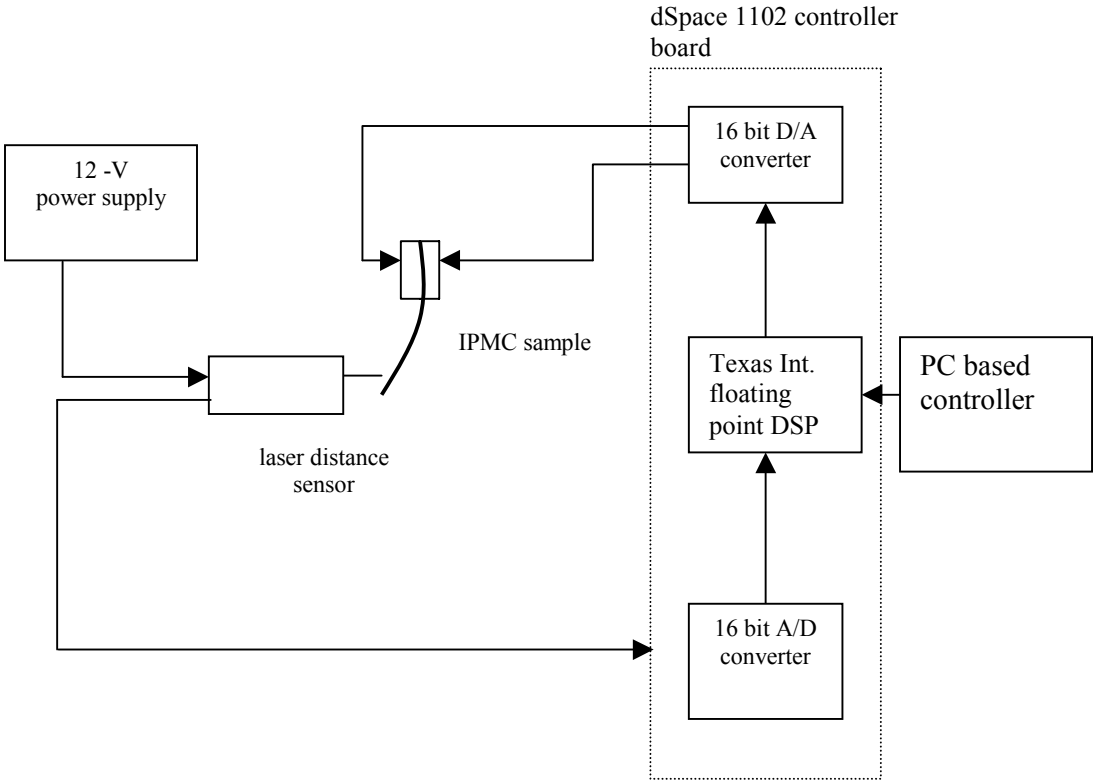

Figure 4.15. Schematic of the setup used for real-time position control.

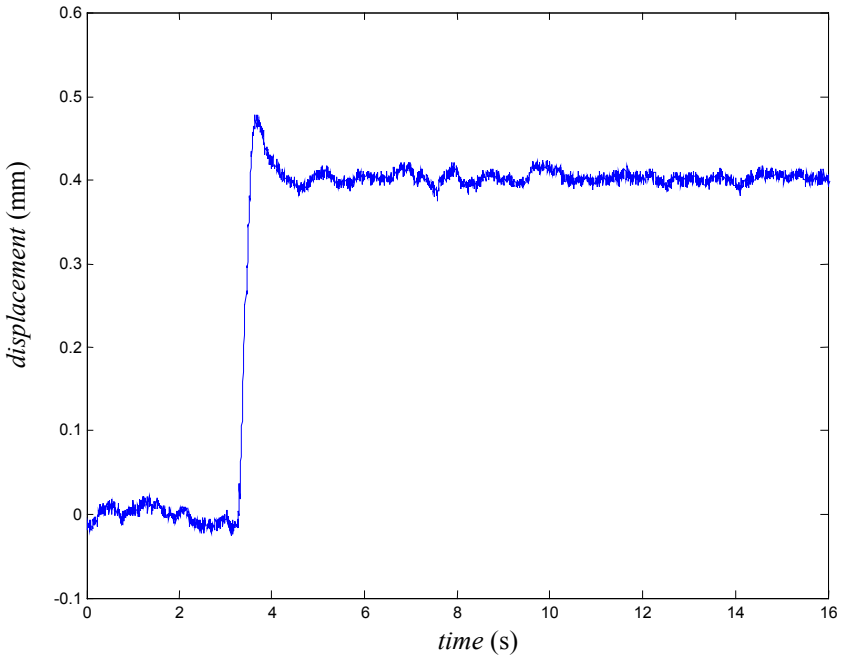

Figure 4.16. Closed-loop position response of IPMC strip to 0.4-mm position input.

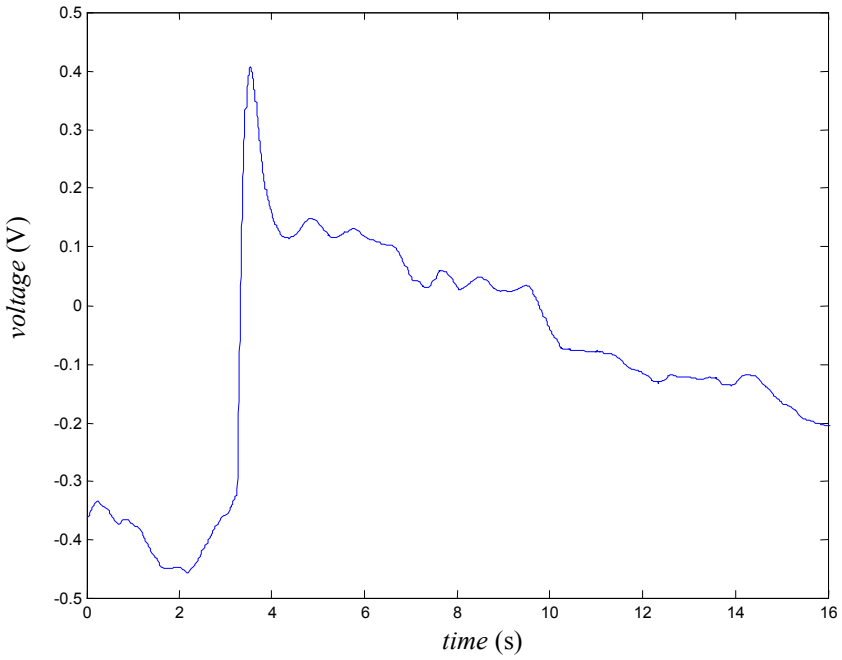

Figure 4.17. Controller output for the 0.4-mm closed-loop response.

4.3 Conclusions for Chapter IV

In this Chapter, a feedback controller for the control of the force produced by IPMC strip *B* has been developed and successfully implemented. The closed-loop settling time was reduced to 1.5 s from about 10 s in open loop, while the percent overshoot was decreased to 30% from nearly 131.62% in open loop. The IPMC strip also followed the commanded force step.

In the second part, a feedback controller for the control of the tip displacement of IPMC strip *C* has been developed and successfully implemented. In this case the closed-loop settling time was reduced to 1 s from 27 s in open loop, while the percent overshoot was decreased to 20% from 205.34 % in open loop. The IPMC strip also could follow the commanded position step.

CHAPTER V

EXPERIMENTAL RESULTS

In this Chapter experimental results obtained after implementing the closed-loop control scheme described in Chapter IV will be shown. Micro-scale force control and position control has been achieved and will be demonstrated. The different performance characteristics of the IPMC achieved in closed loop such as speed, holding capacity without rehydration, and actuator saturation effects will be described.

5.1 Closed-Loop Force Responses

After implementing the control scheme described in Chapter IV on IPMC strip *B*, the primary objective was to achieve micro-scale force control. Initially different step responses were commanded to examine whether the IPMC response followed the commanded values. Figures 5.1–5.3 show the closed-loop force responses to 100 μN, 20 μN, 50 μN commanded step values respectively. The IPMC strip was able to follow the commanded force quite well as long as the controller output is within the permitted values of ±2 V.

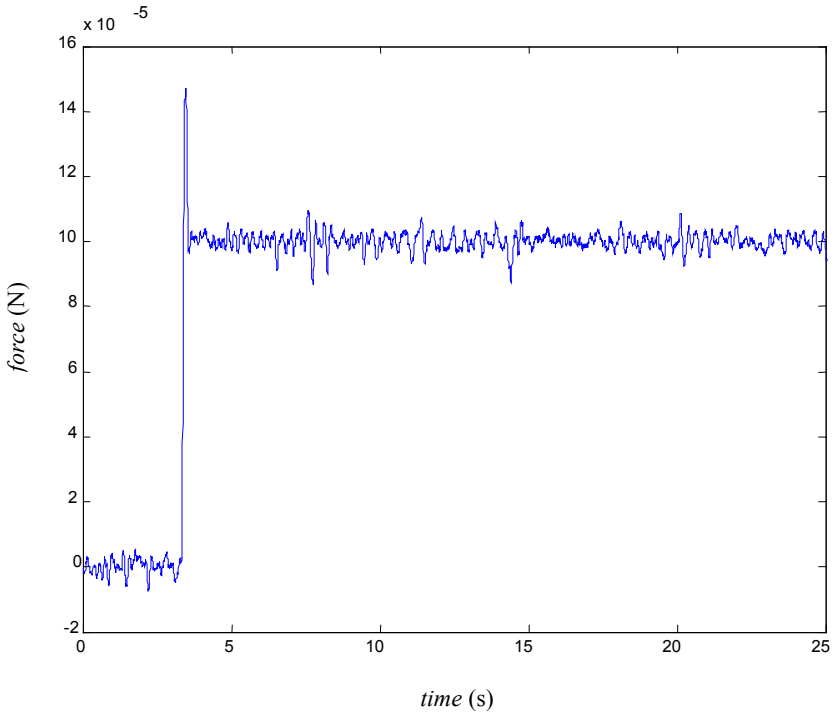

Figure 5.1 Closed-loop response to 100 μN step input.

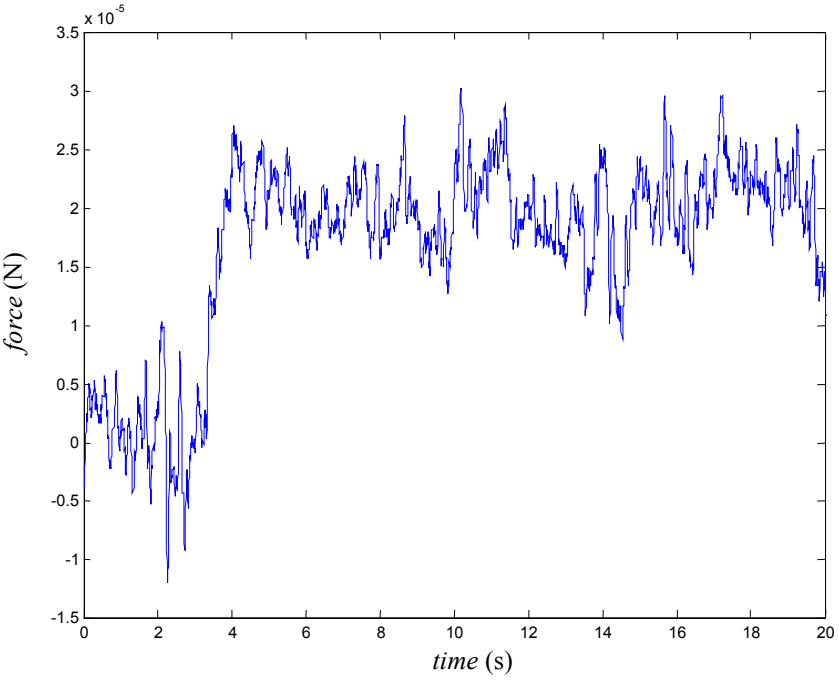

Figure 5.2. Closed-loop response to 20 μN step input.

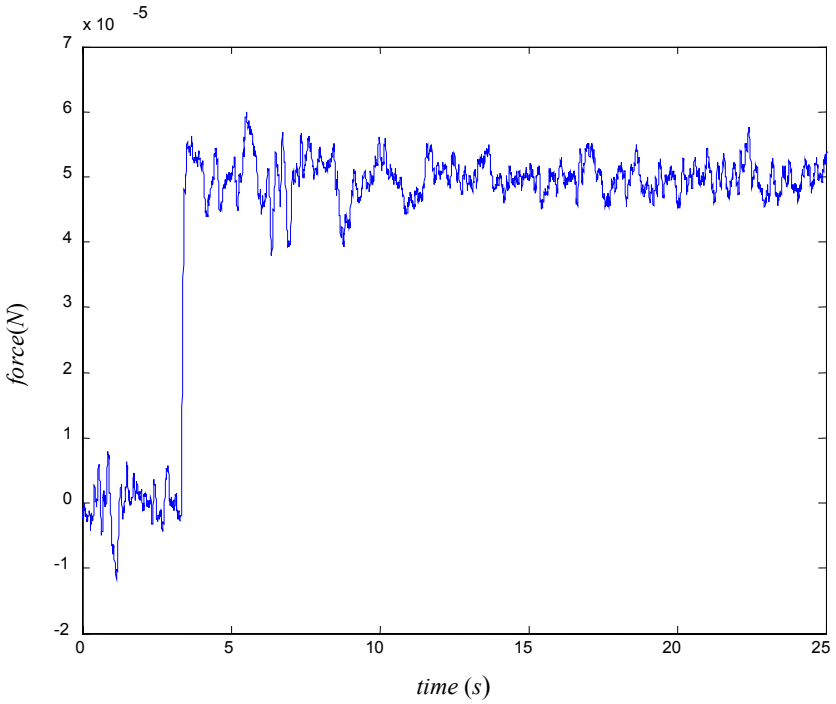

Figure 5.3. Closed-loop response to 50 μN step input.

5.1.1 Micro-Scale Force Control

In Chapter I the importance of micro-scale force control is stated. To use IPMC in next generation, micro or nano-manipulation devices, micro-scale control of force produced by IPMC becomes of primary importance. From the point of view of manipulation micro-scale force control can answer issues like

- Limiting the applied force on micro-objects thus preventing object damage.
- Reduction in adhesion forces between the IPMC fingers in a manipulator and micro-objects.

Figures 5.4–5.5 show closed-loop force control with the step sizes of 8 μN and 4 μN, respectively. The 8 μN step response showed a noise level of 10 μN peak to peak while the 4 μN step response showed a noise level of 4 μN peak to peak. The main reason for

this difference in the noise level was better suppression of the noise due to floor vibration observed at 18.6 Hz. Figures 5.6–5.7 show the frequency response of the 8 μN and 4 μN step responses, respectively. It is observed from the Figures 5.6–5.7 that the magnitude of the 18.6 Hz noise is reduced in case of the 4 μN step response. The experimental setup as mentioned previously was mounted on a vibration isolation table. When the 8 μN step response was taken, the air pressure to the table was not set at a value to obtain the maximum attenuation of the floor vibration noise. When the 4 μN step response was taken, the air pressure was set at a value, which resulted in higher attenuation of the noise due to floor vibration. This 4-μN force control was the finest force achieved with this IPMC strip. The force resolution was therefore 4 μN with a force noise of 4 μN peak to peak or 0.904 μN rms. The sources of this noise can be

- The sensor noise and the ADC electronic noise.
- As discussed previously although the contribution to the noise due to the floor vibration was reduced significantly, this 18 Hz noise was not completely eliminated
- This limit on the resolution may also be attributed due to the internal electro-chemical-mechanical behavior of IPMC.

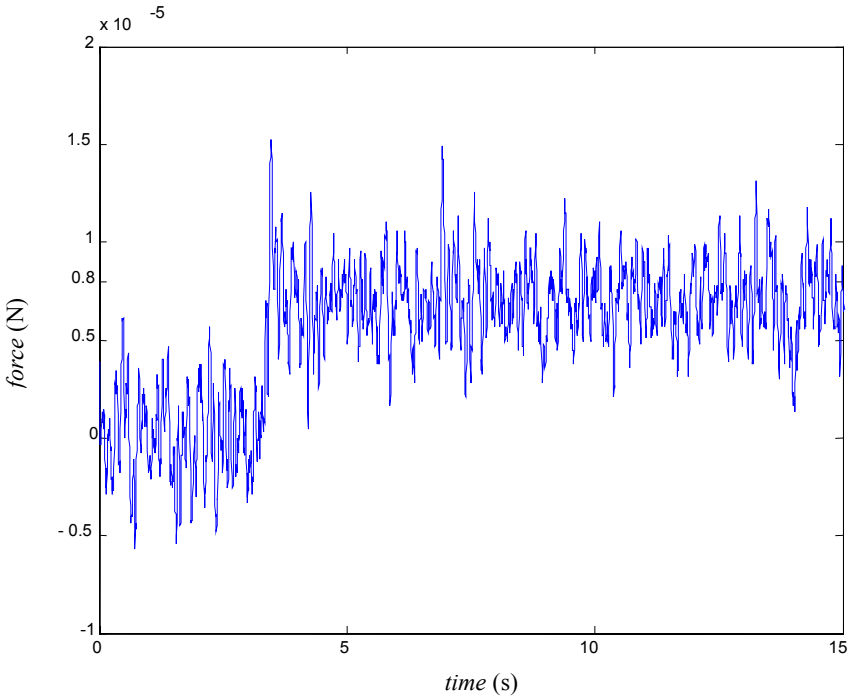

Figure 5.4. Closed-loop response to 8 μN step input.

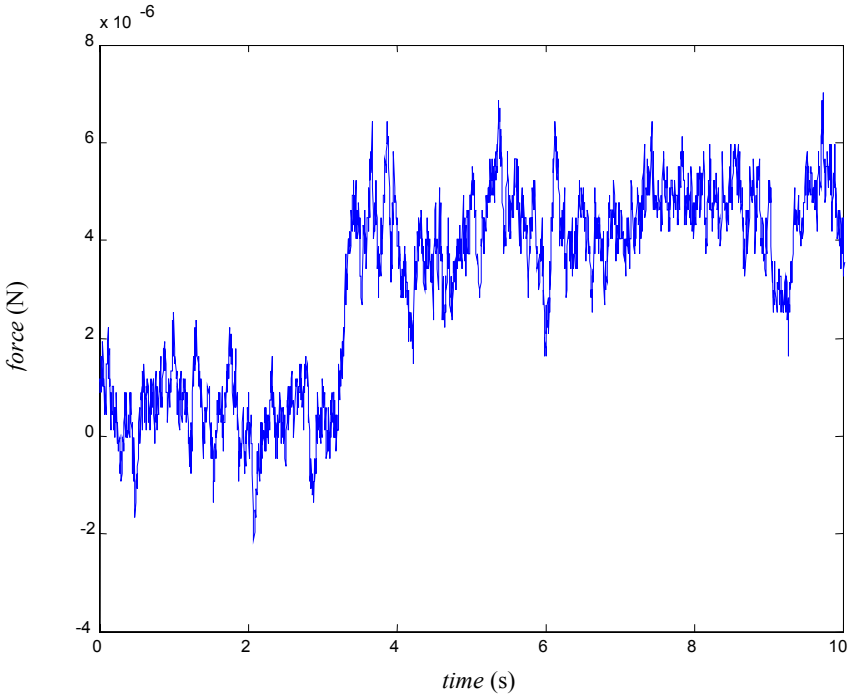

Figure 5.5. Closed-loop response to 4 μN step input.

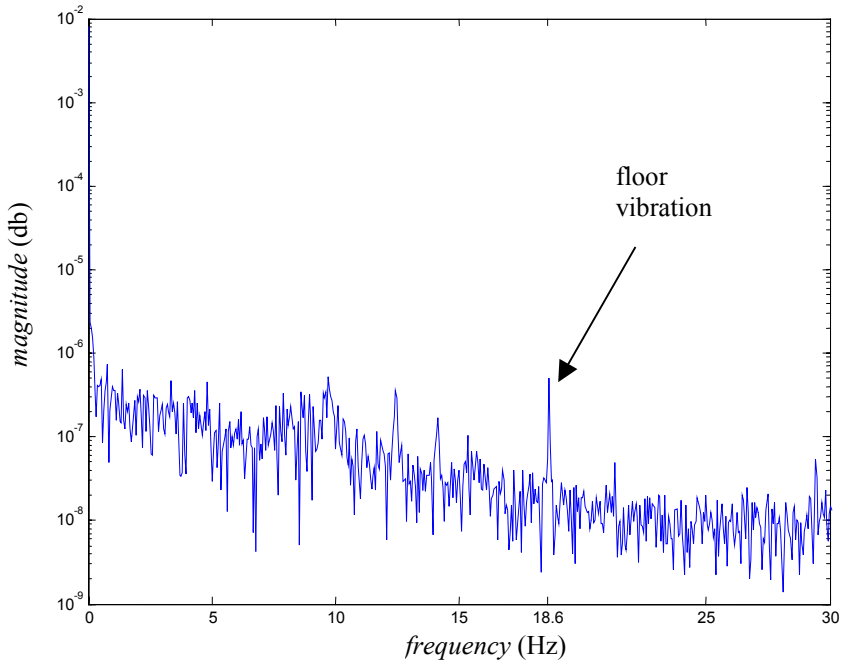

Figure 5.6. Frequency response of the 8 μN step.

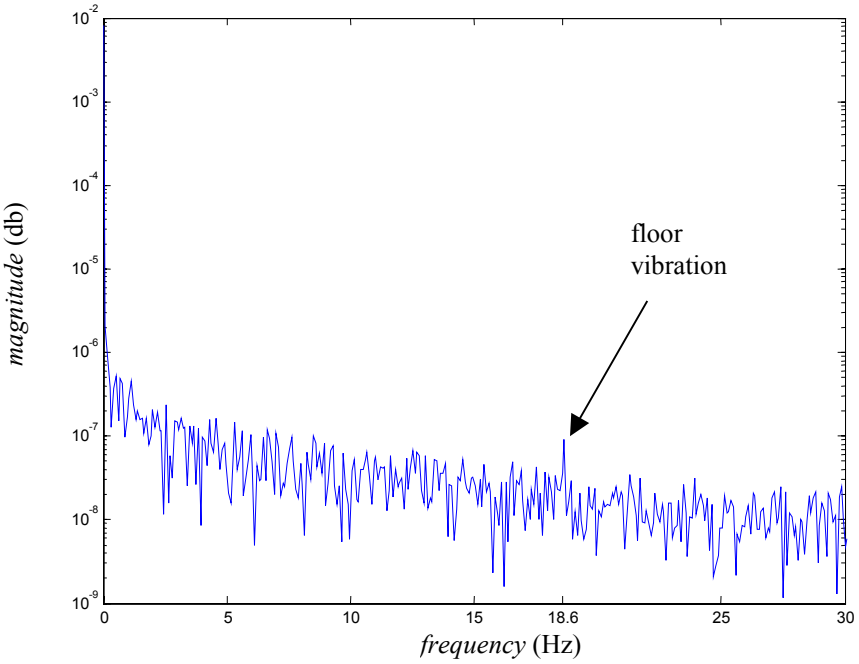

Figure 5.7. Frequency response of the 4 μN step.

5.1.2 Force Capability of IPMC

In the previous section we discuss the force resolution. The maximum force, which was achieved by using the IPMC strip in closed loop, was 1 mN. Figure 5.8 shows the closed-loop 1-mN force response, while Figure 5.9 shows the control voltage required to achieve the force control. The most significant limitation above 1 mN can be attributed to the limited control voltage swing within +2 V and –2 V. The second limitation can be the actual physical limitation of the force generation capability of IPMC. Thus the force generation capability of IPMC is very small as compared to other smart actuators like piezoelectric actuators. However the dynamic force range of 4 μN to 1 mN is large enough for high-resolution force requirement applications such as micro-scale positioning operations and bio-medical micro-surgery devices for which IPMC could be a driving actuator.

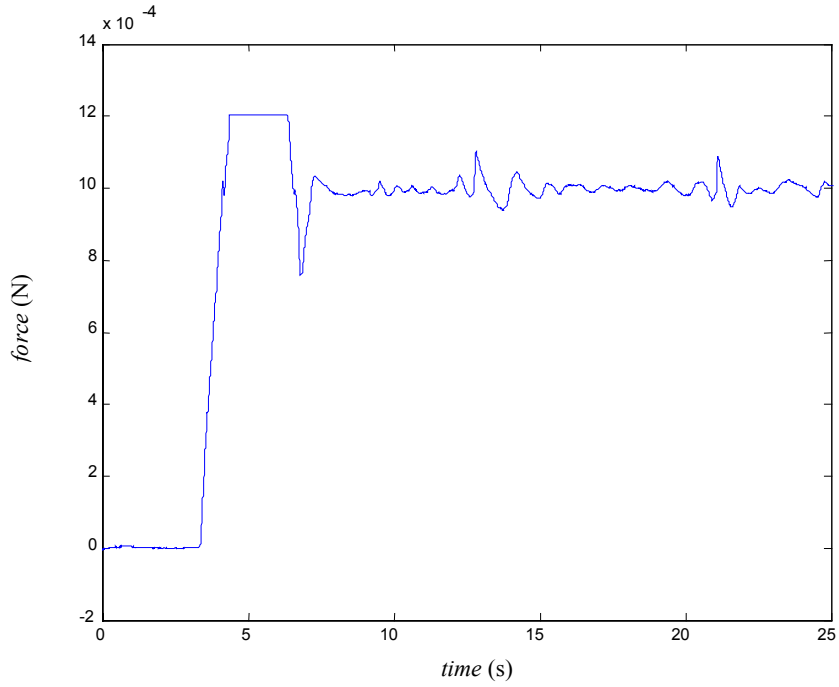

Figure 5.8. Closed-loop response to 1 mN step input.

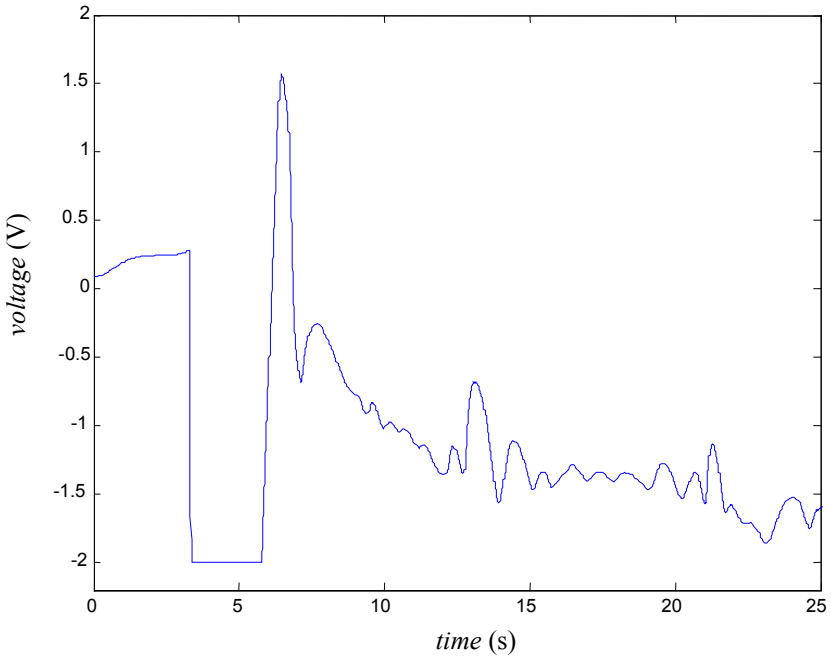

Figure 5.9. Controller output to achieve 1 mN step output.

5.1.3 More Experimental Results

Figure 5.10 shows the closed-loop response to a sine wave of amplitude 100 μN and frequency of 0.5 Hz. The IPMC strip follows the commanded sine wave very well. A closed-loop response of the IPMC strip to a sine wave of 5 Hz frequency was also taken. From the response shown in Figure 5.11 we see an attenuation of 11 dB in the amplitude. Revisiting the closed-loop Bode plot shown in Figure 4.8, we see that at 5 Hz the attenuation was 11.4 dB, which is very close to the actual attenuation obtained. This attenuation was due to the low bandwidth of the close loop system, which was limited at 1.3 Hz due to the resonance behavior of the polymer.

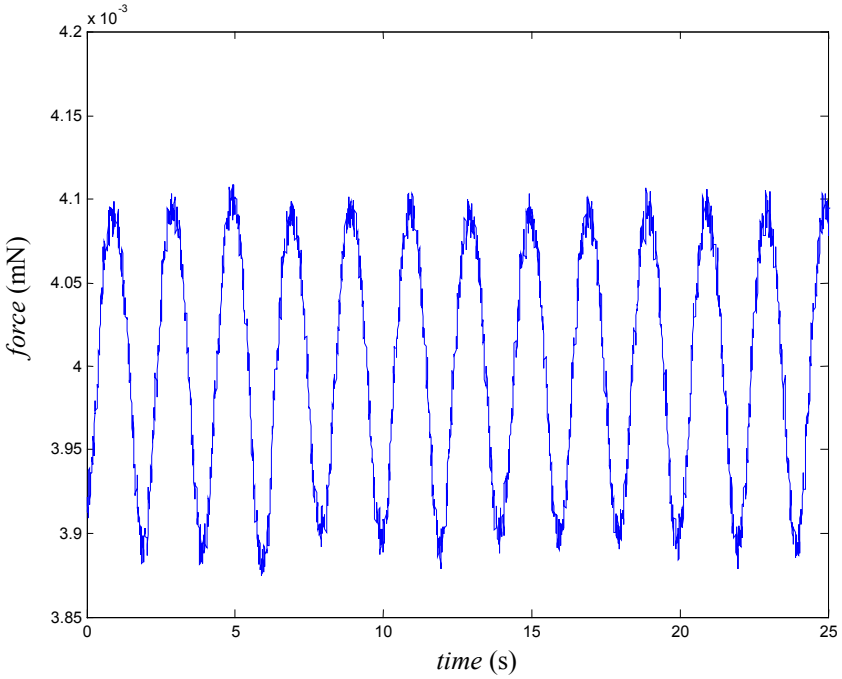

Figure 5.10. Closed-loop response to a sine wave of amplitude 100μN and frequency 0.5 Hz.

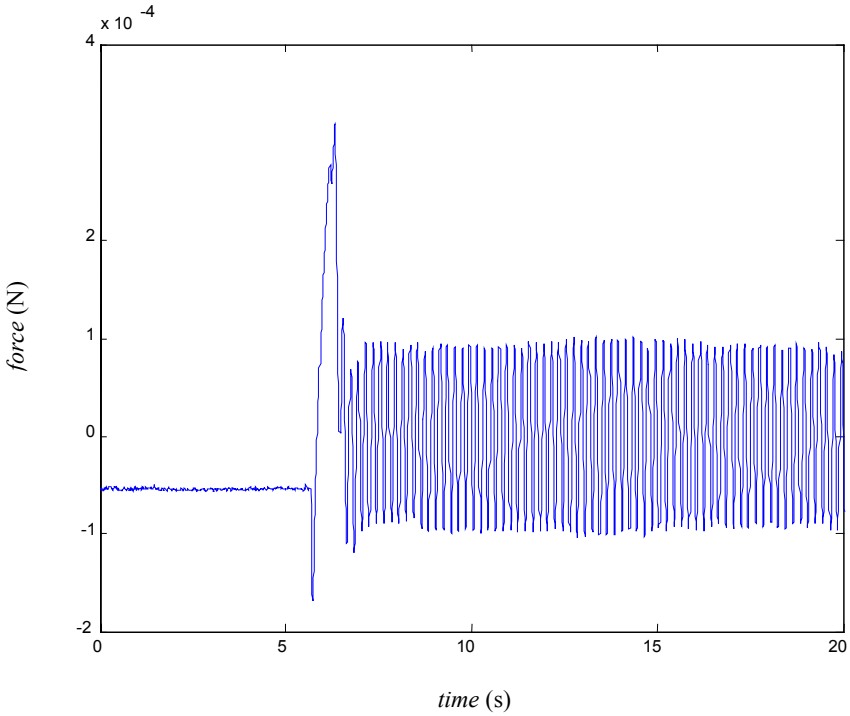

Figure 5.11. Closed-loop response to a sine wave of amplitude 300 μN and 5 Hz frequency.

To demonstrate the capabilities of the IPMC strip to follow several force trajectories under closed-loop control, many responses were taken to different commanded values. Figure 5.12 shows the stair-case wave response of IPMC to 0.01 mN step increment. Figure 5.13 shows the square wave response of IPMC to 0.01 mN amplitude and 0.5 Hz frequency.

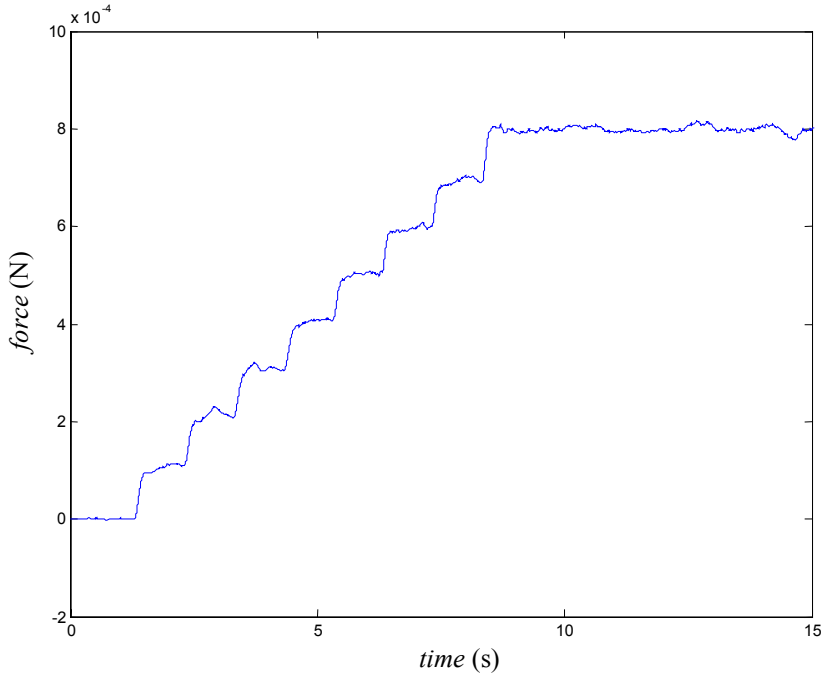

Figure 5.12. Closed-loop response to a staircase wave of step 100 μN and period 0.8 s.

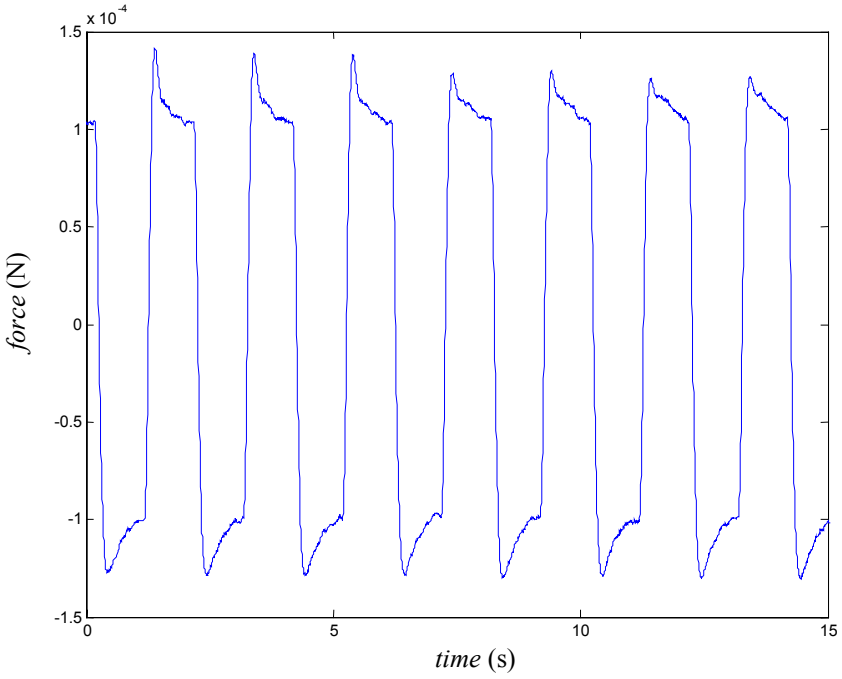

Figure 5.13. Closed-loop response to a square wave of amplitude 100 μN and frequency 0.5 Hz.

5.2 Closed-Loop Position Responses

After successfully achieving precision force control of IPMC, attention was turned to precision position control. As described in Chapter IV, the precision position control was achieved by developing and implementing a digital controller based on the empirical position model developed and described in Chapter III for IPMC strip *C*.

Figure 5.14 shows the 20 μm closed-loop step response of the IPMC strip. The noise level was 30 μm peak to peak or 7.6 μm rms. Figure 5.15 shows the closed-loop response to 50 μm commanded step. The presence of this noise limited the position resolution of the IPMC strip. Some of the probable causes of this noise are as follows:

- The sensor used for sensing the tip position was a laser distance sensor (OADM 20I44/404790). It had a resolution of 5 μm when incident on matt white ceramic. So sensor resolution may be one of the probable causes of this 30 μm peak to peak position noise seen.
- As mentioned in Section 5.1.1, floor vibration maybe one of the contributors to the position noise.
- Other contributors might be the A/D and D/A quantization noise, or the electrical noise.

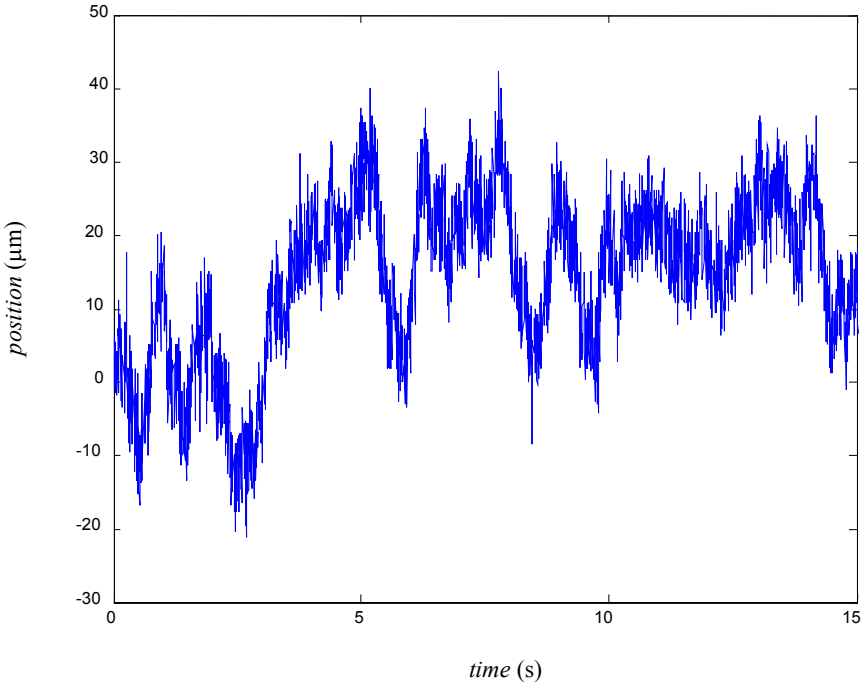

Figure 5.14. Closed-loop position response to 20 μm step.

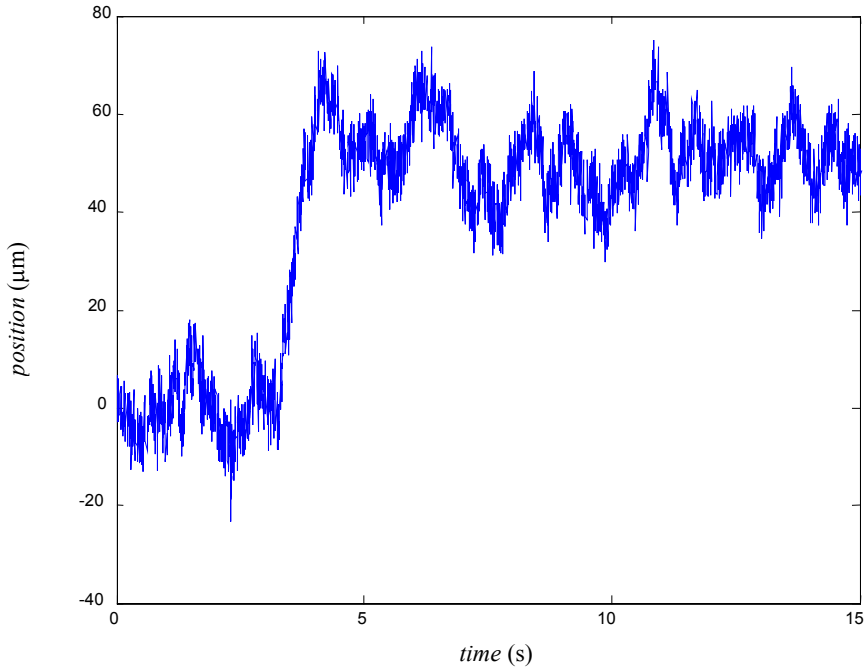

Figure 5.15. Closed-loop position response to 50 μm step.

To check the maximum position the IPMC could traverse under closed-loop control, different step responses were obtained for commanded position of 1 mm, 3 mm and 4 mm. (Figures 5.16–5.18). The controller voltage swing was limited to +2 V and –2 V, hence this limited the range of operation of the IPMC strip. 4 mm was the maximum closed-loop step response obtained for this strip. The controller voltage was limited within the specified values using a saturation block in the control loop (Figure 4.12). Figure 5.19 shows the actual voltage before the saturation block, which the controller generates. From the figure we can see that initially the controller output overshoots well above 2 V, and remains well above 2 V till about 8.33 s. During that period the saturation block limits the voltage being fed to the IPMC to +2 V (Figure 5.20). Thus actually no control action is being taking place on the IPMC, and hence its position starts to fall, so

the error goes on decreasing as seen by the error curve generated in Figure 5.21. The control voltage suddenly drops to negative value, and remains well below –2 V for about 9.6 s and the saturation block clips the actual voltage being supplied to IPMC to –2 V. This again stops the control action for the period the voltage is clipped to – 2 V, and again the error signal is affected by it. Then finally after about 10.4 s the controller output is within +2 V and –2 V, which leads to the control action being effected on the IPMC, and the position being maintained at the commanded position of 4 mm.

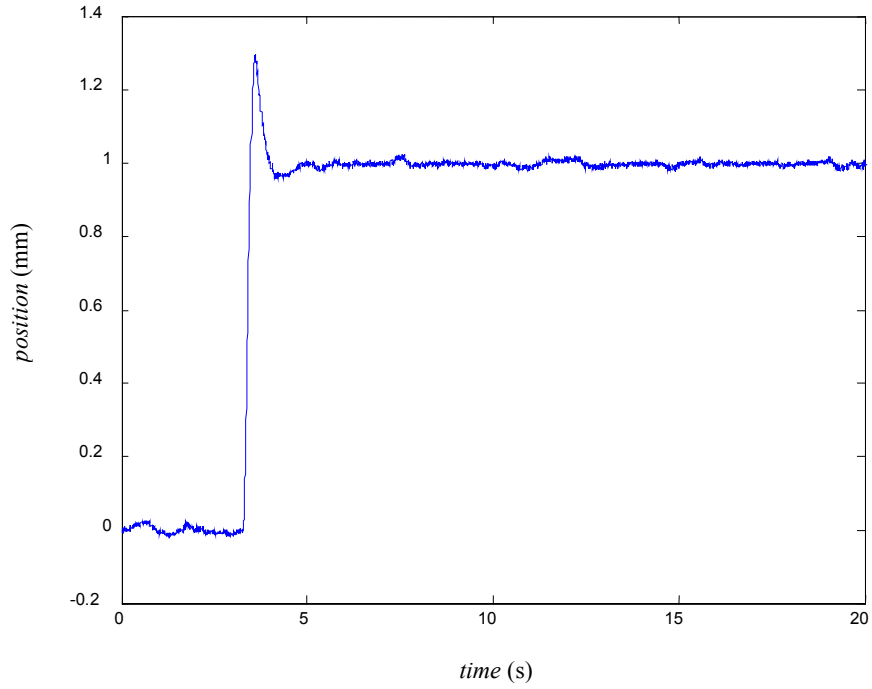

Figure 5.16. Closed-loop position response to 1- mm step.

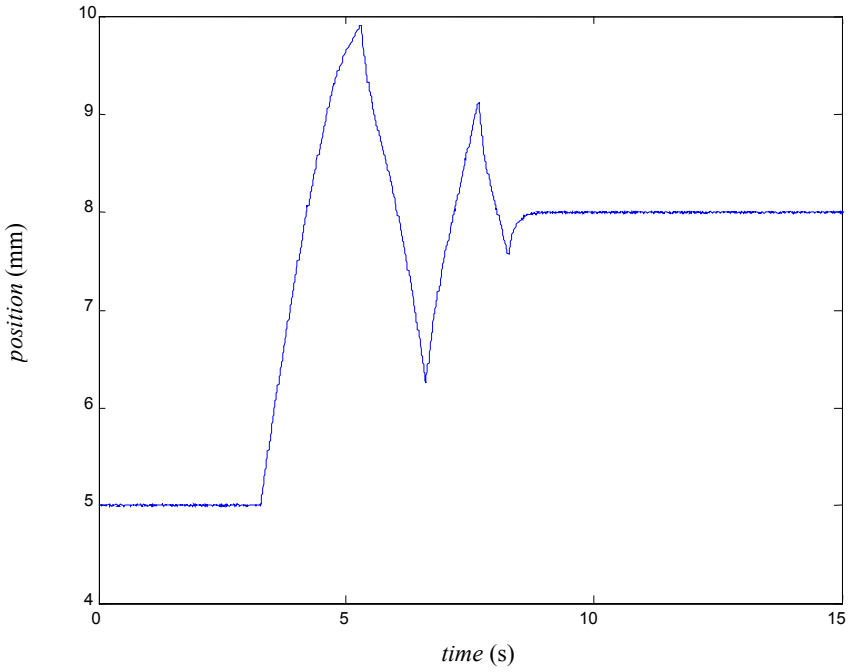

Figure 5.17. Closed-loop position response to 3-mm step.

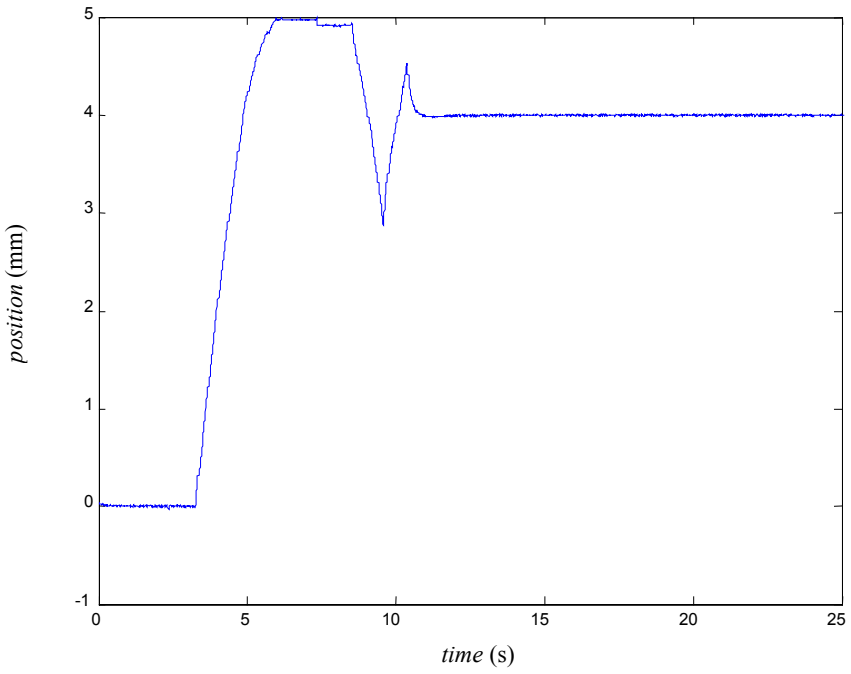

Figure 5.18. Closed-loop position response to 4-mm step.

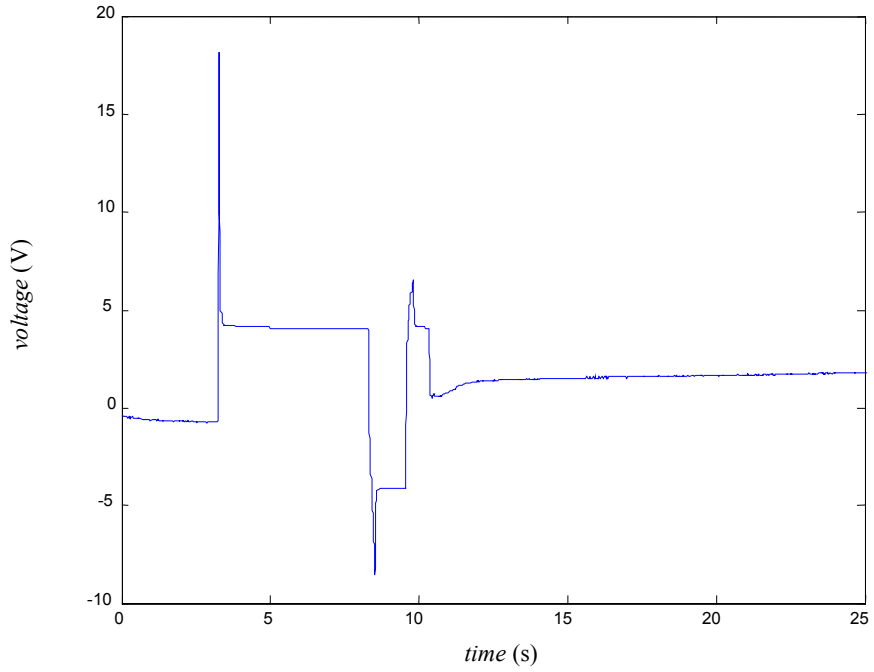

Figure 5.19. Controller output before the saturation block.

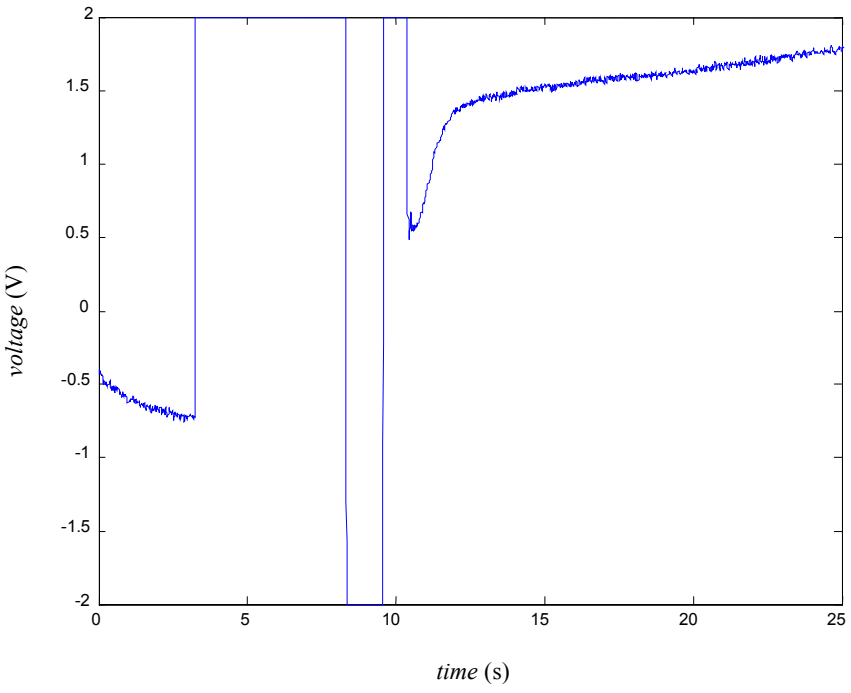

Figure 5.20. Controller output after the saturation block for the 4-mm step response.

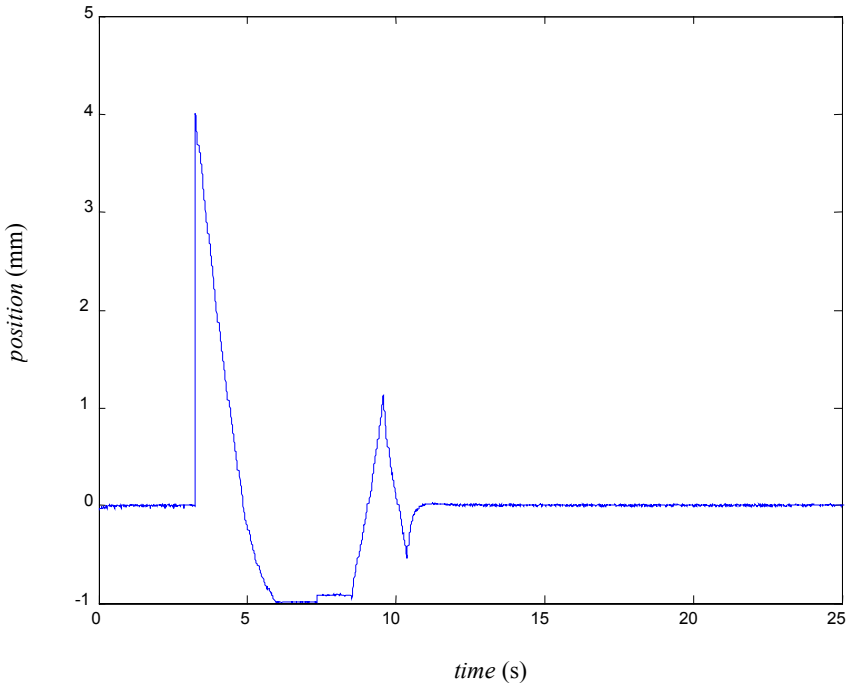

Figure 5.21. Error signal generated for the 4-mm step response.

5.2.1 More Responses

Figure 5.22 shows the actual and commanded closed-loop response of the IPMC strip to a sine wave of amplitude 0.5 mm and 0.25 Hz frequency. The driving frequency is less than the cross over frequency (0.841 Hz), and the IPMC strip follows the commanded signal quite well. Figure 5.23 shows the closed-loop response to a square wave of amplitude 0.5 mm and frequency 0.5 Hz. To demonstrate the different one-dimensional position profiles which the IPMC can follow, the response of IPMC to a ramp trajectory which goes from 0 mm to 1 mm in the time of 10 s is shown in Figure 5.24. Figure 5.25 shows the closed-loop response of IPMC to a combination of increasing and decreasing ramp. It can be seen that as commanded, the IPMC tip position reaches 1mm gradually in 10 s and then after reaching 1mm returns back to its original position in

further 10 s, and stays there. Figure 5.26 shows the IPMC strip following a trapezoidal profile.

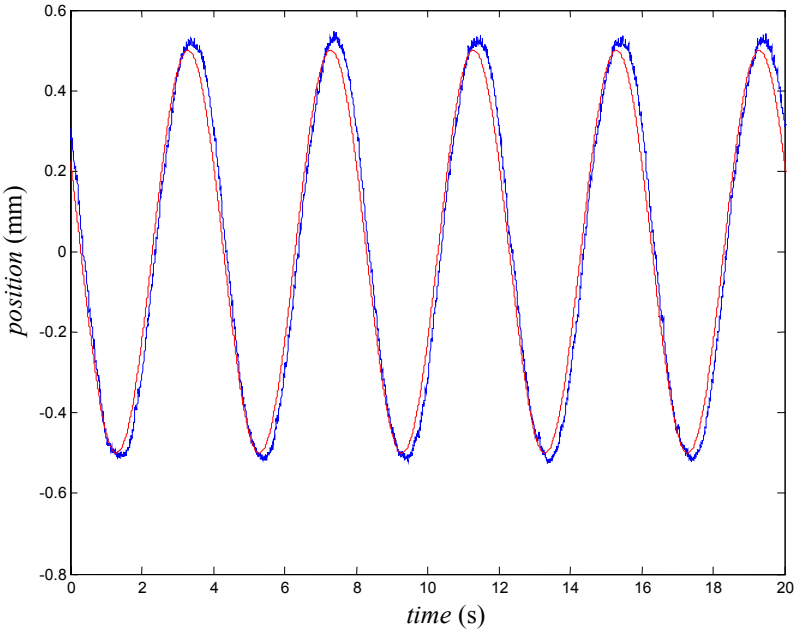

Figure 5.22. Actual and commanded response to a sine wave of frequency 0.25 Hz and amplitude 0.5 mm.

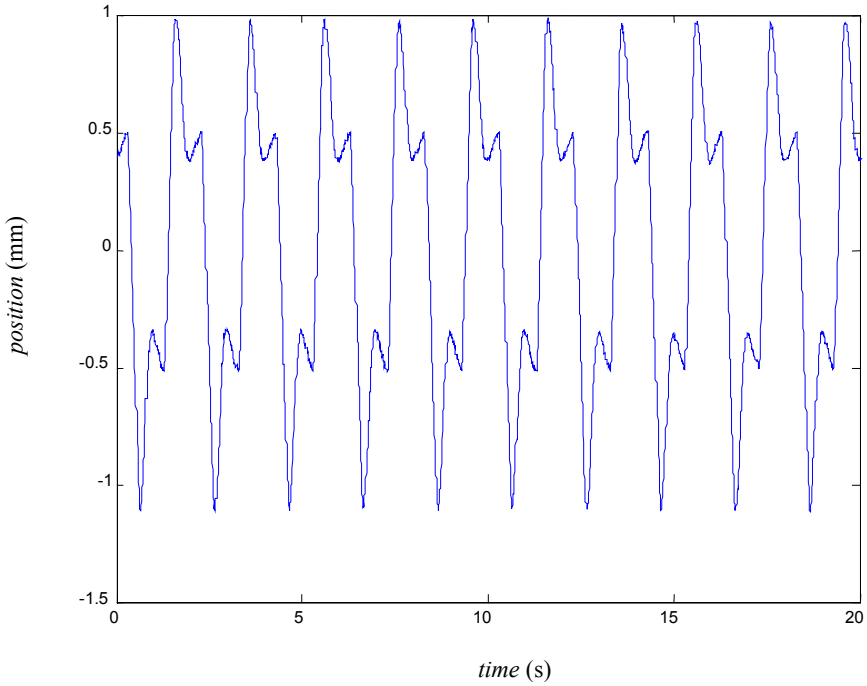

Figure 5.23. Closed-loop response to a square wave of frequency 0.5 Hz and amplitude 0.5 mm.

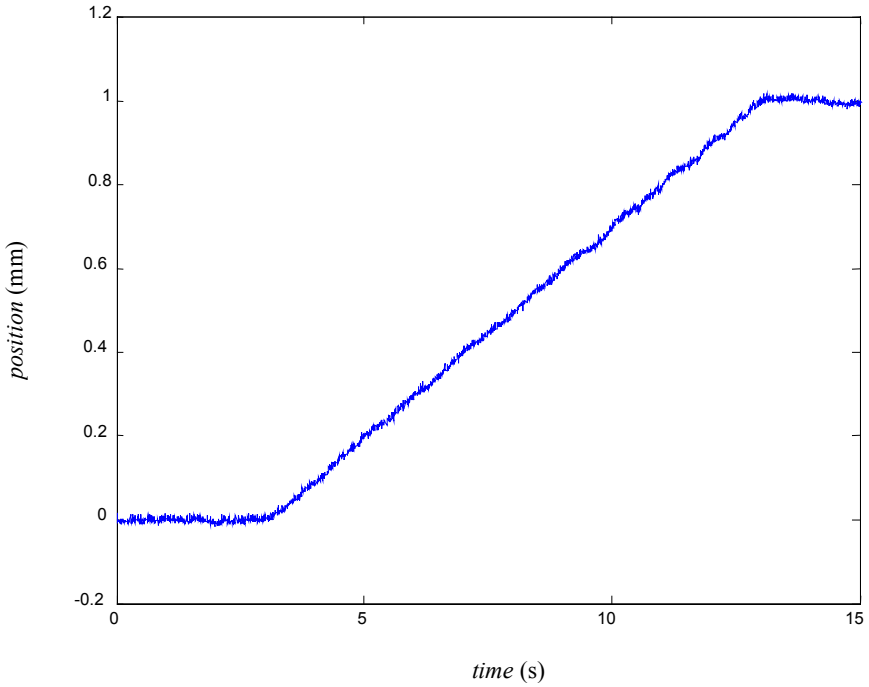

Figure 5.24. Closed-loop response to a ramp profile of slope 0.1 mm/s.

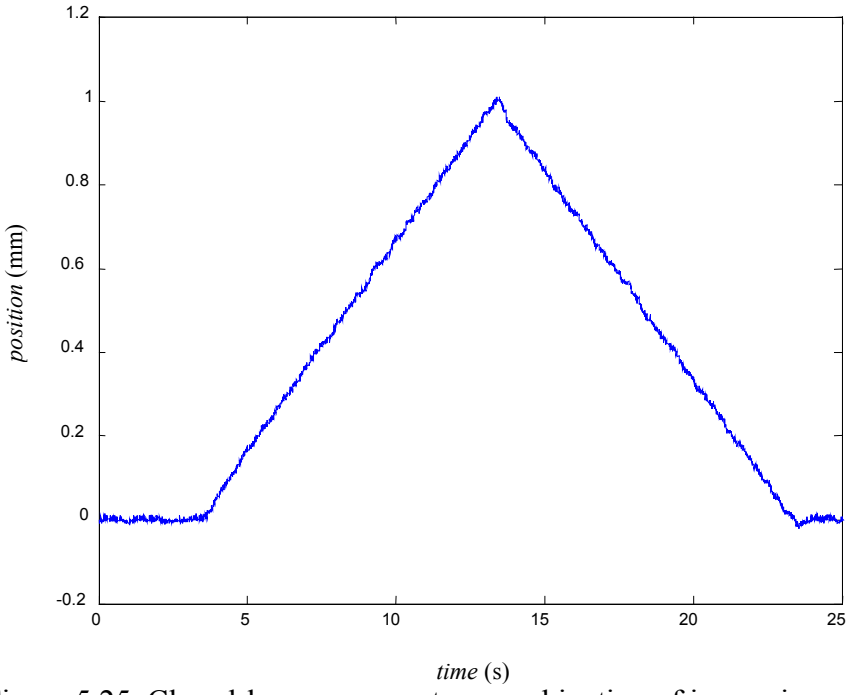

Figure 5.25. Closed-loop response to a combination of increasing and decreasing ramp each having slope of 0.1 mm/s.

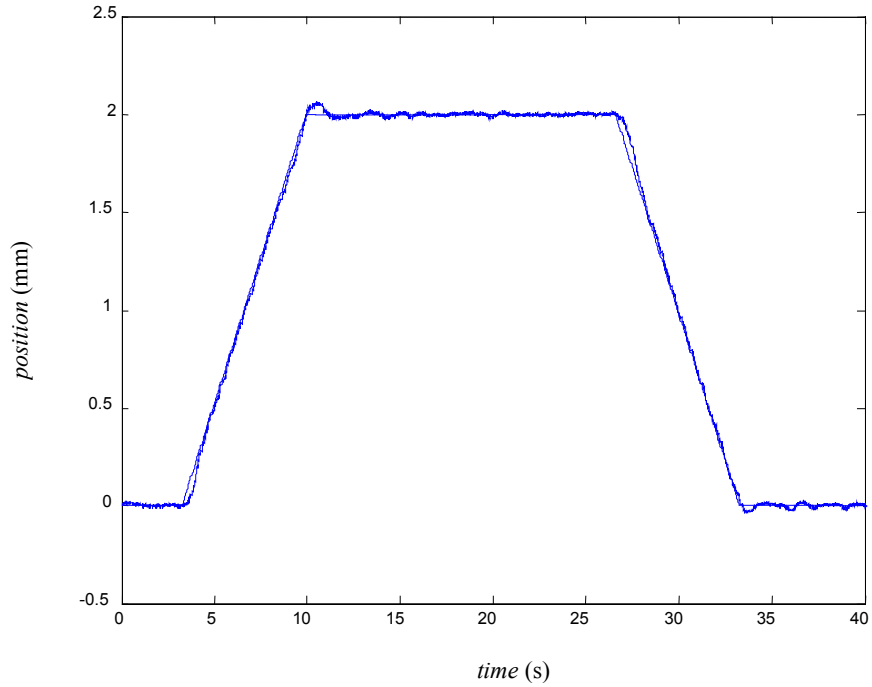

Figure 5.26. Actual and commanded close-loop response to a trapezoidal waveform.

5.3 Performance Characteristics

In Chapter I, the comparison of IPMC actuator with other similar actuators was given. In addition to the parameters mentioned there, some other specifications like the dynamic ranges of force and tip displacement the IPMC can generate under closed-loop control are also important. The knowledge of maximum speed and acceleration which the IPMC can achieve, and the time for which the IPMC can hold its commanded position without any rehyrdration is also important. Though these quantities will vary for different IPMC strips, they can be useful to verify the range of the parameters for comparable size of strips.

To check the maximum speed the IPMC can generate under closed-loop control, a trapezoidal velocity profile was generated using a combination of ramps in Simulink. As

the laser distance sensor could only sense the position and not the velocity, the velocity profile generated was passed through an integrator block in Simulink, and the closed-loop response of IPMC tip displacement was compared to the commanded position curve. Figure 5.27 compares the actual position curve with the commanded one, for a maximum velocity of 0.2 mm/s. It is seen that the IPMC follows the commanded curve very well. Similar curves were generated for velocities of 0.4 mm/s and 1 mm/s as seen in Figures 5.28 and 5.29 respectively. Figure 5.30 shows the commanded and actual profile generated to meet the maximum velocity of 2 mm/s. It can be seen that the IPMC strip does not follow the same curve as commanded, hence cannot achieve the 2 mm/s commanded speed. But the slope of the curve, indicates the reaching of a speed of about 1.5 mm/s. Thus the maximum speed that could be achieved was 1.5 mm/s.

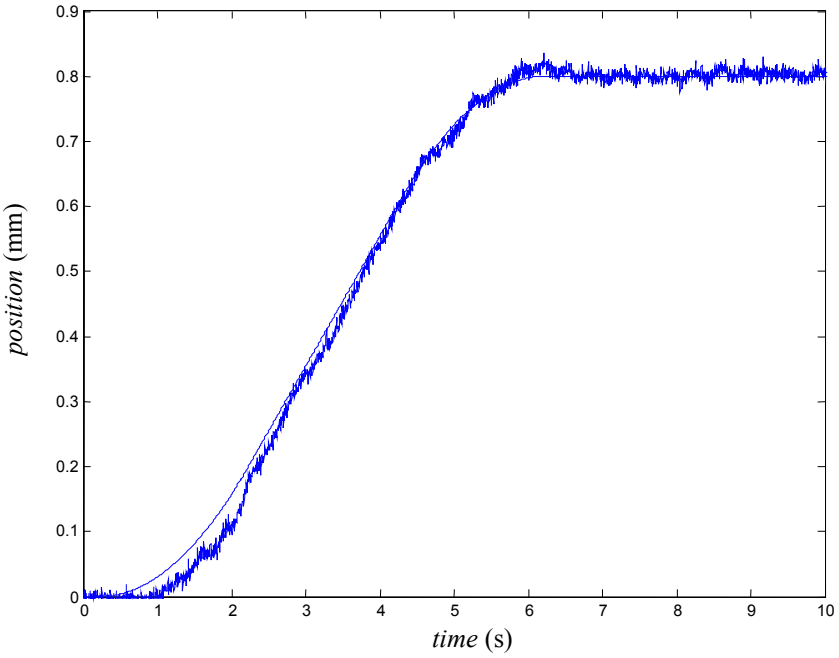

Figure 5.27. Actual and commanded position curve obtained from a trapezoidal velocity profile of maximum velocity 0.2 mm/s.

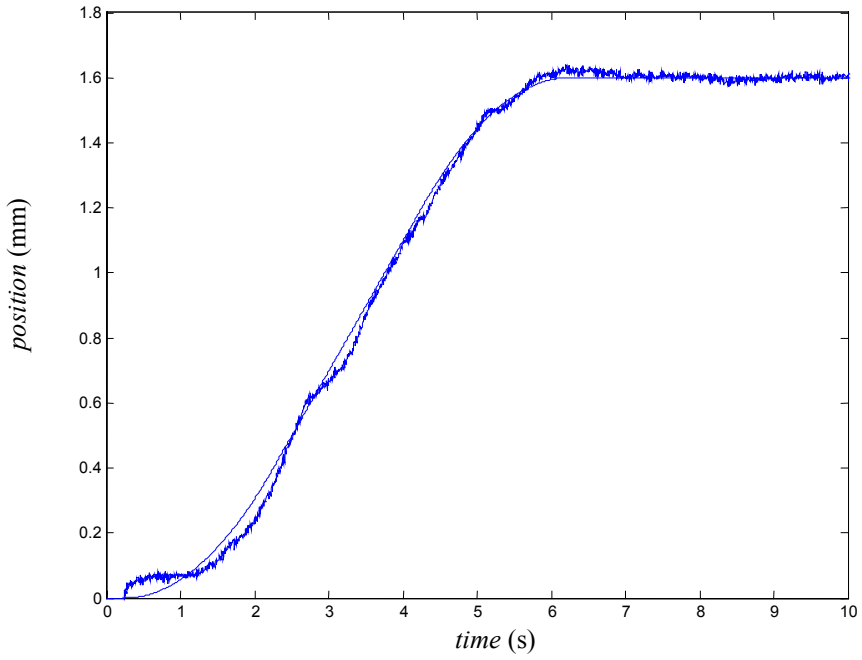

Figure 5.28. Actual and commanded position curve obtained from a trapezoidal velocity profile of maximum velocity 0.4 mm/s.

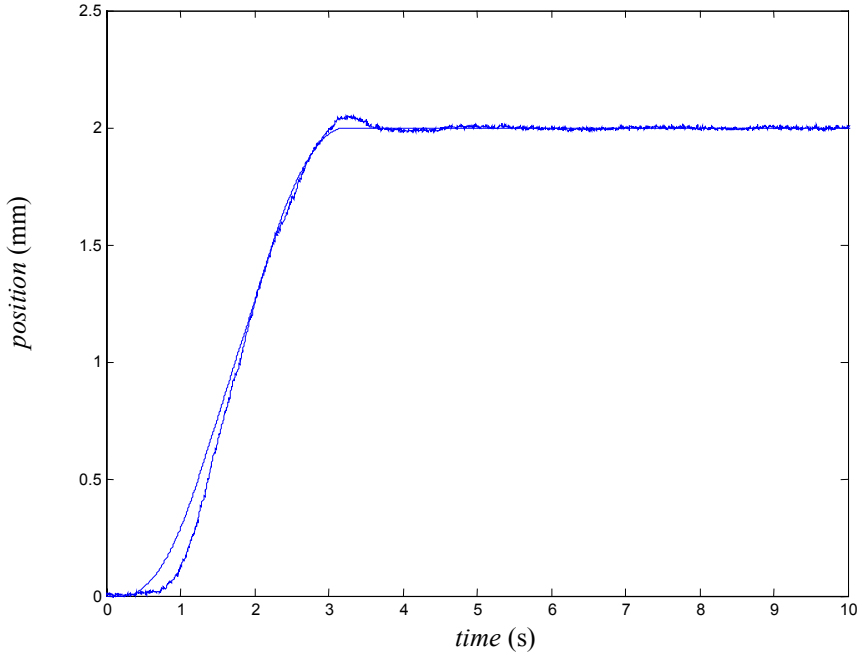

Figure 5.29. Actual and commanded position curve obtained from a trapezoidal velocity profile of maximum velocity 1 mm/s.

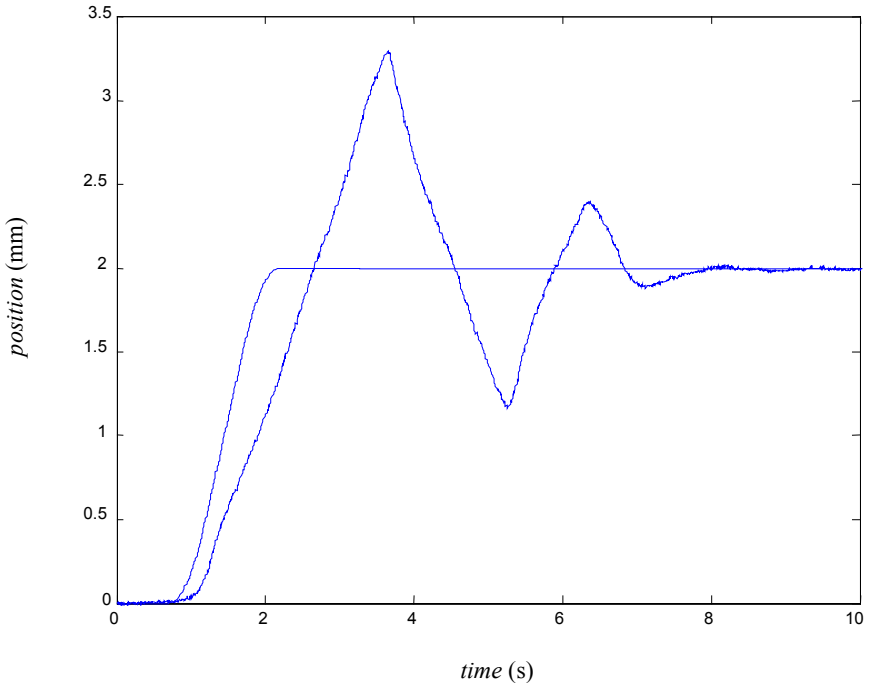

Figure 5.30. Actual and commanded position curve obtained from a trapezoidal velocity profile of maximum velocity 2 mm/s.

As mentioned previously the IPMC requires water for its good performance, and without rehydration, the performance of IPMC goes on degrading. To check the time, for which the IPMC strip could hold its commanded position in air without any rehydration, a closed-loop position test was performed as shown in Figure 5.31. A 0.5-mm step response was commanded, and the tip position data was captured for the time period the IPMC strip could hold its position. From the Figure 5.31, it was observed that the IPMC strip could hold its tip-position at the commanded 0.5 mm for about 39 minutes. A drop in the position after 39 minutes is observed. Figure 5.32 shows the corresponding voltage generated by the controller over time to maintain the tip-position. From the figure it is seen that slowly the voltage is drifting towards the +2 V value, and at 39 minutes it reaches +2 V and the IPMC could not hold its position, as the controller output gets

saturated. The IPMC strip on inspection was found out to be completely dry. As mentioned previously at voltages above 1.23 V hydrolysis reaction starts and electrolysis of water present in the IPMC strip takes place. This causes rapid dehydration of the IPMC strip.

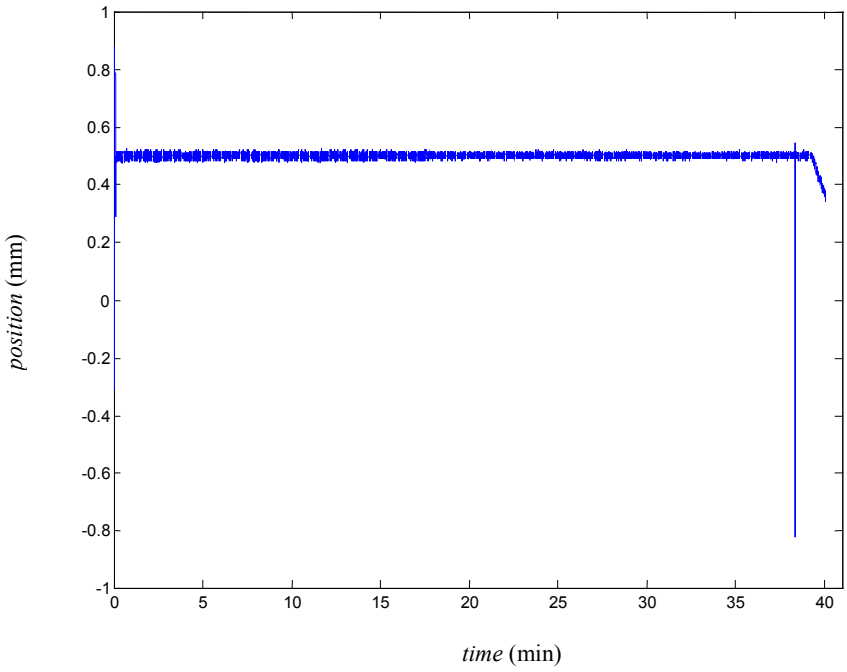

Figure 5.31. Closed-loop step response of the IPMC strip to a 0.5 mm commended value to check the holding capacity of the IPMC strip without rehydration.

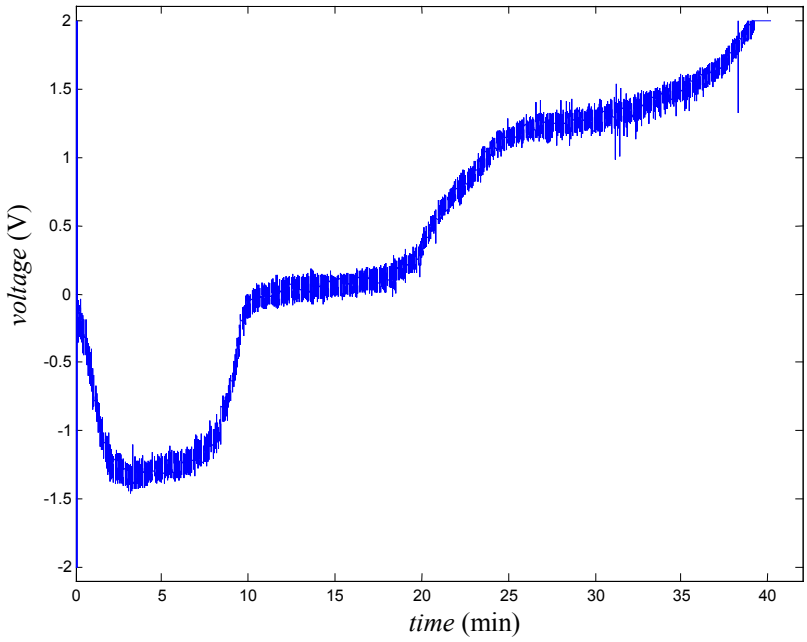

Figure 5.32. The voltage profile after the saturation block which is actually fed to the IPMC strip to get the 0.5-mm step response in the previous figure.

5.4 Actuator Saturation

It was found that the voltage between the two electrodes of the IPMC strip would drift very slowly even without control action. It is possibly due to the electrochemical reaction inside the polymer. Thus, it requires resetting the actuator voltage by discharging the charges accumulated in the polymer before commanding the next control action. If the initial voltage is near the extremes of the voltage swing (+ 2 V and –2 V), the actuator can be saturated upon a control input. To show the effect of such actuator saturation, a force step response of IPMC strip *B* when the lag compensator described in Chapter IV was applied was taken immediately without discharging the charges. Figure 5.33 shows a slower response between 7.5 s and 10 s and the drop in the force after 30 s. From Figure

5.34 we can see that the saturation level is reached in these time intervals. Similar behavior was observed also in case of position control.

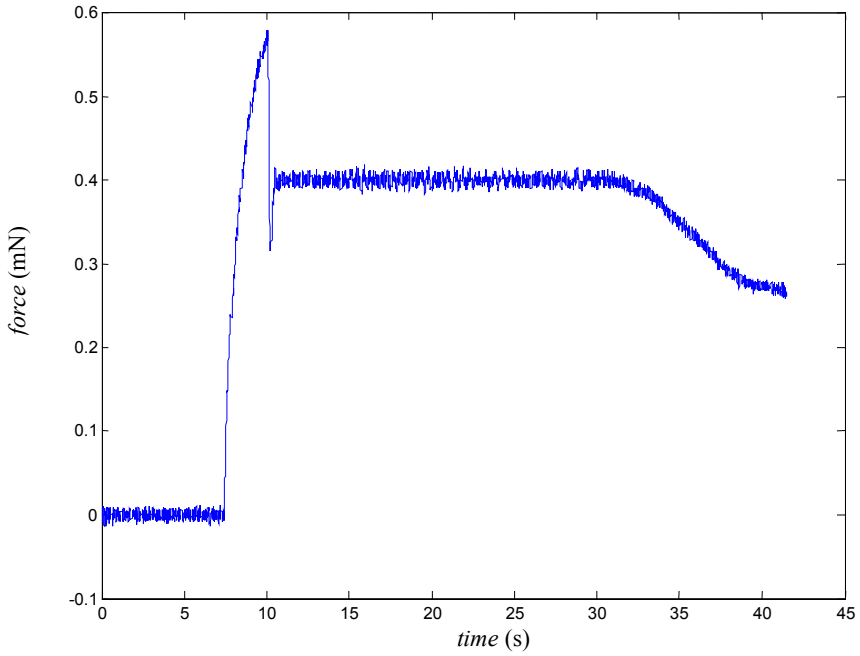

Figure 5.33. Step response of the IPMC strip showing the fall in the force due to actuator saturation.

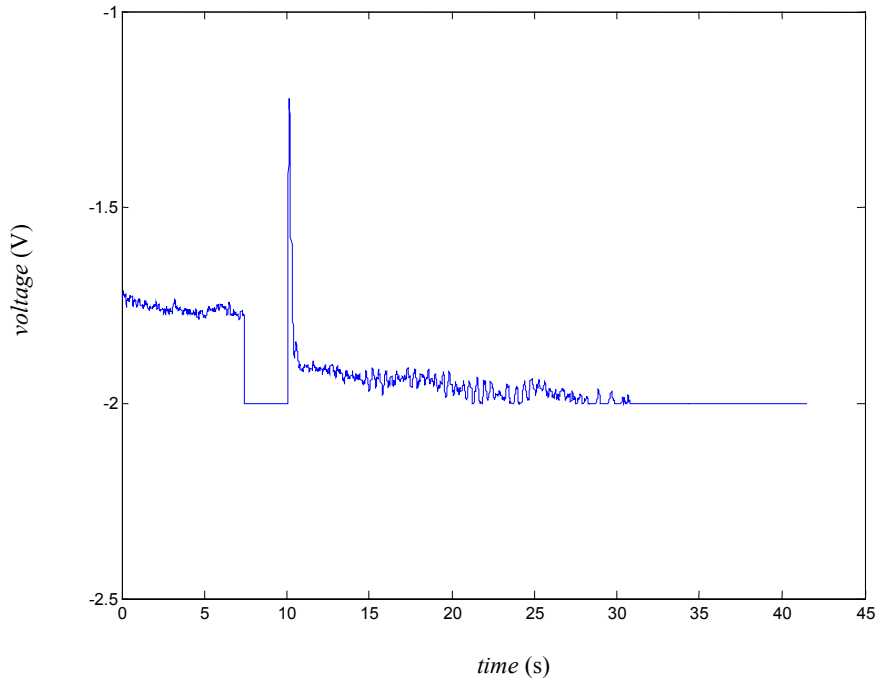

Figure 5.34. Control voltage being generated shows voltage saturation at –2 Volts at the same time the force output falls.

In case of the step response shown Figure 5.33 it took only 30 s for the actuator to saturate but in case of the step response shown in Figure 5.31 it took nearly 39 minutes for the actuator to saturate. The controller output in Figure 5.34 shows that the initial voltage is already close –2 V and the controller output is almost at all times over the ±1.23 V level. This also accelerated the hydrolysis reaction. But in case of the controller output in Figure 5.32 the initial voltage was close to 0 V and also the controller output reached 1.23 V after nearly 25 minutes. Hence one of the factors governing the time when the actuator saturation occurs is the initial voltage level. The other factor might be the accelerated hydrolysis reaction due to voltage above ±1.23 V level, which dehydrates the IPMC strip faster.

5.5 Conclusions for Chapter V

In this chapter the performance characteristics obtained under closed-loop force and position control for the IPMC strips have been stated. The force resolution achieved was 4 μN with an rms force noise of 0.904 μN. The maximum force achieved under closed-loop control was 1 mN. The position resolution attained was 20 μm with a position noise of 7.6 μm rms, while the maximum tip displacement attained under closed-loop control was 4 mm. The IPMC strip could achieve a maximum speed of 1.5 mm/s while it could hold its position without rehydration for 39 minutes.

CHAPTER VI

CONCLUSIONS

6.1 Conclusions

Ionic polymer metal composite was used in a cantilever configuration. A experimental setup used to conduct both force and position experiments was developed and described. Open-loop force response of IPMC strip to a −1.2 V step input was studied. In open loop the per-cent overshoot was found out to be nearly 131.62%, while the settling time was about 10 s. It was also found that the rise time was about 0.08 s on applying a step input. The open-loop tip displacement of IPMC strip to a 1.2 V step input showed overshoot to be about 205.34% while the settling time was about 27 s. It was found that both the force response and position response showed similar behavior but the settling time in case of open-loop force response was smaller than in case of open-loop position response of the IPMC tip.

Based on the step response obtained a fourth-order empirical model between voltage input and force output was derived by using a least-square curve fitting methodology for identifying all the model parameters. It was observed that a model with complex terms as compared to a model with two real exponential decay terms reduced the least-square norm from 3.4774×10^{-5} to 2.7135×10^{-5}.

Based on the position step response obtained a fourth-order empirical model between voltage input and position output was obtained in a similar fashion. It was found that in case of position response, the decrease in the residual norm due to introduction of

complex parameters was minimal as compared to force response. Even a model with two exponential decay terms accounted for the rise time.

A lead-lag compensator was developed based on the force model obtained. The control objectives were to decrease the settling time, the per-cent overshoot and also achieve the goal of reference input following. The phase margin with this controller was 80.714° and the crossover frequency was limited to 1.31 Hz. After implementing this controller on the ionic polymer metal composite system, the overshoot was decreased to 30%, while the settling time was decreased to 1.5 s. A lag compensator was developed based on the position model obtained. The control objectives in this case were also to decrease the settling time, the per-cent overshoot and to achieve reference input following. The phase margin with this controller was 34.5° and the crossover frequency was at 0.842 Hz. After implementing this controller the settling time was reduced to about 1 s while the percent overshoot was decreased to about 20 %.

Micro-scale precision force and position control was achieved and demonstrated. The resolution of the force control achieved was 4 μN with a force noise of 0.904 μN rms or 4 μN peak to peak. In case of position control the resolution achieved was 20 μm with a noise level of 30 μm peak to peak or 7.6 μm rms. 1 mN was the maximum force achieved while 4 mm was the maximum tip displacement achieved under closed-loop force and position control respectively. Reference force tracking was demonstrated by the tracking of different trajectories like staircase wave, sinusoidal wave and square wave under closed-loop force control. Reference position tracking was demonstrated by the tracking of different trajectories like ramp, trapezoidal wave, sinusoidal and square waves under closed-loop position control.

The maximum speed, which the IPMC actuator could achieve under closed-loop position control, was found out to be 1.5 m/s. It was also found that the IPMC strip could hold its position for a period of nearly 39 minutes under closed-loop control.

6.2 Future Work

On the basis of the research work presented in this document the following recommendations on future work are suggested.

- The non-linearities in IPMC like the water dependent behavior etc should be addressed and better models to predict those should be developed.
- A more complete analysis of the behavior of IPMC should be done, and a more generalized and comprehensive model should be developed, which can help develop more accurate control systems based on them.
- Improvements in packaging and manufacturing of IPMC should be done. The water dependant behavior of IPMC makes it difficult to use IPMC in many applications. Also commercial availability of IPMC is an issue which should be addressed to give researchers easy availability of IPMC.
- New control systems should be designed to focus on goal of increasing the closed-loop force and position bandwidths.
- Integrated position and force control strategy should be developed and implemented which would run both, the force and position control loops simultaneously.
- Feedback control systems based on non-linear control scheme and also adaptive control strategy should be developed and applied. Also neural networks may be one solution to getting the maximum performance output out of IPMC.

- Technology should benefit mankind directly or indirectly. Thus applications based on IPMC should be developed, which can reach the stage of commercialization from research labs. Effort in this direction has started recently, with the first commercial application of IPMC the artificial fish robots to be used in aquariums being introduced by Emmax Corp [11].

REFERENCES

1. http://www.crc4mse.org/what/MSE_history.html, in Material Science Engineering Career Resource Center, [Accessed May 2003].
2. Y. Bar-Cohen, *Electroactive polymer [EAP] actuators as artificial muscles*, SPIE Press, Bellingham, Washington, 2001.
3. M. Shahinpoor, Y. Bar-Cohen, J. O. Simpson, and J. Smith, "Ionic polymer-metal composites (IPMCs) as biomimetic sensors, actuators and artificial muscles—a review," *International Journal of Smart Materials and Structures*, vol. 7, pp. R15–R30, September 1998.
4. M. Shahinpoor, "Conceptual design, kinematics and dynamics of swimming robotic structures using ionic polymeric gel muscles," *International Journal of Smart Materials and Structures*, vol. 1, pp. 91–94, May 1992.
5. K. Oguru, Y. Kawami, and H. Takenaka, "Bending of an ion-conducting polymer film-electrode composite by an electric stimulus at low voltage," *Trans. Journal of Micromachine Society*, vol. 5, pp. 27–30, 1992.
6. K. Sadeghipour, R. Salomon, and S. Neogi, "Development of a novel electrochemically active membrane and 'smart' material based vibration sensor/damper," *International Journal of Smart Materials and Structures*, vol. 1, pp. 172–179, May 1992.
7. S. Tadokoro, S. Yamagami, and T. Takamori, "An actuator model of ICPF for robotic applications on the basis of physicochemical hypotheses," in *Proceedings of the 2000*

IEEE International Conference on Robotics & Automation, April 2000, pp. 1340–1346.

8. I. Hunter and S. Lafontaine, "A comparison of muscle with artificial actuators," in *Technical Digest of the IEEE Solid State Sensor and Actuator Workshop*, 1992, pp. 178–185.
9. M. Konyo, S. Tadokoro, T. Takamori and K. Oguru, "Artificial tactile feel display using soft gel actuators," in *Proceedings of IEEE International Conference on Robotics and Automation*, April 2000, pp. 3416–3421.
10. Y. Bar-Cohen, S. Leary, A. Yavrouian, K. Oguru, S. Tadokoro, J. Harrison, J. Smith and J. Su, "Challenges to the application of IPMC as actuators of planetary mechanisms," in *Proceedings of SPIE Symposium on Smart Structures and Materials,* March 2000, vol. 3987, paper no. 21.
11. Eamex, "Fish Robot," EAP in action session, *SPIE International Conference on Smart Materials and Structures*, March 2003.
12. Y. Bar-Cohen, T. Xue, M. Shahinpoor, J. O. Simpson, and J. Smith, "Flexible, low-mass robotic arm actuated by electroactive polymers and operated equivalently to human arm and hand," in *Proceedings of ASCE Robotics 98*, April 1998, pp. 15–21.
13. M. Shahinpoor, "Continuum electromechanics of ionic polymeric gels as artificial muscles for robotic applications," *Smart Materials and Structures*, vol. 3, pp. 367–372, 1994.
14. R. Lumia and M. Shahinpoor, "Microgripper design using electroactive polymers," in *Proceedings of SPIE Symposium on Smart Structures and Materials*, March 1999, vol. 3669, pp. 322–330.

15. W. -J. Kim and N. Bhat, "Microgripper," Disclosure of Invention No. 1868TEES02, Texas A&M University System, February 2002.
16. K. Oguru, http://ndeaa.jpl.nasa.gov/nasa-nde/lommas/eap/IPMC_PrepProcedure.htm, in World wide electroactive polymer actuators webhub, [Accessed May 2003].
17. N. Bhat and W. -J.Kim, "Precision control of force produced by ionic polymer metal composite," *accepted for presentation in 2003 ASME International Mechanical Engineering Congress and Exposition*, November 2003.
18. S. Leary and Y. Bar-Cohen, "Electrical impedance of ionic polymer metal composites," in *Proceedings of SPIE Symposium on Smart Structures and Materials*, March 1999, vol. 3669, paper no. 09.
19. K. Mallavarapu, *Feedback control of ionic polymer actuators*, Master's Thesis, Virginia Polytechnic Institute and State University, July 2001.
20. C. Kothera*, Micro-manipulation and bandwidth characterization of ionic polymer actuators*, Master's Thesis, Virginia Polytechnic Institute and State University, December 2002.
21. Baumer Electric, Measuring at an angle with the OADM 20144 xx and OADM20145 xx, Southington, CT, (Personal Collection, N. Bhat).
22. R. Kanno, S. Tadokoro, M. Hattori, T. Takamori, M. Costaftis, and K. Oguro, "Dynamic model of ICPF (Ionic Conducting Polymer Film) actuator," in *Proceedings of IEEE International Conference on Systems, Man, and Cybernetics: Intelligent Systems for the 21st Century*, October 1995, vol. 1, pp. 177–182.

23. M. Shahinpoor, “Micro-electro-mechanics of ionic polymeric gels as electrically controllable artificial muscles,” *Journal of Intelligent Material Systems and Structures*, vol. 6, pp. 307–314, May 1995.
24. S. Nemat-Nasser and J. Li, “Electromechanical response of ionic polymer metal composites,” in *Proceedings of SPIE Symposium on Smart Structures and Materials*, March 2000, vol. 3987, pp. 82–91.
25. Y. Xiao and K. Bhattacharya, “Modeling electromechanical properties of ionic polymers,” in *Proceedings of SPIE Symposium on Smart Structures and Materials*, March 2001, vol. 4329, pp. 292–300.
26. R. Kanno, A. Kurata, M. Hattori, S. Tadokoro, T. Takamori, and K. Oguro, “Characteristics and modeling of ICPF actuator,” in *Proceedings of Japan-USA Symposium on Flexible Automation*, July 1994, vol. 2, pp. 691–698.
27. K. Mallavarapu, K. Newbury, and D. Leo, “Feedback control of the bending response of ionic polymer-metal composite actuators,” *Proceedings of SPIE Symposium on Smart Structures and Materials*, March 2001, vol. 4329, pp. 301-310.
28. K. Newbury, *Characterization, modeling and control of ionic polymer transducers*, Doctoral thesis, Virginia Polytechnic Institute and State University, September 2002.
29. *Optimization Toolbox*, The Mathworks, Inc., Natrick, MA.
30. N. Bhat and W. -J. Kim, “System identification and control of ionic polymer metal composite,” in *Proceedings of the 10th SPIE Symposium on Smart Materials and Structures*, March 2003, Paper No. 5049-63.
31. G. Franklin, J. Powell, and A. Emami-Naeini, *Feedback control of dynamic systems*, Third Edition, Addison-Wesley, Menlo Park, CA, 1994.

APPENDIX A MATLAB CODES FOR FORCE MODELING AND POSITION MODELING

In this appendix the matlab code (m-file) which was written to obtain empirical model between input voltage and output force is presented. Also the matlab code to obtain empirical model between input voltage and output tip-displacement is presented. The real step response data was first normalized, and then least-square curve fitting method was used to obtain the best model.

A.1 M-file for Obtaining Force Model

```
clear all;
%clc;
%close all;

load step5;  % load the file containing the step response data
 % Take the Data
% Output Data
output =double(step5.Y(2).Data)/100*9.81/1000;  % out force found out from the load cell is converted to newtons
time =  step5.X.Data;  % Change
std(output)%standard deviation
max1=max(output);
figure,plot(time,output)
xlabel('time(s)');
```

```
ylabel('Force(N)');
title('Step response of IPMC to 1.2 Volt input signal')
grid on;
% Input data
input=double(step5.Y(1).Data);
Fs = 1/step5.X.Data(2);
Ts=1/Fs;%sampling period
figure,plot(time,input)
xlabel('time(s)');
ylabel('Voltage(V)');
title('Input signal');
grid on;
% Taking the FFT of the data
f = Fs*(0:length(output)-1)/length(output);
signalfft = fft(output);
signalmag = abs(signalfft)*(2/length(output));
N = length(output);
figure, semilogy(f,signalmag);
title('FFT of Force respose of IPMC to step signal')
xlabel('Frequency (Samples/sec)')
ylabel('Force (N)')
grid on;
% Normalizing the data to remove the initial residual force sensed by the force sensor
```

```
normal=3.9778*10^-3

t=time;

for i=1:15417

tnorm(i)=t(i)-7.152;

end

tnew=tnorm(1788:15417);

for i=1:15417

outnorm(i)=output(i)-3.9778*10^-3;

end

for i=1:15417

unorm(i)=input(i)-0;

end

u=unorm(1788:15417);

outnew=outnorm(1788:15417);

figure,plot(tnew,outnew);

figure,plot(tnew,u)

xlabel('time(seconds)');

ylabel('force(Newtons)');

grid on;



% finding the model by using non linear curve fit methodology
```

```
% By using 1 decay term
fun1=inline('x(1)*exp(-x(2)*tnew)+0.4*10^-3','x','tnew');
[x,resnorm2]=lsqcurvefit(fun1,[5e-003 7.442*10^-3],tnew,outnew)
y=x(1)*exp(-x(2)*tnew)+0.4*10^-3;
figure,plot(tnew,y)
hold on
plot(tnew,outnew);
grid on;
title('Simulated verves normalised response of the step by using model wih 1 exponential
decay term');
xlabel('time');
ylabel('Force N');
% By using 2 decay terms
fun = inline(' x(1)*exp(-x(2)*tnew)+x(3)*exp(-x(4)*tnew)+0.4*10^-3','x','tnew');
[x,resnorm1] = lsqcurvefit(fun,[5e-003 7.442*10^-3 12.79602*10^-3 5.55*10^-
3],tnew,outnew);
y=x(1)*exp(-x(2)*tnew)+x(3)*exp(-x(4)*tnew))+0.4*10^-3;
figure,plot(tnew,y);
hold on
plot(time,outnew);
grid on;
title('Simulated verves normalised response of the step by using model wih 2 exponential
decay terms');
```

```
xlabel('time');
ylabel('Force N');
%By using complex parameters
fun = inline(' x(1)*exp(-x(2)*tnew)+x(3)*exp(-x(4)*tnew)-x(5)*(exp((x(6))*tnew)-
exp((x(7))*tnew))+0.4*10^-3','x','tnew');
[x,resnorm1] = lsqcurvefit(fun,[5e-003 7.442*10^-3 12.79602*10^-3 5.55*10^-3 -2.1i -
0.01+0.9i -0.01-0.9i ],tnew,outnew);
y=x(1)*exp(-x(2)*tnew)+x(3)*exp(-x(4)*tnew)-x(5)*(exp((x(6))*tnew)-
exp((x(7))*tnew))+0.4*10^-3;
figure,plot(tnew,y);
hold on
plot(time,outnew);
grid on;
title('Simulated verves normalised response of the step by using model wih complex
parameters');
xlabel('time');
ylabel('Force N');
% generating the transfer function in s-domain
s = TF('s')
Y=x(1)/(s+x(2))+x(3)/(s+x(4))-x(5)/(s-x(6))+x(5)/(s-x(7))+0.4*10^-3/s;
U=-1.2/s;
model=Y/U;
figure,lsim(model,u,tnew)
```

```
hold on;
plot(tnew,outnew);% creating a final version of the model for further use
Num=[-0.0002365 -0.002947 -0.004299 -0.002266 -0.0002065]
Den=[ 1.2 4.577 6.14 3.314 0.6194 ]
modelwithfreq=tf(Num,Den)
```

A.2 M-file for Developing the Position Model

```
 clear all;
load step1  % loading the file containing the step response data
 % Take the Data
output =double(step1.Y(2).Data)
time =  step1.X.Data;  % Change
std(output)%standard deviation
max1=max(output);
figure,plot(time,output)
xlabel('time(s)');
ylabel('position(mm)');
title('Step response of IPMC to 1.2 Volt input signal')
grid on;



% the conversion factor is 1V=1mm.
% obtaining the input data
```

```
input=double(step1.Y(1).Data);
Fs = 1/step1.X.Data (2);
Ts=1/Fs; %sampling period
figure,plot(time,input)
xlabel('time(s)');
ylabel('Voltage (V)');
title('Input signal');
grid on;

% Taking the FFT of the data
f = Fs*(0:length(output)-1)/length(output);
signalfft = fft(output);
signalmag = abs(signalfft)*(2/length(output));
N = length (output);
figure, semilogy(f,signalmag);
title('FFT of Force respose of IPMC to step signal')
xlabel('Frequency (Samples/sec)')
ylabel('position (mm)')
grid on;


% Normalizing the data
% step starts at 8.31 seconds
```

```
% the step started from 5 mm
t=time;
for i=1:55570
   tnorm(i)=t(i)-8.310;
end
tnew=tnorm(8310:55570);
for i=1:55570
   outnorm(i)=output(i)-5;
end
for i=1:55570
   unorm(i)=input(i)-0;
end
u=unorm(8310:55570);
outnew=outnorm(8310:55570);
figure,plot(tnew,outnew);
figure,plot(tnew,u)
xlabel('time(seconds)');
ylabel('position(mm)');
grid on;



% finding the position model by using non linear curve fit methodology
% the steady state value is taken as 0.54 mm
```

```
% By using just one pole
fun1=inline('a(1)*exp(-a(2)*tnew)+0.54','a','tnew');
[a,resnorm2]=lsqcurvefit(fun1,[0.8 0.7],tnew,outnew)
y=a(1)*exp(-a(2)*tnew)+0.54;
% comparing the actual step response and the simulated response
figure,plot(tnew,y);
hold on
plot(tnew,outnew);
title('Simulated verves normalized response of the step by using model with 1 pole');
xlabel('time (s)');
ylabel('position (mm)');

%By using 2 poles
fun1=inline('b(1)*exp(-b(2)*tnew)+b(3)*exp(-b(4)*tnew)+0.54','b','tnew');
[b,resnorm3]=lsqcurvefit(fun1,[0.8 0.6 0.7 0.65],tnew,outnew)
y=b(1)*exp(-b(2)*tnew)+b(3)*exp(-b(4)*tnew)+0.54;
figure,plot(tnew,y);
hold on
plot(tnew,outnew);
title('Simulated verves normalised response of the step by using model wih 2 pole');
xlabel('time s');
ylabel('position mm');
% model with the complex parameters
```

```
fun=inline('x(1)*exp(-x(2)*tnew)+x(3)*exp(-x(4)*tnew)-x(5)*(exp((x(6))*tnew)-
exp((x(7))*tnew))+0.54','x','tnew');
[x,resnorm1] = lsqcurvefit(fun,[0.8 0.6 0.7 0.65 -2.1i -0.01+0.9i -0.01-0.9i
],tnew,outnew);
y=x(1)*exp(-x(2)*tnew)+x(3)*exp(-x(4)*tnew)-x(5)*(exp((x(6))*tnew)-
exp((x(7))*tnew))+0.54;
figure,plot(tnew,y);
hold on
plot(tnew,outnew);
grid on;
title('Simulated verves normalised response of the step by using model wih complex
parameters');
xlabel('time (s)');
ylabel('position (mm)');
% Generating a transfer function in s-domain to again compare the modeled and
simulated response
s = TF('s')
Y=x(1)/(s+x(2))+x(3)/(s+x(4))-x(5)/(s-x(6))+x(5)/(s-x(7))+0.54/s;
U=1.2/s;
model=Y/U;
figure,lsim(model,u,tnew)
hold on;
plot(tnew,outnew);
```

```
%After the model is decided creating final version of model for further use.
Num=[0.006895 1.735 3.034 2.078 0.1332]
Den=[1.2 4.467 6.345 3.256 0.296]
positionmodel=tf(Num/Den)
```

APPENDIX B SIMULINK BLOCK DIAGRAMS USED FOR IMPLEMENTING CLOSED-LOOP CONTROLLERS

The block diagrams used to implement the real time force and position control were created as simulink block diagrams first. The dSPACE 1102 board has a internal interface with Matlab/Simulink environment. Hence after the controller block diagrams were established, they were build and a real time controller file was generated by Matlab/dSPACE and it was loaded on to the dSPACE DSP. ControlDesk software was used to create the real-time interface.

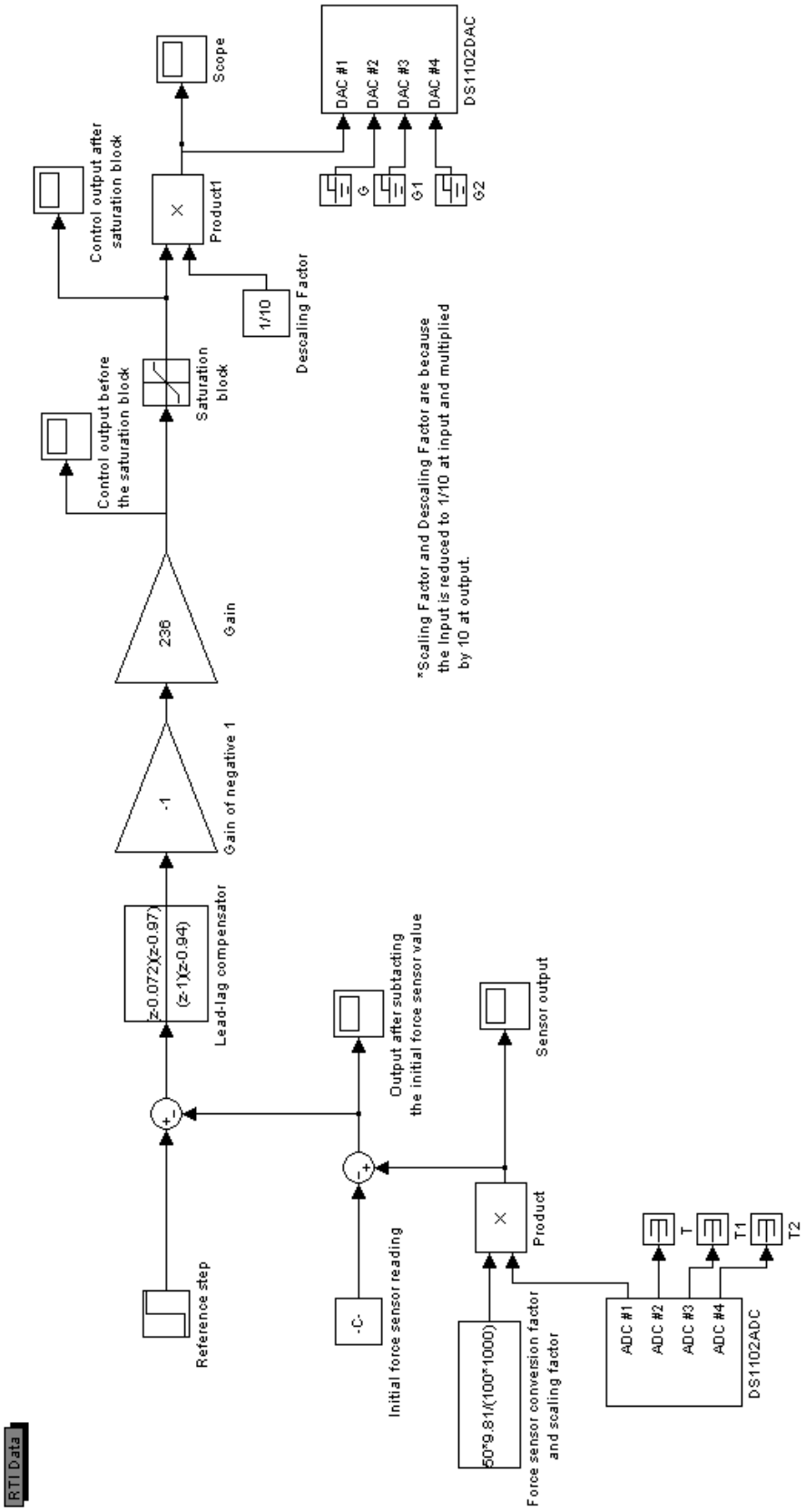

Figure B.1. Simulink block diagram used for real-time force controller implementation on the IPMC strip

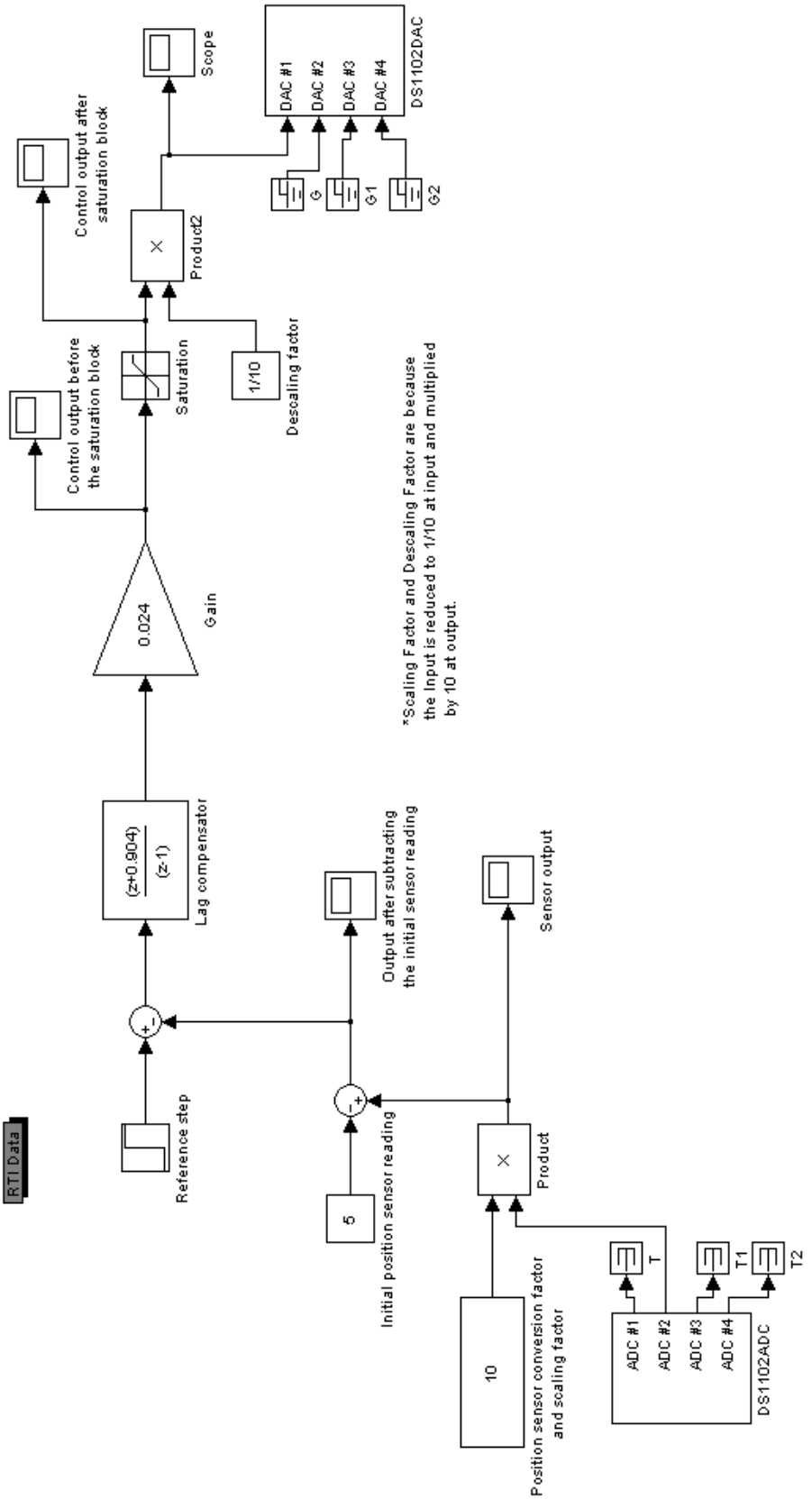

Figure B.2. Simulink block diagram used for real-time position controller implementation on the IPMC strip.

VITA

Nikhil Dilip Bhat was born on November 9th 1979 in Nasik, Maharashtra in India. He spent almost his entire life in Pune (previously Poona) a city near Mumbai in Maharashtra. He graduated from College of Engineering Pune with his Bachelor's Degree in Mechanical Engineering in May 2001. He joined Texas A&M University, College Station, in August 2001, and is pursuing his Master's of Science degree in Mechanical Engineering there.

His permanent address is

Flat no 12, Plot no 29

Rambaug Colony, Paud Road

Pune 4110038

Maharashtra, India.

His local address is

311, Stasney Street, #1100

College Station, Texas 77840

USA.

Phone No: 979-324-6023

Email address: nikhilbhat@hotmail.com